Comparative Fatigue Performance of Steel-Reinforced and Steel–Free Concrete Bridge Deck Slabs

By

Amjad Hussain Memon

A Dissertation

Submitted to the Faculty of Graduate Studies

In Partial Fulfilment of the Requirements for the Degree of

DOCTOR OF PHILOSOPHY

Department of Civil Engineering

The University of Manitoba

Winnipeg, Manitoba, Canada

THE UNIVERSITY OF MANITOBA

FACULTY OF GRADUATE STUDIES

*****

COPYRIGHT PERMISSION

Comparative Fatigue Performance of Steel-Reinforced and Steel-Free Concrete Bridge Deck Slabs

BY

Amjad Hussain Memon

A Thesis/Practicum submitted to the Faculty of Graduate Studies of The University of Manitoba in partial fulfillment of the requirement of the degree

Of

Ph. D.

Acknowledgements

The author would like to express his deepest gratitude to Dr. Aftab A. Mufti for his guidance, continuous encouragement and financial support throughout this research work. In addition to his support, he has provided the unwavering source of inspiration, determination and leadership that was so essential for the successful execution of this research work. The support provided by the Network of Centres of Excellence on the Intelligent Sensing of Innovative Structures (ISIS Canada) is also gratefully acknowledged.

The author is very grateful to Dr. Dimos Polyzois for his comprehensive assistance in reviewing and editing this thesis, and his helpful suggestions on improving the final outcome. The author would like to thank Dr. Douglas J. Thomson for his constructive comments and encouragements throughout the research. Thanks are extended to Dr. S. A. Sheikh from University of Toronto for reviewing the thesis as the external examiner.

The author would like to thank Dr. L. G. Jeager, Dr. B. Bakht and Dr. J. Newhook for their valuable advice regarding development of the theoretical model, analysis of the fatigue data and using the PUNCH Program is greatly acknowledged.

The author would also like to express his thanks to M. McVey, G. Whiteside, S. Sparrow, C. Klowak and L. Han for their valuable assistance during the fabrication, construction and testing of the specimens. Help from fellow graduate students was greatly appreciated as well. Also recognized is the valuable administrative and clerical

assistance provided by ISIS Canada. Special thanks are extended to N. Fehr for editing this thesis.

The patience, love and support of my mother, brothers and sisters, all my family members, my wife, my daughter and my son cannot be praised enough; to them this thesis is dedicated.

Abstract

In concrete bridge deck slabs supported on longitudinal girders, longitudinal cracks are developed to initiate the arching action. When the deck slab is confined externally, as in steel-free concrete deck slabs, and contains no crack-control grid, longitudinal cracks tend to be quite wide.

This study investigates the fatigue behaviour of a cast-in-situ full-scale concrete bridge deck slab with various kinds of internal reinforcement. The deck slab was cast-in-situ compositely on two steel girders at a center-to-center spacing of 2.0 m through the use of shear connectors, with a 500 mm long cantilever overhang beyond the center of the each girder. In the longitudinal direction, the deck slab was 9.0 m long and 175 mm thick. Although cast monolithically, this full-scale 9.0 m long model of a deck slab was divided into three 3.0 m segments (A, B and C). Segments B and C were both confined externally with steel straps and contained a crack control grid of CFRP and a GFRP respectively. Segment A was confined internally and contained two meshes of steel reinforcement. To investigate fatigue behaviour, a cyclic load was applied through a hydraulic actuator; and the performance of all three segments of the concrete bridge deck slab was monitored using a number of sensors, including linear variable displacement transducers (LVDTs), strain gauges, pi-gauges and linear motion transducers (LMTs).

Each of the three slab segments was tested under a central pulsating load representing the dual tires of a heavy truck. In each cycle, the pulsating load peaked at approximately 25 tonne and all three segments completed 1,000,000 cycles which

satisfied the serviceability criterion. All three segments failed under a cyclic load which peaked at 60 tonne. The internally confined Segment A, with two meshes of steel bars, failed after 23,162 cycles. The externally confined deck slabs, Segment B with a crack control grid of CFRP, failed after 198,863 cycles, and the Segment C, with GFRP crack control grid, failed after 420,682 cycles. This outcome shows that deck slabs having the same thickness but confined differently have significantly different fatigue resistance. An internally confined deck slab with two meshes of steel bars has the least fatigue resistance, whereas an externally confined deck slab has the most favourable fatigue resistance.

On the basis of measured data, this study concluded that the externally confined deck slab with a GFRP crack control grid provides the best fatigue resistance for concrete bridge deck slabs. Based on the limited experimental results and fatigue curves, a simple theoretical model is developed to estimate the fatigue strength of steel-free concrete bridge deck slabs.

I believe this study will make possible to construct the durable steel-free concrete bridge deck slabs. The hybrid system consisting of internal a GFRP crack control grid and an external steel strap results in an efficient, economical, and corrosion-free second generation steel-free concrete bridge deck slab that satisfies the serviceability, ultimate and fatigue limit states criterion.

Table of Contents

Acknowledgement ---------- i

Abstract ---------- iii

Table of Contents ---------- v

List of Symbols ---------- x

List of Tables ---------- xiii

List of Figures ---------- xiv

Chapter 1. Introduction

1.1 General ---------- 1

1.2 Concept of the Steel-Free Concrete Bridge Deck Slab ---------- 1

1.3 Focus of the Study ---------- 3

1.4 Research Objectives ---------- 4

Chapter 2. Background To Concrete Bridge Deck Slabs

2.1 History of Reinforced Concrete Bridge Deck Slabs ---------- 5

2.1.1 Flexural Design Method ---------- 5

2.1.2 Development of Empirical Design Method ---------- 6

2.1.3 Development of Steel-Free Concrete Bridge Deck Slab ---------- 8

2.2 Field Application of Steel-Free Concrete Bridge Deck Slabs in Canada ---------- 13

2.2.1 Salmon River Bridge ---------- 13

2.2.2 Chatham Bridge ---------- 14

2.2.3 Crowchild Trail Bridge---------- 15

2.2.4 Waterloo Creek Bridge---------- 15

2.2.5 Lindquist Creek Bridge ---------- 15

2.3 Dynamic Tests on Steel-Free Concrete Bridge Deck Slab---------- 16

2.3.1 Single Moving Wheel ---------- 16

2.3.2 Sequential Wheel Load---------- 17

2.3.3 Single Pulsating Wheel Load---------- 18

2.4 Wheel Load Data---------- 18

2.5 Theoretical Approach for Punching Shear (PUNCH Program) ---------- 20

Chapter 3. Design Of Steel-Free Concrete Bridge Deck Slabs

3.1 General ---------- 26

3.2 Design of Concrete Deck Slabs ---------- 27

3.2.1 Design of Segment A (Steel Reinforcement) ---------- 28

3.2.2 Design of Segment B and C (Steel-Free Concrete Deck Slabs)---------- 31

3.3 Design of Steel Girder---------- -37

3.4 Design of Shear Connectors ---------- 38

3.5 Design of Edge Beams and Diaphragm---------- 42

Chapter 4. Test Program For Fatigue Behaviour Of Steel Free Concrete ArchPanel® And Bridge Deck Slabs

4.1 General ---------- 43

4.2 Pre-Cast Steel-Free ArchPanel® ---------- 43

4.2.1 Instrumentation for ArchPanel®----------45

4.2.2 Testing Detail of ArchPanel®----------46

4.3 Full-Scale Specimen of Concrete Bridge Deck Slab ----------47

4.3.1 Construction of Full-Scale Specimen Concrete Deck Slab ----------48

4.3.2 Instrumentation for Concrete Bridge Deck Slab ----------54

4.3.3 Testing Detail of Concrete Bridge Deck Slab ----------56

Chapter 5. Test Results Of Pre-Cast Concrete Archpanel®

5.1 General----------57

5.2 Deflection behaviour in ArchPanel®----------58

5.3 Strain in the steel strap behaviour in ArchPanel® ----------60

5.4 Crack width behaviour in ArchPanel®----------61

Chapter 6. Test Results of Cast-in-situ Concrete Deck Slab

6.1 General----------64

6.2 Segment C (steel-free concrete deck slab with internal GFRP crack control grid and external steel straps)----------64

6.2.1 Deflection behaviour in Segment C (GFRP) ----------66

6.2.2 Strain behaviour in Segment C (GFRP)----------70

6.2.3 Crack width behaviour in Segment C (GFRP) ----------73

6.2.4 Outward movement of steel girders behaviour in Segment C (GFRP) ------74

6.3 Segment A (conventional design with steel reinforcement)----------75

6.3.1 Deflection behaviour in Segment A (Steel) ----------77

6.3.2 Strain behaviour in Segment A (Steel) ---------- 82

6.3.3 Crack width behaviour in Segment A (Steel) ---------- 84

6.3.4 Outward movement of steel girders behaviour in Segment A (Steel) ------- 86

6.4 Segment B (steel-free concrete deck slab with internal CFRP crack control grid and external steel straps) ---------- 87

6.4.1 Deflection behaviour in Segment B (CFRP) ---------- 89

6.4.2 Strain behaviour in Segment B (CFRP) ---------- 94

6.4.3 Crack width behaviour in Segment B (CFRP) ---------- 97

6.4.4 Outward movement of steel girders in Segment B (CFRP) ---------- 98

6.5 Fatigue performance comparison of segments A, B and C ---------- 100

6.5.1 Deflection comparison of segments A, B and C ---------- 100

6.5.2 Reinforcement and steel strap strain comparison of segments A, B and C ---------- 103

6.5.3 Crack width comparison of segments A, B and C ---------- 105

Chapter 7. Estimate of the Fatigue Strength of Steel-Free Deck Slab

7.1 General ---------- 107

7.2 Modifying Matsui's P-N Curve ---------- 107

7.3 Estimate Equivalent Number of Cycles at Two Load Levels ---------- 111

7.4 Recommended Approach for Fatigue ---------- 112

7.4.1 Background ---------- 112

7.4.2 Suggested Method ---------- 114

7.4.3 Numerical Example ---------- 115

7.5 Estimate Fatigue Strength of Segment C---------- 116

7.6 Estimate Fatigue Strength of Segment B---------- 118

7.7 Fatigue Strength of Steel-free Concrete Bridge Deck Slab---------- 120

Chapter 8. Conclusions & Recommendations

8.1 Conclusions---------- 121

8.2 Recommendations for future research---------- 124

References ---------- 125

Appendices

Appendix-A1 Details of concrete mix proportions for Grade-35 and properties --- 131

Appendix-A2 Compressive and Tensile strength of concrete cylinders ---------- 132

List of Symbols

AASHTO	American Association of State and Highway Transportation Officials
ACI	American Concrete Institute
ADT	Average Daily Traffic
ADTT	Average Daily Truck Traffic
$ADTT_{SL}$	Average Daily Truck Traffic in a Single Lane
ASTM	American Society for Testing and Materials
CFRP	Carbon Fibre Reinforced Polymers
CHBDC	Canadian Highway Bridge Design Code
FRP	Fibre Reinforced Polymers
GFRP	Glass Fibre Reinforced Polymers
ISIS	Intelligent Sensing for Innovative Structures
LMT	Linear Motion Transducer
LVDT	Linear Variable Displacement Transducer
OHBDC	Ontario Highway Bridge Design Code
RC	Reinforced Concrete
FRC	Fibre Reinforced Concrete
F_s	A factor given in Clause 16.7 of CHBDC
$\Delta\phi$	Angle inscribed by the two radial cracks forming the sides of wedge
ψ	Angle of rotation of wedge
P	Applied cyclic load
P	Applied Point Load
P_1	Applied cyclic load at level 1
P_2	Applied cyclic load at level 2

Δ	Deflection of deck
A_s	Area of reinforcement bars
A_s	Cross-sectional area of strap
c_1	Base of conical shell
R	Circumferential compressive force
f_c'	Compressive strength of concrete in bridge deck
M	Constant Factor for material
c_2	Depth of compressive stress block
d	Effective depth of concrete
B	Diameter of equivalent circle for loaded area
y	Distance of the neutral axis from the top surface
Δ_L	Lateral deflection
F_w	Lateral restraint force on a wedge
N_1, N_2	Limiting number of cycles
E	Modulus of elasticity of steel strap
E_s	Modulus of elasticity of steel strap
M_r	Moment resistance
N	Number of cycles
n_1	Number of cycles at P_1
n_2	Number of cycles at P_2
R_1, R_2	Ratio of applied cyclic load to static failure load
ρ	Reinforcement ratio
S	The centre-to-centre spacing of beams supporting a deck slab

f_y	Specified minimum yield strength of reinforcing steel
P_s	Static failure load
P_u	Static failure load
T	Tension force
S_s	Spacing between straps
S_l	The Spacing of straps
S_l	Length of strap
t	Thickness of slab
K	Transverse restraint stiffness
V_r	Vertical shear resistance
b	Width of compression face of the member

List of Tables

Table 2.1 Comparison of theoretical and experimental results----------25

Table 3.1: Load Deflection from PUNCH Program (Design for Segment A) --------31

Table 3.2: Load Deflection from PUNCH Program (Design for Segments B and C)33

Table 3.3: Sectional properties of W920 x 387 and W760 x 196 ----------37

Table 3.4: Permissible and maximum deflection of W920 x 387 and W760 x 196 --38

List of Figures

Fig. 1.1 Cross-section of a steel-free concrete deck slab----------3

Fig. 1.2 Cross-section of 2nd generation of steel-free concrete bridge deck slab ----3

Fig. 2.1 Failure by bending ----------6

Fig. 2.2(a) Empirical design method----------8

Fig. 2.2(b) Failure by punching shear----------8

Fig. 2.3 Steel-free concrete deck slab----------10

Fig. 2.4(a) Construction of Salmon River Bridge----------10

Fig. 2.4(b) Bottom view of Salmon River Bridge ----------11

Fig. 2.5 Salmon River Bridge opens for traffic----------11

Fig. 2.6 Crack pattern underside of the Salmon River Bridge----------12

Fig. 2.7 Wheel load statistics----------20

Fig. 2.8(a) Plan view of slab with crack pattern----------23

Fig. 2.8(b) Rigid body rotation of wedges----------23

Fig. 3.1 Reinforcement details of segments A, B, and C----------27

Fig. 3.2 (a) Top-view of Segment A, (b) Cross-section of Segment A ----------30

Fig. 3.3 (a) Top-view of Segment B, (b) Cross-section of Segment B`----------35

Fig. 3.4 (a) Top-view of Segment C (b) Cross-section of Segment C ----------36

Fig. 3.5 Shear studs on top flange of steel girder ----------41

Fig. 3.6 Detail of edge beam and diaphragm----------42

Fig. 4.1 Top view and typical cross-sections of ArchPanel® ----------44

Fig. 4.2 Schematic view of test setup----------45

Fig. 4.3 View of LVDTs----------46

Fig. 4.4 View of test setup----------47

Fig. 4.5 Steel frameworks for the supporting steel-free concrete deck slab --------49

Fig. 4.6 Reinforcement details and formwork ----------49

Fig. 4.7(a) Detail of steel reinforcement in Segment A----------50

Fig. 4.7(b) Detail of CFRP-grid and steel straps in Segment B----------50

Fig.4.7(c) Detail of GFRP-grid and steel strap in Segment C----------50

Fig. 4.8(a) Pouring of concrete----------52

Fig. 4.8(b) Concreting of Segment A----------52

Fig. 4.9 Concreting of Segment B----------53

Fig. 4.10 Concreting of Segment C----------53

Fig. 4.11 Concrete deck slab after casting----------54

Fig. 4.12 Test setup and instrumentation----------55

Fig. 4.13 Bottom view and instrumentation----------55

Fig. 5.1 Load–deflection behaviour under 20, 25, 35 and 50 tonne (ArchPanel®)-59

Fig. 5.2 Deflection behaviour under 20, 25, 35, and 50 tonne (ArchPanel®)-------59

Fig. 5.3 Deflection behaviour under 50 tonne (ArchPanel®)----------60

Fig. 5.4 Strain behaviour under 20, 25, 35 and 50 tonne (ArchPanel®)----------61

Fig. 5.5 Strain behaviour under 50 tonne (ArchPanel®)----------62

Fig. 5.6 Crack width behaviour under 25, 35, and 50 tonne (ArchPanel®)---------62

Fig. 5.7 Crack width behaviour under 50 tonne (ArchPanel®)----------63

Fig. 6.1 Load-deflection behaviour under 25, 50 and 60 tonne (Segment C)-------67

Fig. 6.2 Deflection behaviour under 25, 50 and 60 tonne (Segment C)----------67

Fig. 6.3 Punching shear failure mode (Segment C)----------68

Fig. 6.4 Deflection profile along transverse direction (Segment C)----------69

Fig. 6.5 Deflection profile along longitudinal direction (Segment C)----------69

Fig. 6.6(a) Strain behaviour of GFRP rebar under 25 and 50 tonne (Segment C)-----70

Fig. 6.6(b) Strain behaviour of GFRP rebar under 25 tonne (Segment C)----------71

Fig. 6.7 Strain profile of GFRP rebar along longitudinal direction (Segment C)--71

Fig. 6.8(a) Strain behaviour of steel strap under 25, 50 and 60 tonne (Segment C)--72

Fig. 6.8(b) Strain behaviour of steel strap under 25 tonne (Segment C)----------73

Fig. 6.9 Crack width behaviour under 25, 50 and 60 tonne (Segment C)----------74

Fig. 6.10 Outward movement of girders behaviour under 25, 50 and 60 tonne (Segment C)----------75

Fig. 6.11 View of LVDTs and test setup (Segment A)----------76

Fig. 6.12 View of the pi-gauge and LMT (Segment A)----------77

Fig. 6.13 Load-deflection behaviour under 25 and 60 tonne (Segment A)----------78

Fig. 6.14 Deflection behaviour of Segment A under 25 and 60 tonne (Segment A)79

Fig. 6.15 Deflection behaviour of Segment A under 60 tonne (Segment A)---------79

Fig. 6.16 Punching shear failure mode (Segment A)----------80

Fig. 6.17 Deflection profile along transverse direction at different no. of cycles (Segment A)----------81

Fig. 6.18 Deflection profile along longitudinal direction at different no. of cycles (Segment A)----------82

Fig. 6.19 Strain behaviour from bottom transverse rebar under 25 and 60 tonne (Segment A)----------83

Fig. 6.20 Strain behaviour under 60 tonne (Segment A)----------83

Fig. 6.21 Strain profile from bottom transverse rebar along longitudinal direction (Segment A)----------84

Fig. 6.22 Crack width behaviour under 25 and 60 tonne (Segment A)----------85

Fig. 6.23 Crack width behaviour under 60 tonne (Segment A)----------85

Fig. 6.24 Outward movement of girders behaviour under 25 and 60 tonne (Segment A)----------86

Fig. 6.25 Outward movement of girders behaviour under 60 tonne (Segment A)---87

Fig. 6.26 View of LVDTs and test setup (Segment B)----------88

Fig. 6.27 Bottom view of Segment B and instrumentation (Segment B)----------89

Fig. 6.28 Load-deflection behaviour under 25 and 60 tonne (Segment B)----------91

Fig. 6.29 Deflection behaviour under 25 and 60 tonne (Segment B)----------91

Fig. 6.30 Deflection – No. of cycles behaviour at 60 tonne load level (Segment B)92

Fig. 6.31 Punching shear failure mode (Segment B)----------92

Fig. 6.32 Deflection profile along transverse direction (Segment B)----------93

Fig. 6.33 Deflection profile along longitudinal direction (Segment B)----------94

Fig. 6.34 Strain behaviour of CFRP rebar under 25 and 60 tonne (Segment B)-----95

Fig. 6.35 Strain behaviour of transverse CFRP rebar under 60 tonne (Segment B)-95

Fig. 6.36 Strain profile of transverse CFRP rebar under 25 and 60 tonne (Segment B)----------96

Fig. 6.37 Strain behaviour of the steel strap under 25 and 60 tonne (Segment B)---96

Fig. 6.38 Crack-width behaviour under 25 and 60 tonne (Segment B)----------97

Fig. 6.39 Crack-width behaviour under 60 tonne (Segment B)----------98

Fig. 6.40 Outward movement of girders behaviour under 25 and 60 tonne (Segment B)----------99

Fig. 6.41 Outward movement of girders behaviour under 60 tonne (Segment B)---99

Fig. 6.42 Deflection behaviour of segments A, B and C under 25 tonne----------101

Fig. 6.43 Deflection behaviour of Segment C under 50 tonne----------101

Fig. 6.44 Deflection behaviour of Segment C under 60 tonne----------102

Fig. 6.45 Deflection behaviour of segments A, B and C under 60 tonne----------102

Fig. 6.46(a) Steel reinforcement (Segment A) and steel strap strain (Segments B & C) behaviour under 25 tonne ----------103

Fig. 6.46(b) Steel reinforcement (Segment A) and steel strap strain (Segments B & C) behaviour under 60 tonne ----------104

Fig. 6.47 Strain behaviour of CFRP and GFRP under 25 tonne----------104

Fig. 6.48 Crack width behaviour of segments A, B and C under 25 tonne ---------105

Fig. 6.49 Crack width behaviour of Segment C under 50 tonne----------106

Fig. 6.50 Crack width behaviour of segments A, B and C under 60 tonne ---------106

Fig. 7.1 Comparison of P-N Curves----------109

Fig. 7.2 P-N curves for ArchPanel® and bridge deck slabs ----------110

Fig. 7.3 Load – number of cycles----------113

Fig. 7.4 Load – deflection curve----------115

Fig. 7.5 Load–number of cycles of suggested method----------116

Fig. 7.6 Fatigue curve of Segment C ----------117

Fig. 7.7 P-N Curve for Segment C to estimate fatigue strength----------118

Fig. 7.8 Fatigue curve for Segment B ----------119

Fig. 7.9 P-N curve for Segment B to estimate fatigue strength----------119

Fig. 7.10 P-N Curve for steel-free concrete bridge deck slab----------120

Chapter 1

Introduction

1.1 General

Reinforced concrete deck slabs require constant maintenance due to corrosion of the reinforcing steel, which is caused by de-icing salts, temperature and thermal cracking, dynamic fatigue and fracture of the concrete. To avoid the corrosion of steel reinforcement, Mufti et al. (1991) proposed the concept of a steel-free concrete bridge deck slab. This concept has been applied to four highway bridges and one forestry bridge in Canada (Bakht and Mufti, 1998). These deck slabs have been instrumented extensively and are being monitored for their performance, under the influence of both environmental effects and vehicle loads.

1.2 Concept of the Steel-Free Concrete Bridge Deck Slab

A steel-free concrete deck slab is based on the concept that the concrete deck slab is entirely free of any internal steel reinforcement. In a steel-free concrete deck slab, steel straps are partially studded and placed at the top of the girder, as shown in Fig. 1.1, providing lateral restraint to the top flange of the girders, resulting in compressive force being developed in the deck slab. Stresses develop in bridge decks as a result of traffic loads. Once the bridge deck cracks, traffic loads are resisted through arching action, as shown in Fig. 1.1, and failure takes place by punching shear. This concept led to the world's first steel-free concrete bridge deck slab over the Salmon River on the Trans-Canada Highway in Nova Scotia, which was opened to

traffic in December 1995 (Mufti et al. 1999). Six months later longitudinal cracks that were approximately 1 mm wide were observed at the soffit of the deck slab, roughly midway between the girders. Periodic visual inspection has shown that the widths and pattern of the cracks have not changed significantly during the past nine years. Laboratory investigation under simulated rolling wheel tests on steel-free concrete bridge deck slab conducted by Bakht and Selvadurai (1996) observed longitudinal cracks similar to those observed in the field. Limaye (2004) reported that longitudinal cracks in a steel-free concrete deck slab did not affect the safety of the deck slab. However, since these cracks are aesthetically unpleasing and can result in public unease, engineers are not comfortable with them.

Therefore, to reduce the development of longitudinal crack width in future steel-free concrete bridge deck slabs, a research study was conducted at the University of Manitoba to examine the fatigue behaviour of an ArchPanel® and a full-scale specimen of a cast-in-situ bridge deck slab, internally reinforced with either a GFRP crack control grid or a CFRP crack control grid, and externally reinforced with steel straps, as shown in Fig. 1.2. Due to this hybrid system of either a GFRP crack control grid or a CFRP crack control grid and steel straps, corrosion can be completely eliminated from the deck slab, and crack widths can be reduced significantly resulting in an economical and durable bridge deck system. The above hybrid system is called the second generation of steel-free concrete bridge deck slabs. The first application of a second generation steel-free concrete bridge deck slab was introduced in the Red River Bridge in Winnipeg, Manitoba, Canada in 2003 and later, in 2004, one was constructed in Toma County, Iowa, USA.

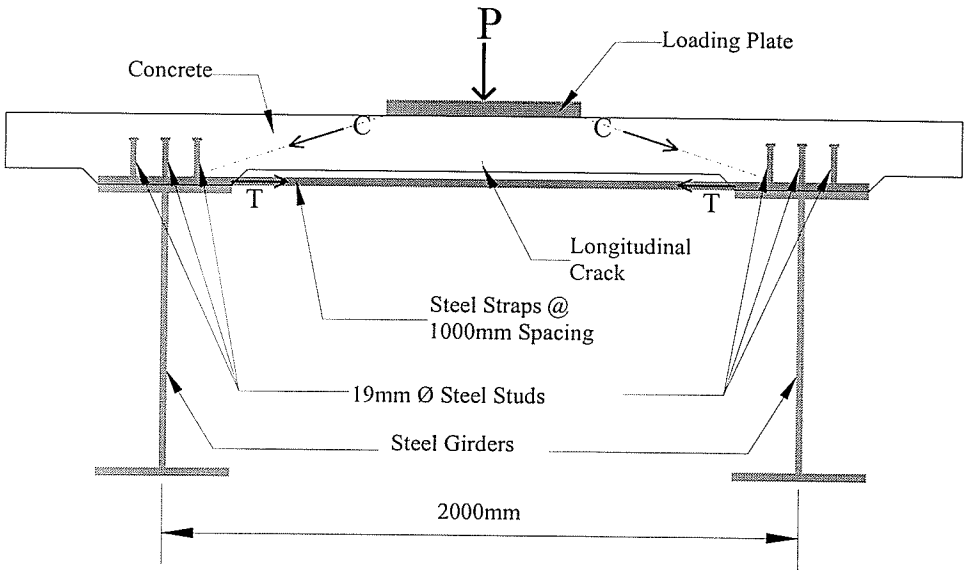

Fig. 1.1: Cross-section of a steel-free concrete deck slab

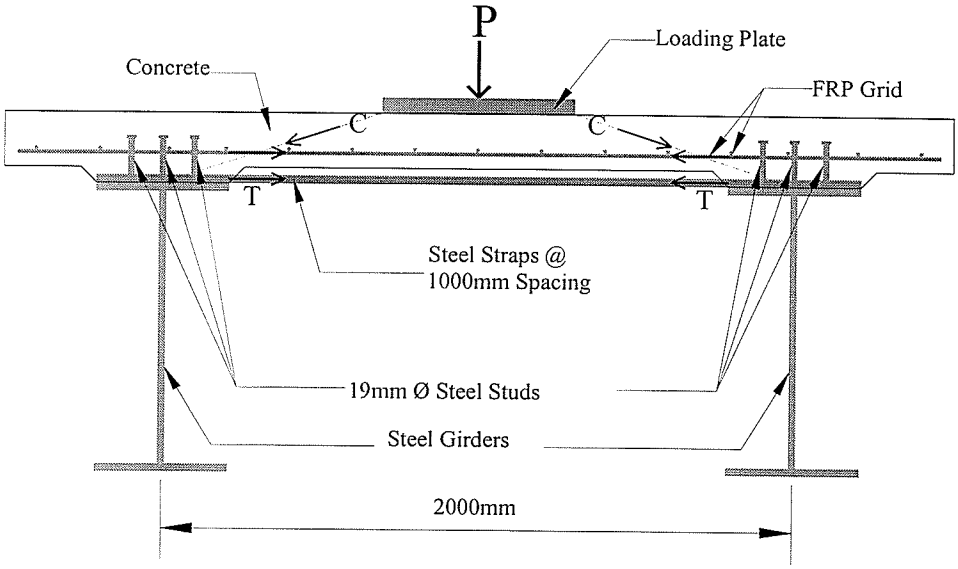

Fig. 1.2: Cross-section of 2nd generation of steel-free concrete bridge deck slab

1.3 Focus of the Study

The focus of this study was the performance of steel-free concrete deck slabs under cyclic loading. The phenomenon of fatigue resulting from cyclic loading in this study

refers to the growth of the crack width that leads to failure when the crack becomes large enough. In order to study the fatigue behaviour of steel-free concrete bridge deck slabs, an experimental investigation of the fatigue behaviour of a non-composite ArchPanel® was conducted first. Finally, a cast-in-situ full scale specimen steel-free concrete bridge deck slab was tested to investigate fatigue behaviour. Based on the results, P-N Curves (load versus number of cycle curve) were developed.

1.4 Research Objectives

The overall objectives of this research were to investigate the fatigue behaviour of steel-free concrete bridge deck slabs and to propose a theoretical model to estimate the fatigue strength of steel-free concrete bridge deck slabs. The specific objectives of this research are summarized as follows:

- Investigate the fatigue behaviour of steel-free concrete ArchPanel® and cast-in-situ bridge deck slabs under cyclic loading and develop P-N Curves;
- Investigate the load-deformation response, as well as cracking behaviour under cyclic load;
- Compare the fatigue performance of a deck slab reinforced with steel reinforcement, a CFRP crack control grid with steel straps and a GFRP crack control grid with steel straps; and
- Propose a theoretical model to estimate the fatigue strength of steel-free concrete bridge deck slabs.

Chapter 2

Background to Concrete Bridge Deck Slabs

2.1 History of Reinforced Concrete Bridge Deck Slabs

Since the 1920s, slab-on-girder bridges have been common in North America. Slab-on-girder bridges consist of a number of parallel longitudinal girders surfaced with a concrete deck slab. The girders are typically made from either steel or concrete and are supported at intermediate interior points and ends. The concrete deck slab transfers the vehicle loads to the longitudinal girders and ultimately to the supports. With this system, the deck slab can contribute significantly to the longitudinal flexural stiffness of the girders, provided that certain design considerations are utilized to ensure the concrete deck slab and girders act synergistically. This type of system is referred to as a composite slab-on-girder superstructure.

2.1.1 Flexural Design Method

Originally, concrete bridge deck slabs were designed using the flexural design method and assumptions of flexural bending and failure, as shown in Fig. 2.1. This design technique was mainly based on live load transverse moments, which were obtained from plate bending analysis. The flexural design method specified in American Association of State Highway and Transportation Officials (AASHTO, 1998) results in concrete deck slabs in which the steel reinforcement is between 3.2% and 4.0% of the volume of the

concrete. Reinforced concrete deck slabs designed according to the flexural design method specified in AASHTO (1998) have been used in Canada, as well as many other countries around the world.

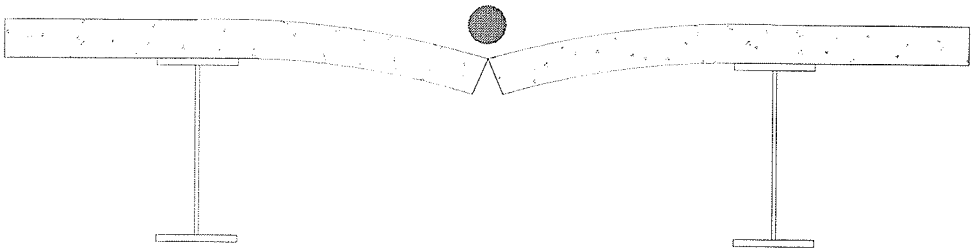

Fig. 2.1: Failure by bending

2.1.2 Development of Empirical Design Method

About thirty years ago, bridge engineers in Ontario observed that highway bridges designed by the flexural design method specified in AASHTO (1998) were performing well despite truck loads being almost twice the recommended weight. At that time, an extensive field and laboratory testing program was initiated by the Ministry of Transportation of Ontario (Dorton et al., 1977) and was undertaken mainly at Queen's University, Kingston, Ontario (Hewitt and Batchelor, 1975). At the onset of this research, deck slabs with the reinforcement specified by the flexure design method were tested and the failure mode was found to be quite different from that of flexure. This led to the realization that concrete deck slabs develop an internal arching action. As a result of this arching action, the concrete slabs fail in the punching shear mode, rather than the flexure mode, and at a much higher load than the analytically predicted failure loads of pure

flexural behaviour. A prototype test bridge was constructed in Ontario in 1975 to verify the research test results (Dorton et al., 1977). Variations in slab thickness and reinforcing ratios were incorporated into the slab of the bridge in order to study the influence of these variables on the deck behaviour while under concentrated test loads and in-service loading. From this structure, it was established that a total reinforcing ratio of 1.2% distributed orthotropically in two layers provided an acceptable safety margin for both the ultimate and serviceability conditions. In 1979, the Ontario Highway Bridge Design Code (OHBDC, 1979) was developed, which included design provisions for this empirical design method. Bakht and Markovic (1986) provided a state-of-the-art report on the research that led to this code development.

In 2000, the Canadian Highway Bridge Design Code (CHBDC, 2000) included a section on the empirical design method. According to this method, the deck slabs contain two layers, top and bottom each way, and a total steel reinforcement of about 1.2% of the volume of concrete and fail by punching shear, as shown in Fig. 2.2(a) and (b). This percentage is much less than that given by the flexural design method. Khanna et al. (2000) tested a model deck slab under static load and found that the failure was due to punching shear.

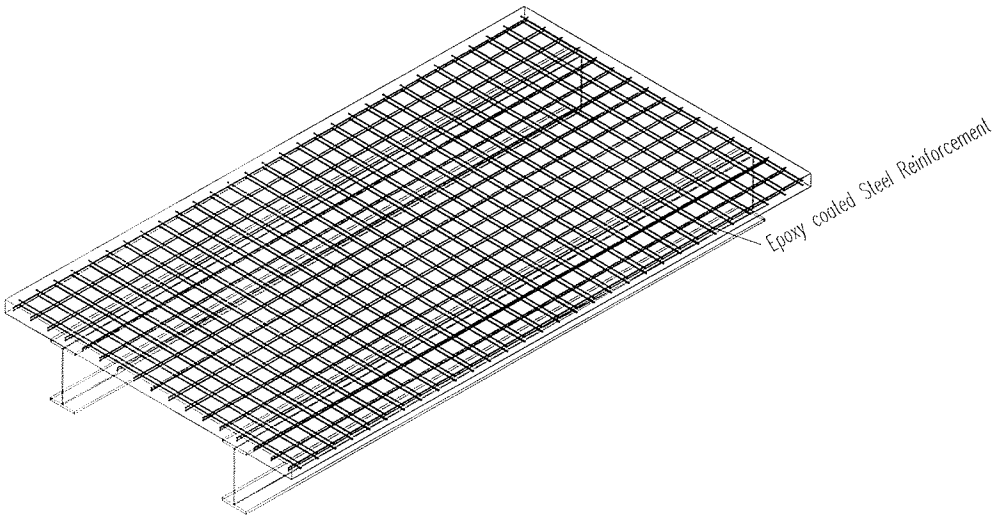

Fig. 2.2(a): Empirical design method

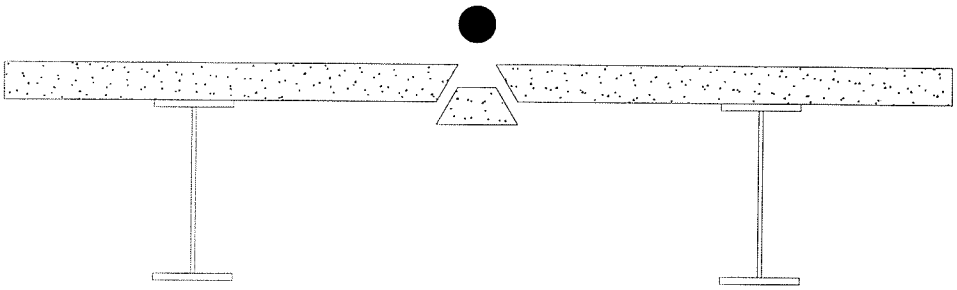

Fig. 2.2(b): Failure by punching shear

2.1.3 Development of Steel-Free Concrete Bridge Deck Slab

Mufti et al. (1991) proposed the concept of a steel-free concrete deck slab entirely free of any internal tensile reinforcement. The load carrying capacity of this deck slab depends on an internal arching system. The steel-free concrete deck slab on girder bridges are an extension of the empirically designed bridge decks outlined in the OHBDC (1983). The empirical method implicitly recognizes the presence of an arching system in the bridge

components. The failure loads due to punching are substantially higher than the theoretical flexural failure loads. This design method specifies a minimum reinforcement in two layers, with an orthogonal pattern of steel bars in each layer. According to the OHBDC (1983), this minimum reinforcement provides for shrinkage and thermal cracks in the concrete.

In 1988, researchers at the Dalhousie University (Technical University of Nova Scotia) began further investigations into the punching failure of concrete deck slabs. Mufti et al. (1993) demonstrated that the entire removal of all internal steel reinforcement from a concrete deck slab was possible. The key to the system was to provide sufficient transverse lateral restraint so that compressive membrane forces could be developed for the punching failure mechanism. This lateral restraint was provided by transverse steel straps external to the deck slab, which tied adjacent girders together, as shown in Fig. 2.3. This innovative deck slab was named the Steel-Free Concrete Deck Slab.

This concept led to the world's first steel-free concrete bridge deck over the Salmon River on the Trans-Canada Highway in Nova Scotia, as shown in Fig. 2.4 (a) and (b). This bridge was opened to traffic in December 1995 (Mufti et al., 1999), as shown in Fig. 2.5. Six months later, longitudinal cracks were observed on the soffit of the slab, roughly midway between the girders, as shown in Fig. 2.6.

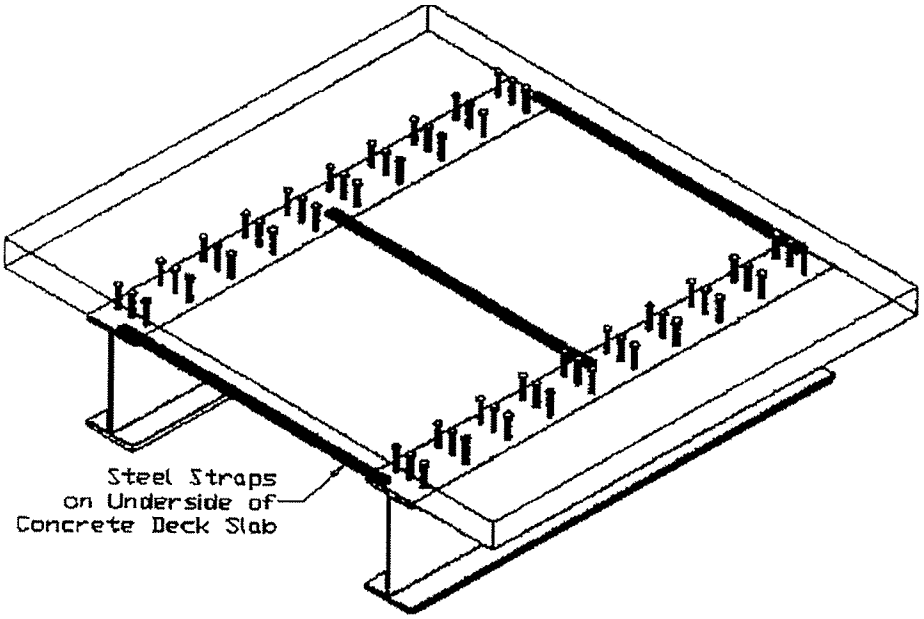

Fig. 2.3: Steel-free concrete deck slab

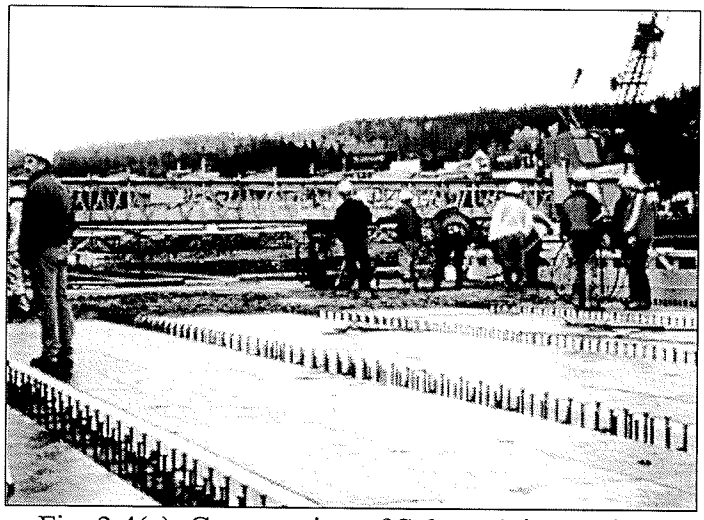

Fig. 2.4(a): Construction of Salmon River Bridge

Fig. 2.4(b): Bottom view of Salmon River Bridge

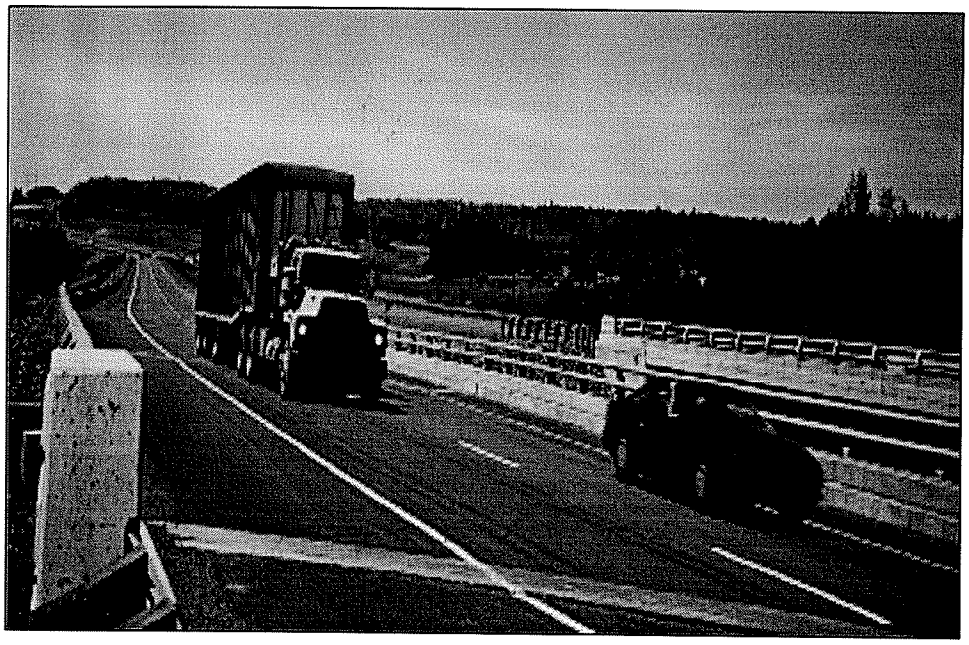

Fig. 2.5: Salmon River Bridge open for traffic

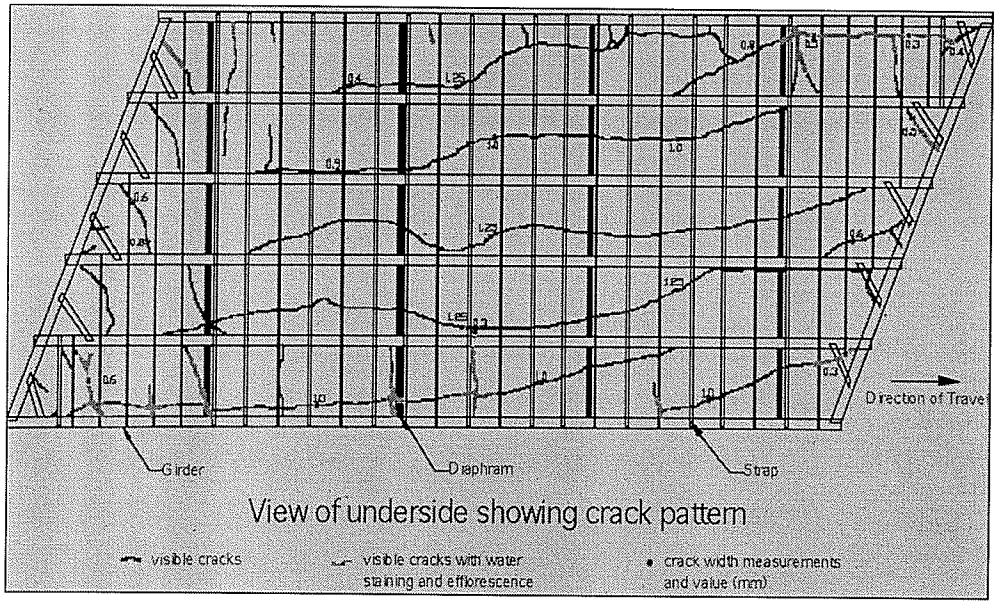

Fig. 2.6: Crack pattern underside of the Salmon River Bridge

Static tests on steel-free concrete bridge decks and ArchPanel® were conducted at Dalhousie University, Nova Scotia. Results showed that the static punching shear failure load of the steel-free concrete deck slabs was significantly higher than that of the design wheel loads, but the crack initiation and propagation did not extensively show. Although fatigue tests carried out in Canada, the U.S.A. and Japan provided excellent information on steel reinforced decks, more fatigue testing was required to understand how steel-free concrete decks would respond in fatigue behaviour.

Extensive Japanese testing of deck slabs under rolling wheels highlighted the importance of developing a base of dynamic test data. Fatigue tests conducted under the wheel running machine by Matsui et al. (2001) concluded that a steel-free deck slab exhibits significantly higher fatigue resistance than a conventional reinforced concrete (RC) slab of the same thickness. Perdikaris and Beim (1988) demonstrated that concrete deck slabs

reinforced with reduced amounts of steel have a higher fatigue resistance under moving loads than more heavily reinforced deck slabs. According to Perdikaris and Beim (1988), this is because fatigue cracks in concrete initiate from the steel bar. Therefore, using more steel promotes a greater increase in degradation of the concrete than would be experienced by using less steel. It is postulated that replacing the steel in concrete deck slabs with very small diameter FRPs will improve the fatigue resistance of the deck slab by eliminating degradation.

2.2 Field Application of Steel-Free Concrete Bridge Deck Slabs in Canada

The concept of a steel-free concrete deck slab has been applied to four highway bridges and one forestry bridge in Canada (Bakht and Mufti, 1998) as follows:

- Salmon River Bridge
- Chatham Bridge
- Crowchild Trail Bridge
- Waterloo Creek Bridge
- Lindquist Creek Forestry Bridge

2.2.1 Salmon River Bridge

The first field application of the steel-free concrete deck slab was cast in October 1995 across the Salmon River on the Trans Canada Highway in the province of Nova Scotia, Canada. The Salmon River Bridge has two simply supported spans, each 31.2 m long with a skew angle of 22°. One of the spans is comprised of a 225 mm thick concrete slab with steel reinforcement based on the empirical design method. The other span has a

200 mm thick concrete slab with no internal tensile reinforcement and is supported on steel girders at spacings of 2.7 m. The transverse confinement in the steel-free concrete deck slab was provided by means of 100 x 12 mm steel straps welded to the top flange of the girders at spacings of 1.2 m. The Salmon River Bridge was opened to traffic on December 5, 1995.

2.2.2 Chatham Bridge

The second application of the steel-free concrete deck slab was constructed on Kent County Road No. 10 Bridge in Chatham, Ontario, Canada. It is a replacement structure for a 4-span bridge that crosses Highway 401. The deteriorated deck slab of the bridge was replaced in the fall of 1996. The two inner 20 m spans of this structure consist of a conventionally reinforced deck slab while the 13 m end spans consist of the steel-free concrete deck system. The bridge has five girders spaced at 2.1 m. The deck slab has a 0.9 m wide cantilever overhang beyond each outer girder. The middle two spans have a 225 mm thick concrete deck slab with steel reinforcement and were designed according to the empirical design method. The two outer spans have a 175 mm thick steel-free concrete deck slab. The cantilever overhangs and the outer panels of this slab have a grid of CFRP placed near the top surface. This reinforcement is provided only for the negative moments, which are induced due to loads on the cantilever overhang. The transverse confinement of the steel-free concrete deck slab was provided by means of 20 x 50 mm galvanized steel straps welded to the top flanges of the girders at spacings of 1.0 m. The rehabilitated Chatham Bridge was opened to traffic on November 29, 1996.

2.2.3 Crowchild Trail Bridge

The Crowchild Trail Bridge in Calgary, Alberta, is the third application of the steel-free concrete bridge deck slab in Canada. The girders are spaced at 2.0 m with a 185 mm steel-free concrete deck slab. The five girders of the bridge are continuous over three spans of 30, 33 and 30 m. The longitudinal negative moment above the two intermediate supports has been overcome by longitudinal GFRP bars. The transverse confinement in the steel-free concrete deck slab was provided by means of 50 x 25 mm steel strap at spacings of 1.2 m. Partially studded steel straps were used instead of welding the strap to the top flange of the girders because of fatigue concerns. The Crowchild Trail Bridge was completed by the end of August 1997, one month ahead of schedule, and was opened to traffic in the fall of 1997.

2.2.4 Waterloo Creek Bridge

Waterloo Creek Bridge in British Columbia is the fourth Canadian application of the steel-free concrete bridge deck slab. This is an integral abutment bridge with pre-cast concrete girders having a single span of 25 m. The five concrete girders are spaced at 2.8 m with a 190 mm steel-free concrete deck slab. The transverse confinement in the steel-free concrete deck slab was provided by means of 50 x 25 mm studded steel straps with spacings of 1.25 m. The Waterloo Creek Bridge was opened to traffic early in 1998.

2.2.5 Lindquist Creek Bridge

The Lindquist Creek Bridge in British Columbia is the fifth application of the steel-free concrete bridge deck slab concept in Canada. Forestry bridges in Canada are usually

single-lane, single span structures with two steel girders and a deck of pre-cast reinforced concrete panels. The concept of arching in deck slabs has led to an alternative to the reinforced concrete pre-cast panels typically used for forestry bridges. The alternative is the steel-free concrete ArchPanel® with a thickness of 150 mm at the crown. The ArchPanel® girders are spaced at 3.5 m. The transverse confinement to the panels is provided by 25 x 50 mm studded steel straps at spacings of 1.0 m. By using the steel-free concrete ArchPanel®, the bridge can be opened to traffic within 24 hours after the erection of steel works. The Lindquist Creek Bridge was open to traffic on December 1997.

2.3 Dynamic Tests on Steel-Free Concrete Bridge Deck Slabs

In general, static tests of concrete bridge decks provide little understanding of fatigue resistance. The following section looks at various types of dynamic tests that can be done on concrete bridge deck slabs.

2.3.1 Single Moving Wheel

In a single moving wheel system, the moving wheel of a vehicle is represented by an actual moving single wheel, the weight and speed of which can be controlled. The test arrangement includes an anchoring frame, which guides the moving wheel along a linear path. The load level on the wheel is governed by means of a vertical actuator and the movement of the wheel is controlled by a separate system that uses a horizontal actuator with a relatively long stroke. The primary advantage of this type of test facility is that it replicates exactly the motion of actual wheel loads on the surface of the test specimen.

Limitations of this system include high cost, slow speed, and high noise level. Michael et al. (1994) reported that the single moving wheel assembly, powered by a hydraulic motor, moves back and forth at a maximum speed of about 61 cm/sec or 2.2 km/hr. The wheel speed in their study is much lower than the reasonable measured speed of truck wheels which is 88.5 km/hr. Thus the test results on fatigue response under a constant moving wheel load did not include any possible dynamic effects that would be present at normal traffic speeds.

2.3.2 Sequential Wheel Load

The shortcomings in the single moving wheel system led to the development of the sequential wheel load system. In this system, the action of moving wheels is simulated by means of a number of load pads at fixed locations. The magnitude of a load acting on these pads is sequentially affected in such a way that the load is passed on from one pad to the next according to a pre-determined pattern. This passing of the load from one pad to another is done in such a way that during one cycle of loading the same total of loads is maintained on the test specimen. The sequential wheel load technique was introduced by Selvadurai and Bakht (1995), and demonstrated sequential a loading system simulating a vehicle speed of 40 km/hr. With this system, it is possible to simulate two million passes of a wheel in only two weeks, while the single wheel system will require about 40 weeks for a similar test. The limitation of this system is that only the maximum load of 98 kN (10 tonne) could be applied. With this small magnitude of load, the fatigue behaviour of bridge decks cannot be determined with clear cut conclusions. This system was used to study the steel-free concrete bridge deck model prior to the construction of

Salmon River Bridge deck. Therefore, full depth cracks that appeared were not seen in the laboratory tests conducted by Selvadurai and Bakht (1995).

2.3.3 Single Pulsating Wheel Load

When using a single pulsating wheel load, the load is applied through a hydraulic actuator reacting against a steel loading frame, which is attached to the structural floor of the laboratory. The load patch simulates the dual tire footprint of a heavy highway vehicle. This method of fatigue testing is simple and inexpensive. This system is capable of applying higher wheel loads, so that the test can be completed in a specified time frame. This has the drawback of not simulating moving loads. However, it does simulate pulsating loads.

2.4 Wheel Load Data

During its lifetime, a bridge deck slab is subjected to several hundred millions passes of the wheel loads of trucks. The range of wheel loads varies from the lightest to the heaviest. The numbers of passes of lighter wheels are very large in number, whereas the heavier wheel passes are fewer. By contrast, the laboratory investigation of the fatigue resistance of a deck slab is usually conducted under a test load of constant magnitude. The time available for such investigations is necessarily much smaller than the lifetime of a bridge. Consequently, the test loads are kept large so that the number of passes required to fail the slab in fatigue are manageably small. To the author's knowledge, no method is currently available to correlate actual wheel loads with fatigue test loads. The design

codes (e.g., AASHTO (1998) and CHBDC (2000)) are also not explicit with respect to the design of fatigue loads on deck slabs.

Commentary Clause C3.6.1.4.2 of the AASHTO Specifications (1998) notes that the Average Daily Traffic (ADT) in a lane is physically limited to 20,000 vehicles and the maximum fraction of trucks in traffic is 0.20. Thus the maximum number of trucks per day in one direction (*ADTT*) is 4,000. When two lanes are available to trucks, the number of trucks per day in a single lane averaged over the design life ($ADTT_{SL}$) is found by multiplying *ADTT* by 0.85, giving $ADTT_{SL}$ = 3,400. It is assumed that the average number of axles per truck is four (a conservative assumption) and that the life of a bridge is 75 years. The maximum number of axles that a bridge deck would experience in one lane during its lifetime is: 3400×4×365×75 = 372 million.

The Calibration Report in the Commentary of the Canadian Highway Bridge Design Code (CHBDC, 2000) is based on vehicle weight surveys in four Canadian provinces. From this Calibration report, it can be calculated that the expected annual maximum axle loads in the Canadian provinces of Ontario, Alberta, Saskatchewan and Quebec are 314, 150, 134 and 159 kN respectively. As described by Matsui and Tei (2001), the maximum wheel load observed in Japan is 313 kN (32 tonne). The close correspondence between the expected annual maximum axle weight in Canada and the maximum observed axle load in Japan indicates similarity between the axle loads in the two countries. Matsui and Tei (2001) have also provided a histogram of axle weights observed on 12 bridges in Japan. In the absence of data on Canadian trucks, the histogram developed by Matsui and

Tei (2001) was used to construct the wheel load statistics shown in Fig. 2.7. From Fig. 2.7 it can be seen that the number of wheels of various magnitudes corresponds to a total of 372 million wheel passes.

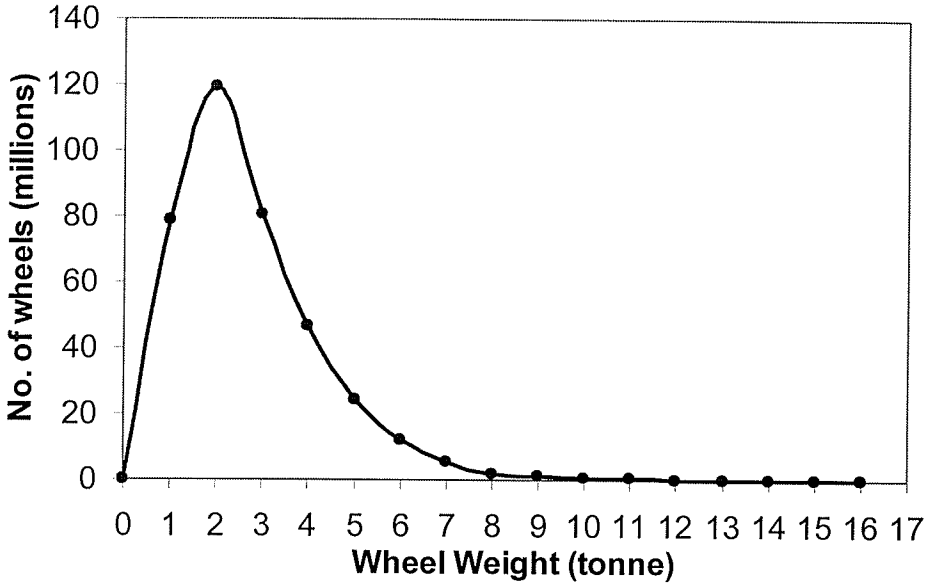

Fig. 2.7: Wheel load statistics

2.5 Theoretical Approach for Punching Shear (PUNCH Program)

Many theoretical approaches (Kinnunen and Nylander (1960), Hewitt and Batchelor (1975), Marzouk and Hussein (1991), and Mufti and Newhook (1998)) have been developed for predicting the punching strength in reinforced concrete deck slabs. The models generally rely on stresses developed in the steel reinforcement as a key parameter. Therefore, it became necessary to develop a model that could predict the behaviour of laterally restrained deck slabs that contained no internal reinforcement. A finite element model study done by Wegner and Mufti (1994) was very successful in providing

guidance for further experimental work; however, the model was found to be very complex and sensitive to modelling parameters. The model developed by Kinnunen and Nylander (1960) and enhanced by Hewitt and Batchelor (1975) to include lateral restraint conditions was adapted for steel-free concrete deck slab conditions. The full mathematical formulation of this model can be found elsewhere, Newhook et al. (1995); only the basic elements of the model are reviewed here.

The important components of the system geometry are the depth of the concrete deck slab, the spacing of the support girders, the spacing and cross-sectional area of the transverse straps, and the dimensions of the loaded area. The essential parameters are the modulus of the transverse strap, area of strap, the yield strain of the straps, the compressive strength of the concrete, and the influence of three dimensional stresses on the compressive strength of concrete, girder spacing and thickness of the deck slab.

The following assumptions were also used by Kinnunen and Nylander (1960) to describe the deck behaviour under idealized conditions. Under low loading, a concrete slab subjected to a concentrated load will form longitudinal cracks on the bottom surface of the slab, originating below the load point. As the load increases, the cracks will also form radially and gradually migrate to the top surface of the slab to become full depth cracks. On the top surface of the slab, circular cracks with a diameter proportional to the lateral stiffness will be formed.

At a load value somewhat less than the failure load, an inclined shear crack will develop, originating on the bottom of the slab at some distance away from the load point, and propagating toward the load point. At punching failure, this inclined crack forms the upper surface of the punch cone. The sections of concrete outside the shear crack can be divided into wedges bound by the shear crack, the radial cracks, and the outside edge of the slab or the outer circular cracks, shown in Fig. 2.8(a). Under further loading, these wedges act as rigid bodies in the radial direction and rotate about a center of rotation, as shown in Fig. 2.8(b). At the intersection of the wedges and the load patch is a state of three-dimensional compressive stress. It is the stresses in this region that will govern the eventual failure of the deck Kinnunen and Nylander (1960).

As a wedge, shown in Fig. 2.8(b), rotates through an angle ψ, it has an associated lateral displacement Δ_L which is restrained by the stiffness of the straps. If we designate $\boldsymbol{K}$ as the stiffness of the strap, in units of force/displacement per unit length of circumference, then the restraining force is calculated as $\boldsymbol{K}\Delta_L$. The magnitude of this restraining stiffness is a key parameter in establishing the level of arching action and hence the ultimate capacity. The value of lateral restraint stiffness, $\boldsymbol{K}$, is determined from the geometry of the straps and the spacing of the girders. For design purposes it is conservative to use Eq. 2.1.

$$K = \frac{EA_s}{\frac{S_l}{2} S_S} \tag{2.1}$$

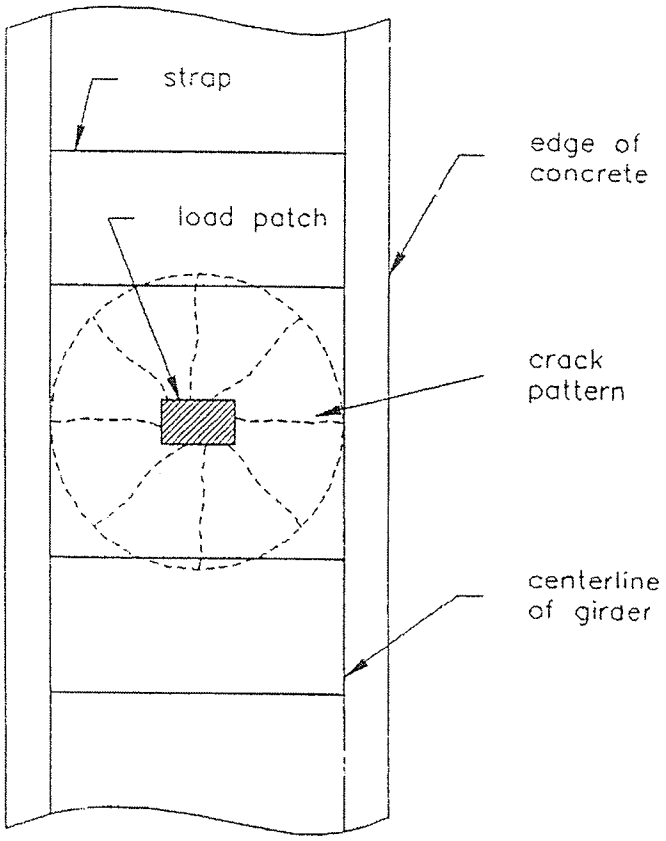

Fig. 2.8(a): Plan view of slab with crack pattern

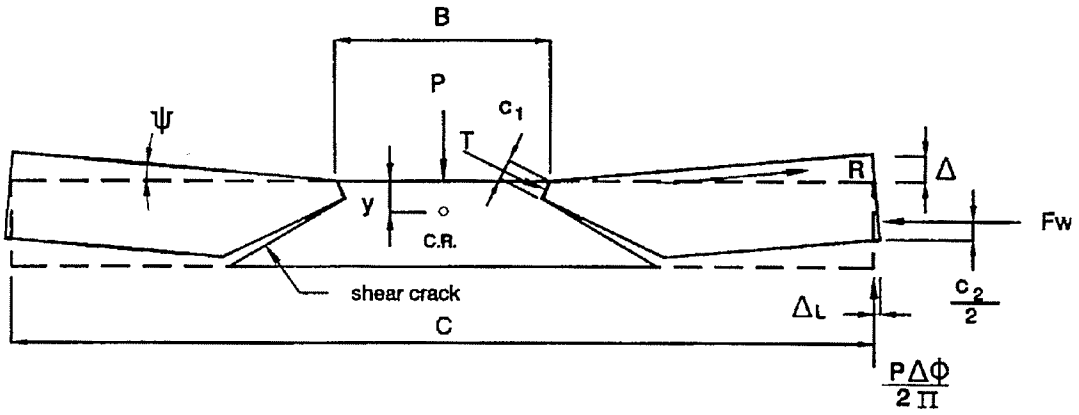

Fig. 2.8(b): Rigid body rotation of wedges

The parameters E, A_s, S_l and $\boldsymbol{S}_S$ represent the modulus of elasticity of the strap, the area of the strap, the length of the strap and the longitudinal spacing of the strap, respectively. For comparison with experimental work; it is necessary to calculate $\boldsymbol{K}$ in a more rigorous manner. This includes consideration of the lateral stiffness of girders. Newhook (1997) and Newhook and Mufti (1998), developed a computer program called the PUNCH Program to predict the ultimate capacity of restrained deck slabs under concentrated loads. A comparison of the theoretical and experimental work is presented in Table 2.1 (Mufti and Newhook, 1998) and has been updated in the work of other authors. The comparison reveals that the PUNCH Program can predict, within reasonable accuracy, the punching failure load of a restrained, fibre-reinforced concrete slab-on-girder bridge deck. For purposes of this research, the PUNCH Program was used to predict the punching failure load of the full scale model of a concrete bridge deck slab.

Table 2.1: Comparison of theoretical and experimental results (Mufti & Newhook, 1998)

Test	f_c' N/mm^2	Girder Spacing mm	Straps mm^2 @ mm c/c	Deck depth mm	K N/mm^2	P Theor kN	P Exp kN	P theor / P exp
Half-Scale (Mufti et al. 1993; Newhook et al. 1995)								
1	45.0	1067	640 @ 457	100	630	415	418	0.99
2	46.1	1067	640 @ 547	100	630	409	418	0.98
3	41.8	1067	640 @ 547	95	630	362	370	0.98
4	41.8	1067	640 @ 547	95	630	362	388	0.93
5	43.0	1067	640 @ 610	95	472	315	313	1.01
Skewed (Bakht and Agarwal 1995)								
6	55.0	800	608 @ 400	80	921	388	323	1.20
7	55.0	800	608 @ 400	80	921	388	352	1.10
Full Scale (Thorburn and Mufti 1995; Newhook and Mufti 1996; Mufti et al. 1999)								
8	27.0	2000	2500 @ 1000	175	705	1147	1127	1.02
9	27.0	2000	1250 @ 1000	175	460	930	923	1.01
10	27.0	2000	950 @ 1000	175	370	830	911	0.91
11	27.0	2000	650 @ 1000	175	300	730	844	0.86
12	27.0	2000	650 @ 1000	175	300	730	576	1.27
13	27.0	2000	650 @ 1000	175	300	730	715	1.03
14	39.0	2700	1250 @ 1200	300	297	1269	1275	1.00
15	39.0	2700	650 @ 1000	300	86	937	951	0.99
Repaired (Thorburn and Mufti 2001)								
16	27.0	2000	2500 @ 1000	175	700	1143	785	1.46
17	27.0	2000	650 @ 1000	175	300	730	687	1.06
Reinforced Concrete (Mufti et al. 1999; Bakht and Lam 2000)								
18	30.0	2000	Steel Rebar	175	211	819	808	1.01
19	30.0	2000	Steel Rebar	175	218	834	793	1.05
20	35.0	2000	Steel Rebar	175	218	888	888	1.0
21	35.0	2000	GFRP Rebar	175	211	873	756	1.15
22	-	2133	Steel Rebar	190	200	627	631	0.99
23	-	2000	Steel Rebar	150	428	629	622	1.01

Chapter 3

Design of Steel-Free Concrete Bridge Deck Slabs

3.1 General

The full-scale specimen of a concrete bridge deck slab with dimensions of 9000 mm x 3000 mm was constructed compositely on two steel girders spaced at 2000 mm, through the use of shear connectors. In composite construction, longitudinally, the slab and the steel girders are assumed to act compositely; that is, it is assumed that no slippage occurs at the concrete slab/ steel girder interface. The slab is assumed to act simply as a cover plate attached to the compression flange of the girder. In other words, a portion of the slab functions much like a steel cover plate over the compression flange of the steel beam, adding significantly to the compression flange's strength and stiffness. Thus a composite girder section comprises a concrete slab at the top and steel I-girder at the bottom. The concrete deck slab acting as the top flange of the composite section is always in longitudinal compression, no tensile reinforcement is required in the slab in the longitudinal direction. The composite construction of the bridge deck slab requires the proper design of the concrete deck slab, the longitudinal steel girders supporting the deck and the shear connectors to resist the horizontal shear.

3.2 Design of Concrete Deck Slabs

The full-scale specimen of a concrete bridge deck slab with dimensions 9000 mm x 3000 mm was conceptually divided into three segments A, B and C as shown in Fig. 3.1. All three segments were designed according to CHBDC (2000) and are explained in the following sections. All three segments were tested under cyclic loading to investigate fatigue behaviour. The three segments A, B and C were designed to have almost equal ultimate capacities, so that a direct comparison between the segments under fatigue could be made. The static capacity of all three segments was computed according to Program PUNCH (Newhook and Mufti 1998). This program was developed to evaluate the behaviour of laterally restrained concrete slab-on-girder bridge decks under the wheel loads of heavy trucks. The program requires the input of specific geometric and material properties and will provide a value for the ultimate failure capacity of a specimen deck slab. The complete description of the PUNCH Program based on the rational model can be found in Newhook et al. (1995). The user manual of the PUNCH Program is described in Newhook and Mufti (1998).

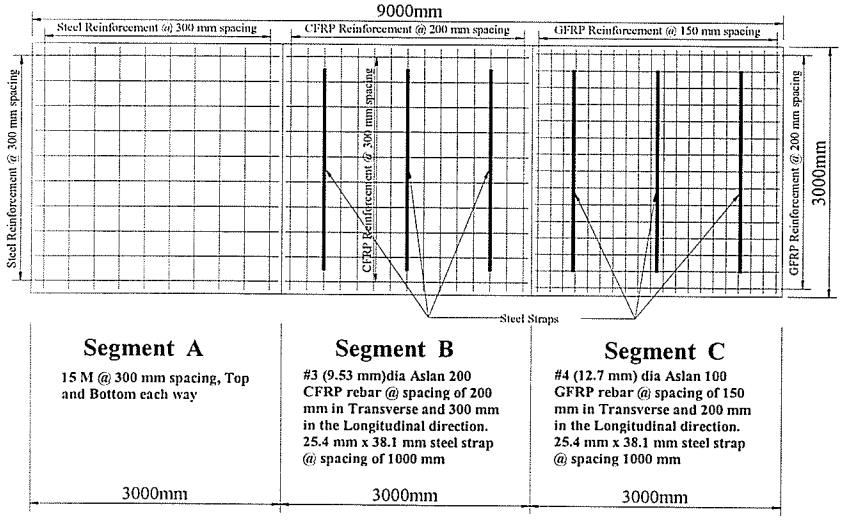

Fig. 3.1: Reinforcement details of segments A, B, and C

3.2.1 Design of Segment A (Steel Reinforcement)

Segment A is designed according to CHBDC (2000), Section 8.18. The provisions of this Clause apply to deck slabs supported on steel girders. When proportioned in accordance with the empirical design method of Clause 8.18.4, these deck slabs do not need be analyzed. This method is applicable to that portion of the deck slab which is of, nearly, uniform thickness and bounded by exterior supporting beams satisfying the following conditions:

(a) The deck slab is composite with the supporting beams, which are parallel to each other, and the lines of supports for the beams are also parallel to each other;

(b) The ratio of the spacing of the supporting beams to the thickness of the slab is $\leq$ 18.0;

(c) The spacing of the supporting beams does not exceed 4.0 m; and

(d) The minimum slab thickness shall not be less than 175 mm.

The empirical design method according to the CHBDC (2000) is applicable, when the full-depth cast-in-situ deck slab contains two orthogonal assemblies of reinforcement near the top and bottom of the slab, respectively, with reinforcement ratio (ρ) in each direction in each assembly being at least 0.3% of the volume of the concrete. The spacing of reinforcement in each direction and in each assembly does not exceed 300 mm. Segment A satisfies the above conditions more specifically;

Thickness of slab = 175 mm (minimum thickness)		O.K.
Spacing of the supporting beams = 2.0 m	(<4.0)	O.K
The ratio of the spacing of the supporting beams to the thickness of the slab =11.43	(<18.0)	O.K

The minimum Area of steel in each assembly (A_s) = $\rho.b.d$ (3.1)

Where,

$\rho = 0.003$

$b = 3000mm$

$d = (175 - 40 - 8) = 127mm$ (Thickness of slab –Clear cover-Dia of bar/2)

According to Eq. 3.1, the minimum Area of Steel becomes:

$A_s = 1143mm^2$ (In each direction and in each assembly)

As mentioned in Chapter 1, the focus of this research is to conduct fatigue behaviour on a full-scale specimen of a bridge deck slab. In this research program, three segments A, B and C were constructed. In practice, deck slabs designed by conventional design methods use the equivalent area of steel ($A_s = 667mm^2/m$). For this research program, Segment A of the deck slab, contained an area of steel (in transverse direction) of about 2000 mm^2 in each layer, which gives the reinforcement ratio of 0.53%. In the construction of slab-on-girder bridges, the typical size of reinforcing steel bar used is 15M. Therefore, the top and bottom layers of isotropic reinforcement each consist of 15M bars at a spacing of 300 mm in each of the longitudinal and transverse directions. The detail of the reinforcement in the deck slab for Segment A is shown in Fig. 3.2. The ultimate capacity of Segment A was computed to be approximately 1144 kN (116.6 tonne) by the PUNCH Program (Table 3.1).

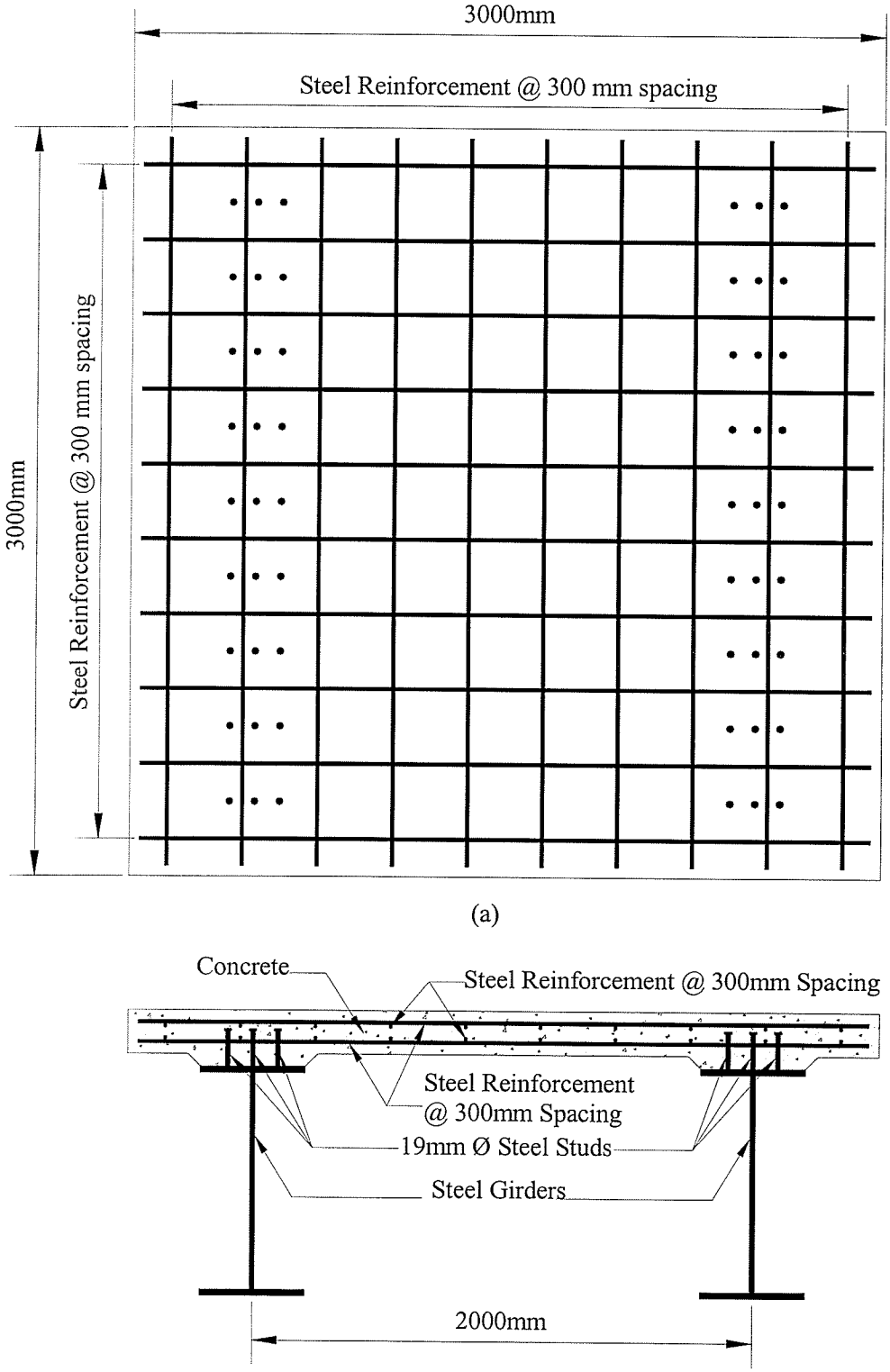

Fig. 3.2: (a) Top-view of Segment A, (b) Cross-section of Segment A

Table 3.1: Load Deflection from PUNCH Program (Design for Segment A)

Load (kN)	Deflection (mm)
0	0.00
60	0.64
118	1.29
175	1.93
230	2.57
284	3.21
337	3.86
389	4.50
439	5.14
489	5.79
538	6.43
586	7.07
633	7.71
679	8.36
724	9.00
769	9.64
813	10.29
856	10.93
898	11.57
940	12.21
981	12.86
1022	13.50
1062	14.14
1101	14.79
1144	15.43

3.2.2 Design of Segments B and C (Steel-Free Concrete Deck Slabs)

Segments B and C are designed according to CHBDC (2000), Section 16.7. The provisions of this clause apply to FRC deck slabs supported by steel girders and satisfying the following conditions:

(a) The deck slab is composite with the parallel supporting beams;

(b) The spacing of the supporting beams, S, does not exceed 3.0 m;

(c) The deck slab thickness, t, is at least 175 mm, and not less than S/15;

(d) The supporting beams are connected with transverse diaphragms;

(e) The height of the haunch between the deck slab and the top of a supporting beam is between 25 and 125 mm, and the projection of the shear connecting devices in the deck slab, t_s, is a minimum of 75 mm;

(f) The top flanges of all adjacent supporting beams are connected by an external transverse confining system, comprised of straps that are connected perpendicular to the supporting beams, as in partially studded straps;

(g) The spacing of the straps, S_l , is not more than 1.25 m;

(h) Each strap has a minimum cross-sectional area, A, in mm^2, given by

$$A = \frac{F_s . S^2 . S_l}{E.t} 10^9 \qquad (3.2)$$

This Eq. 3.2 is similar to the Eq. 2.1, since the CHBDC (2000) make it simple, so that explicitly calculate the minimum cross –sectional area of the steel strap.

Where,

$F_s = 6.0$ for outer panels,

$F_s = 5.0$ for inner panels,

E is the modulus of Elasticity of the strap material (MPa),

S is the spacing of the supporting beams (m),

S_l is the spacing of the straps (m),

t is the thickness of the slab (mm); and

(i) The connection of the strap to the supporting beams is designed to have a shear strength of at least $200\,A$ (N).

Based on the conditions in Section 16.7 of the CHBDC (2000), as outlined above, the following parameters were considered:

S (spacing of supporting steel beams) = 2.0 m (<3.0 m) O.K

t (thickness of slab) = 175 mm (>S/15) O.K

S_l (spacing between straps) =1.0 m (<1.25 m) O.K

According to Eq. 3.2, the minimum area of steel strap becomes:

$A_{s(\min)} = 686 \text{ mm}^2$

According to Eq. 3.1, this $A_{s(\min)}$ gives the reinforcement ratio 0.4%, which is less than the reinforcement ratio of 0.53% (Segment A). According to PUNCH Program, the area of steel strap was selected for segments B and C, 967 mm^2, which gives the reinforcement ratio of 0.55%. The ultimate capacity of segment B and C was computed approximately 1145 kN (116.7 tonne) by the PUNCH Program (Table 3.2), which is closer to that of Segment A.

Table 3.2: Load Deflection from PUNCH Program (Design for Segments B and C)

Load (kN)	Deflection (mm)
0	0
87	0.64
170	1.29
251	1.93
330	2.57
406	3.21
480	3.86
553	4.5
623	5.14
692	5.79
760	6.43
826	7.07
891	7.71
955	8.36
1018	9
1079	9.64
1145	10.29

Summary of Design of Segment B (with CFRP crack control grid) :

Size of Steel Strap:	25.4 mm x 38.1 mm
Spacing between straps:	1000 mm
Transverse reinforcement:	#3 Aslan 200 (CFRP) at spacing of 200 mm
Longitudinal reinforcement:	#3 Aslan 200 (CFRP) at spacing of 300 mm
Modulus of elasticity :	#3 Aslan 200 (CFRP) is 121 GPa
Ultimate tensile strength:	#3 Aslan 200 (CFRP) is 1310 MPa

Summary of Design of Segment C (with GFRP crack control grid):

Size of Steel Strap:	25.4 mm x 38.1 mm
Spacing between straps:	1000 mm
Transverse reinforcement:	#4 Aslan 100 (GFRP) at spacing of 150 mm
Longitudinal reinforcement:	#4 Aslan 100 (GFRP) at spacing of 200 mm
Modulus of elasticity :	#3 Aslan 100 (GFRP) is 40.8 GPa
Ultimate tensile strength:	#3 Aslan 100 (GFRP) is 690 MPa

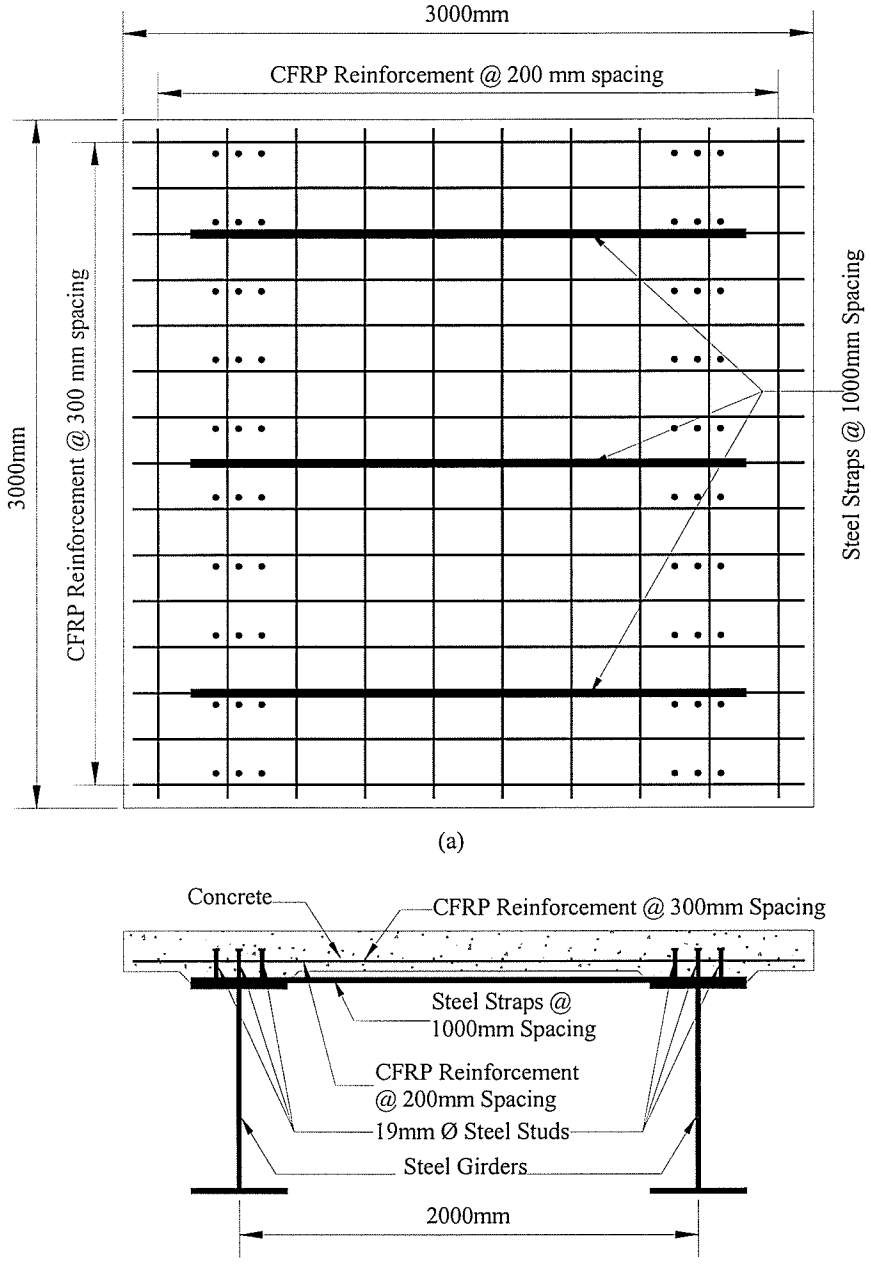

Fig. 3.3: (a) Top-view of Segment B, (b) Cross-section of Segment B

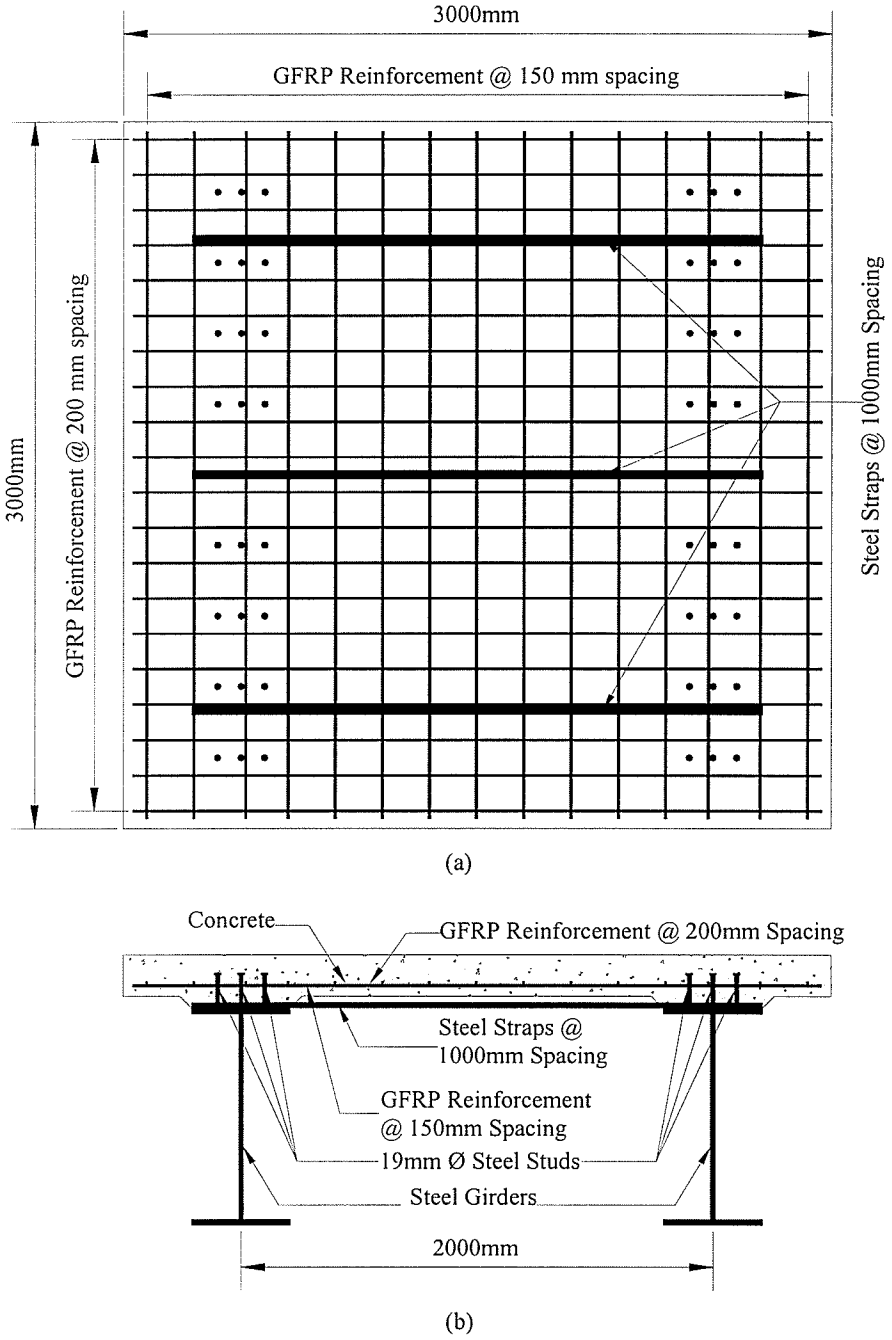

Fig. 3.4 (a) Top-view of Segment C (b) Cross-section of Segment C

3.3 Design of Steel Girder

The steel girders supporting the deck slab transferred the applied loads to the structural floor through concrete blocks spaced at 9000 mm. Cyclic loads were applied at various stages varying from 196 kN (20 tonne) and 588 kN (60 tonne). The steel girders used in this program were W920 x 387 and W760 x 196. The ArchPanel® was supported on two W760 x 196 steel girders while the deck slab was supported on two W920 x 387 steel girders. The sectional properties of these girders along with shear and moment resistance, computed according to CAN/CSA-S16.1-94 (CISC, 2000) are shown in Table 3.3.

Table 3.3: Sectional properties of W920 x 387 and W760 x 196

Steel Girder	**Units**	**W920 x 387**	**W760 x 196**
Dead Load	kN/m	3.8	1.93
Total Area	mm^2	49,300	25,100
Depth	mm	921	770
Width of Flange	mm	420	268
Thickness of Flange	mm	36.6	25.4
Thickness of Web	mm	21.3	15.6
Shear Resistance (Vr)	kN	4,020	2,460
Moment Resistance (Mr)	kN-m	4,560	973

The shear and moment resistance values shown in Table 3.3, are good for monotonic load conditions and satisfy the ultimate limit state. The calculations shown in Table 3.3 are based on an assumed steel grade 350W with F_y of 350 MPa. The steel girders in this experimental program undergo cyclic loading. The maximum cyclic load was

applied to steel girders W760 x 196 from zero to 490 kN (50 tonne) and to steel girders W920 x 387 from zero to 588 kN (60 tonne). Therefore, to design the girders for fatigue, Clause 14 of the CAN/CSA-S16.1-94 was used. According to this Clause 14, the steel girders W920 x 387 and W760 x 196 were able to handle approximately 15,768,000 and 1,752,000 cycles respectively. According to CAN/CSA-S16.1 (CISC, 2000), the serviceability criterion for deflection is considered to be 1/360 deflection to span ratio. The maximum deflection for total load at the center of the steel girder and permissible deflection of the sections are shown in Table 3.4.

Table 3.4: Permissible and maximum deflection of W920 x 387 and W760 x 196

Steel Girder	Units	W920 x 387	W760 x 196
Maximum deflection	mm	5.53	13.8
Permissible deflection	mm	25	25

3.4 Design of Shear Connectors

In composite structures consisting of a steel beam and a concrete deck slab, the resistance to shear at the interface between the slab and the beam is provided by mechanical shear connectors. The number of shear connectors is calculated as follows:

According to CHBDC, the factored compressive resistance of the slab used in computing the factored resistance of the section shall be the smaller of C_1 and C_2, computed from the following Equations:

$$C_1 = C_c + C_r \qquad (3.3)$$

$$C_2 = \phi_s A_s F_y \tag{3.4}$$

Where,

$$C_c = 0.85\phi_c b_e t_c f_c' \tag{3.5}$$

$$C_r = \phi_r A_r f_y \tag{3.6}$$

Since,

$A_s = 49{,}300$ mm^2 (Area of the steel girder W920 x 387)

$F_y = 350$ MPa

$\phi_s = 0.95$

$\phi_c = 0.75$

$f_c' = 35$ MPa

$b_e = 1000$ mm

$t_c = 175$ mm

$\phi_r = 0.85$

$A_r = 1200$ mm^2

$f_y = 300$ MPa

According to Equations (3.5) and (3.6), C_c and C_r becomes:

$C_c = 3{,}905$ kN

$C_r = 306$ kN

According to Equation (3.3), C_1 becomes:

$C_1 = 4{,}211$ kN

According to Equation (3.4), C_2 becomes:

$C_2 = 16{,}392$ kN

Since,

$C_1 < C_2$

Therefore, the plastic neutral axis in steel and the factored force (P) to be transferred by shear connectors will be,

$P = C_1 = 4{,}211$ kN

The number of shear connectors between points of maximum and zero moment can be computed by the following Equation:

$$N = \frac{P}{q_r} \tag{3.7}$$

The factored shear resistance q_r of an end welded stud shear connector shall be computed by the following relationship:

$$q_r = 0.5\phi_{sc} A_{sc} \sqrt{f_c' E_c} \leq \phi_{sc} F_u A_{sc} \tag{3.8}$$

Where,

$\phi_{sc} = 0.85$

$A_{sc} = 283.5mm^2$ (Cross-sectional area of shear stud)

$f_c' = 35MPa$

$F_u = 410MPa$ (Minimum tensile strength for commonly available steel studs)

$W_c = 2300kg/m^3$

$$E_c = W_c^{1.5} 0.043\sqrt{f_c'} \tag{3.9}$$

According to Equation (3.9), the modulus of concrete becomes,

$E_c = 28{,}060MPa$

According to Equation (3.8), the shear resistance becomes,

$q_r = 119.4 \leq 98.8$

Therefore consider the smaller value as a factored shear resistance

$q_r = 98.8kN$

Substitute the values of P and q_r in Equation (3.7), the number of studs become,

$N = 43$

If considering three (3) studs in one row, the spacing becomes,

$Spacing = 317mm$

Therefore, $3\ \#\ \frac{3}{4}$ ***in Diameter of Shear Stud at a Spacing of 300 mm are used.***

The top view of the steel girder with shear studs is shown in Fig. 3.5

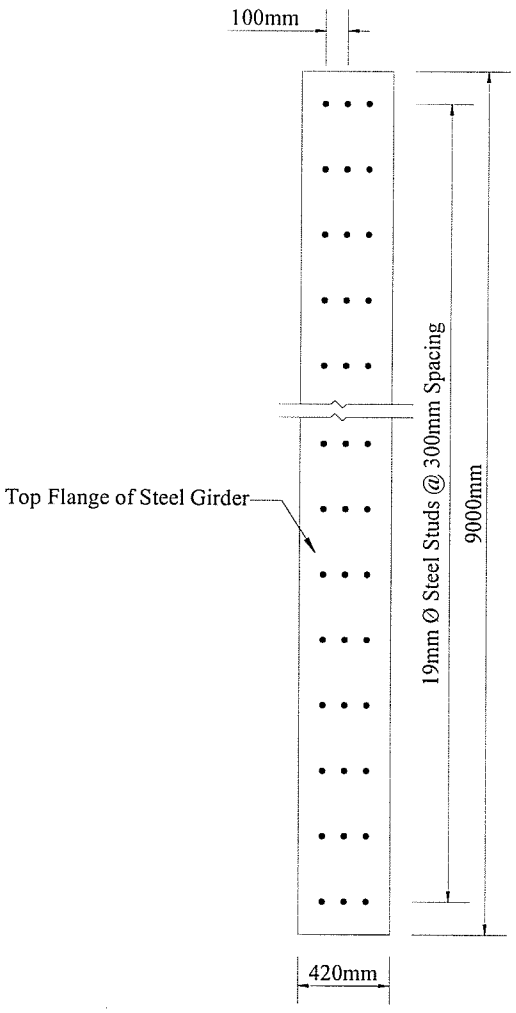

Fig. 3.5: Shear studs on top flange of steel girder

3.5 Design of Edge Beams and Diaphragms

The transverse edge beams were designed according to CHBDC (2000), Section 16.7(k). Furthermore, as required by CHBDC (2000), 2 – 22 mm diameter studs were provided at a spacing of 300 mm to help edge beams resist the shear force. Details of the edge beam with shear studs are shown in Fig. 3.6. As required by CHBDC, Clause 16.7(d), the supporting beams were connected with transverse diaphragms or cross frames at the ends, as shown in Fig. 3.6. These diaphragms are designed to provide stability to the steel girder system due to lateral loads.

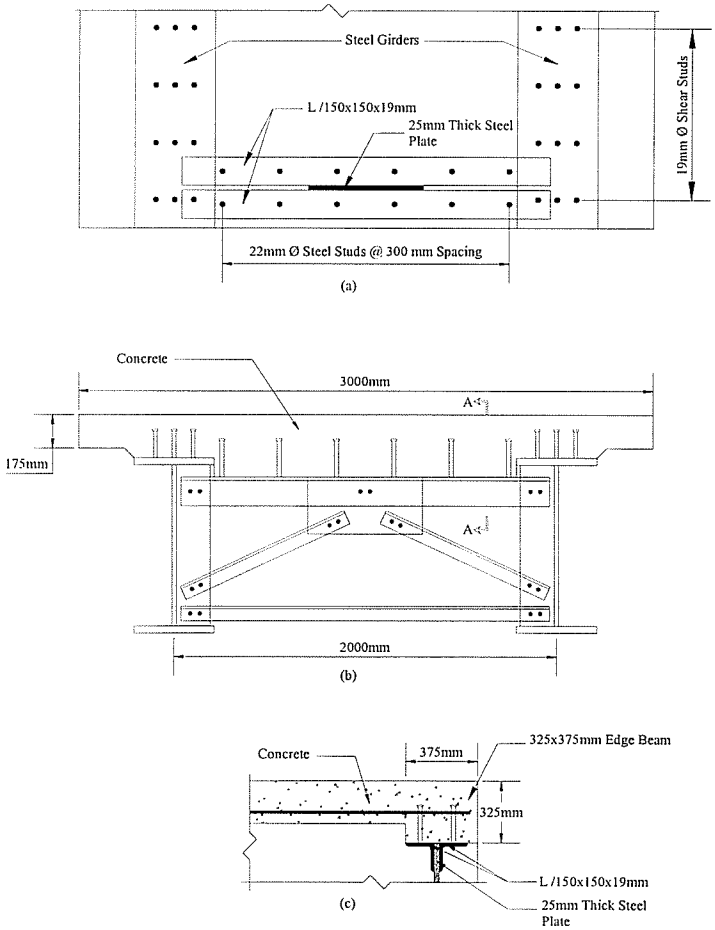

Fig. 3.6: Detail of edge beam and diaphragm

Chapter 4

Test Program for Fatigue Behaviour of Steel-Free Concrete ArchPanel® and Bridge Deck Slabs

4.1 General

As mentioned in Chapter 3, the full-scale specimen of a concrete bridge deck slab was conceptually divided into three segments A, B and C, as shown in Fig. 3.1. All three segments were designed according to CHBDC (2000) and are explained in Chapter 3. To understand the fatigue behaviour, first the ArchPanel® was tested and then the full-scale specimen bridge deck slab. The purpose of this component of the research program was to investigate the fatigue behaviour of segments A, B and C. The experimental program was divided into two parts:

(a) Testing of non-composite pre-cast steel-free ArchPanel®; and

(b) Construction and testing of a cast-in-situ full-scale specimen of a concrete bridge deck slab.

4.2 Pre-Cast Steel-Free ArchPanel®

A non-composite pre-cast steel-free ArchPanel® was tested under cyclic loading to investigate fatigue behaviour. Typical cross-sections are shown in Fig. 4.1. A 175 mm thick concrete slab was supported by two steel girders spaced at 3500 mm centre-to-

centre and had a longitudinal span of 3000 mm, as shown in Fig. 4.2. The girders were simply supported and the deck slab projected 400 mm beyond the centerline of each girder. The ArchPanel® was entirely free of any internal tensile reinforcement. It was designed by making use of the principle of steel-free deck slabs that are confined transversely by steel straps. The dimensions of the steel strap were 25 x 50 mm. Since this ArchPanel® is non-composite, two longitudinal steel straps were used to provide longitudinal confinement. The ArchPanel® was constructed with edge-stiffening beams at both transverse edges. The concrete was ordered 35 MPa, but when tested the compressive strength of concrete was found 51.3 MPa. The concrete contained 2 kg/m^3 polypropylene fibres to control the shrinkage and thermal cracks.

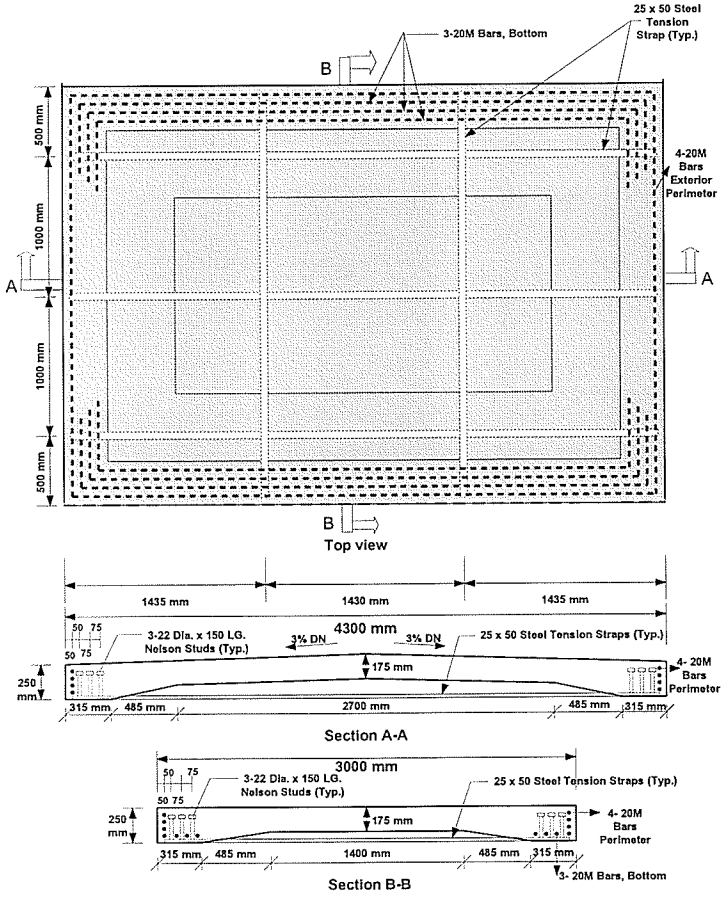

Fig. 4.1: Top view and typical cross-sections of ArchPanel®

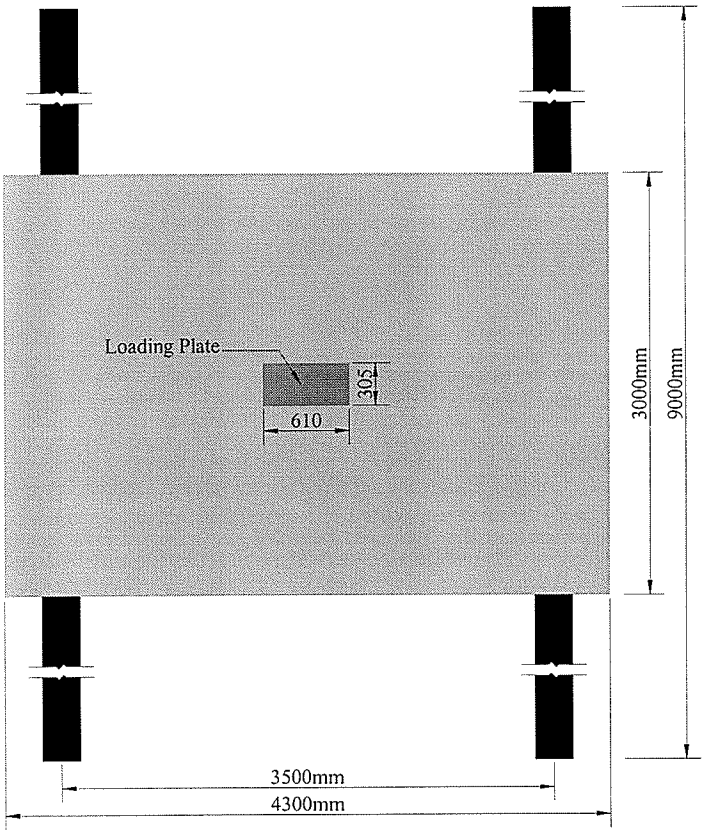

Fig. 4.2: Schematic view of test setup

4.2.1 Instrumentation for ArchPanel®

To investigate the performance under cyclic loading, the ArchPanel® was monitored through a number of sensors, including linear variable displacement transducers (LVDTs), strain gauges and pi-gauges. Vertical deflection of the ArchPanel® was measured by LVDTs. The displacement transducers (5 LVDTs) were attached to steel beams resting directly above the center of the girders as shown in Fig. 4.3 in order to measure deflection of the deck slab with respect to the girders. Displacement transducer locations were selected at mid span and all four sides in the direction of both longitudinal and transverse centerline of the ArchPanel®. Due to the locations of the displacement transducers, longitudinal and transverse profiles of deflection were

monitored with respect to increasing the number of cycles. In order to monitor the performance of the steel straps, a strain gauge was mounted on the middle of each strap. To monitor the longitudinal crack width of the ArchPanel®, pi-gauges were used.

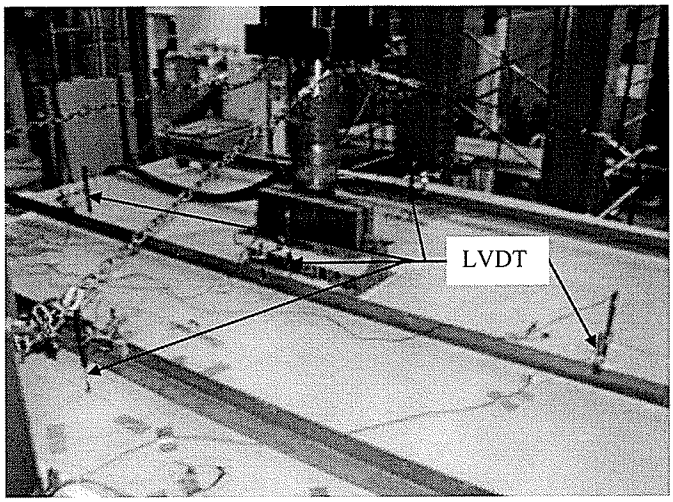

Fig. 4.3: View of LVDTs

4.2.2 Testing Detail of ArchPanel®

To understand the fatigue behaviour of the non-composite pre-cast steel-free ArchPanel®, cyclic tests were conducted at various load levels. The fatigue investigation of the non-composite steel-free concrete ArchPanel® was tested between 196 kN (20 tonne) and 490 kN (50 tonne) load levels. The load was applied with a hydraulic actuator. The load cell had a capacity of 1000 kN (102 tonne). The deck slab was tested under a central rectangular patch load measuring 610 x 305 mm, with the latter dimension being in the longitudinal direction of the ArchPanel®. The test setup is shown in Fig. 4.4. The test results are discussed in Chapter 5.

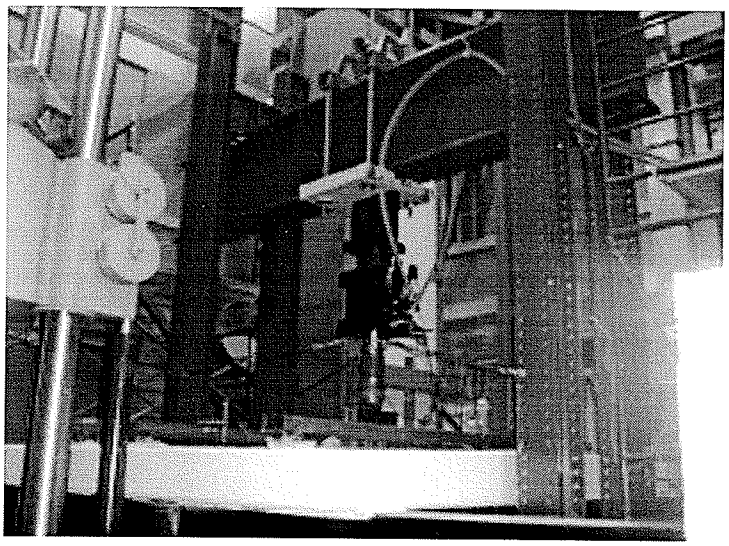

Fig. 4.4: View of test setup

4.3 Full-Scale Specimen of Concrete Bridge Deck Slab

In this study, the fatigue behaviour of a cast-in-situ full-scale concrete bridge deck slab specimen was investigated. The specimen deck slab consisted of three segments 3000 mm each with overall dimensions of 9000 x 3000 mm and a thickness of 175 mm and a haunch of 50 mm. The deck slab was cast-in-situ compositely on two steel girders at a center-to-center spacing of 2000 mm through the use of shear connectors. The deck slab had a 500 mm long cantilever overhang beyond the center of the each girder. In the longitudinal direction, the deck slab was 9000 mm long. Although cast monolithically, this full-scale specimen was divided into three segments (A, B and C), as shown in Fig. 3.1. All three segments were designed according to the CHBDC (2000) and explained in Chapter 3.

4.3.1 Construction of Full-Scale Specimen Concrete Deck Slab

The specimen deck slab was designed according to the CHBDC (2000), as described in the previous section. Full details about the design of the specimen deck slab are given in Chapter 3. The construction of the full scale specimen deck slab on two steel girders was simply supported at the free ends. The spacing between the girders was 2000 mm center-to-center. This specimen deck slab was a cast-in-situ composite deck slab, in order to provide the composite action between the steel girders and the concrete deck slab, three ¾ inch (19 mm) diameter shear studs at a spacing of 300 mm were used. According to the CHBDC (2000), two end diaphragms were installed during the erection of the girders. In a steel-free concrete deck slab, edge beams are necessary to achieve punching shear failure behaviour. For that purpose, a set of two angles (L 150 x 150 x 19) were installed and made composite with the deck slab by using the shear studs, as shown in Fig. 4.5. Once the steel framework was completed (Fig. 4.5), six partially studded steel straps were placed on top of the steel girders at a spacing of 1000 mm, can be seen in Figs. 4.7 (b) and (c). After that, formwork was made and the steel reinforcement, CFRP grid and GFRP grid were placed, as shown in Fig. 4.6. The reinforcement detail of the steel reinforcement, the CFRP grid and GFRP grid are shown in Figs. 4.7(a), (b) and (c) respectively. From Figs. 4.7 (a), (b) and (c), it can be seen that some of the bars were instrumented with electrical resistance strain gauges and placed in transverse as well as longitudinal direction. Since this specimen deck slab was a steel-free concrete deck slab, it was decided to use concrete chairs instead of steel and plastic to support the bars and maintain the concrete cover, as shown in Figs. 4.7 (a), (b) and (c).

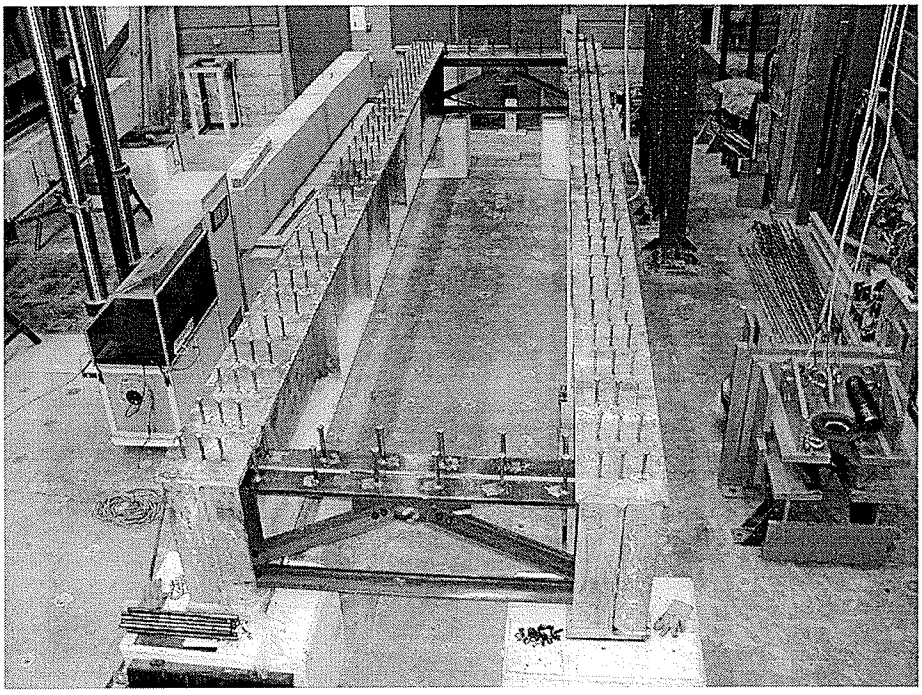

Fig. 4.5: Steel frameworks for the supporting steel-free concrete deck slab

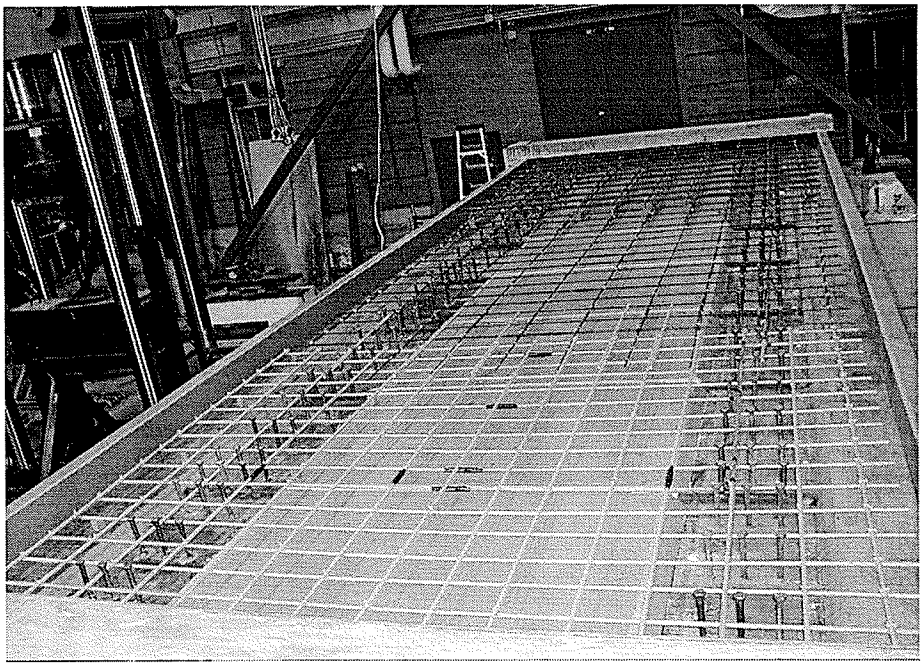

Fig. 4.6: Reinforcement details and formwork

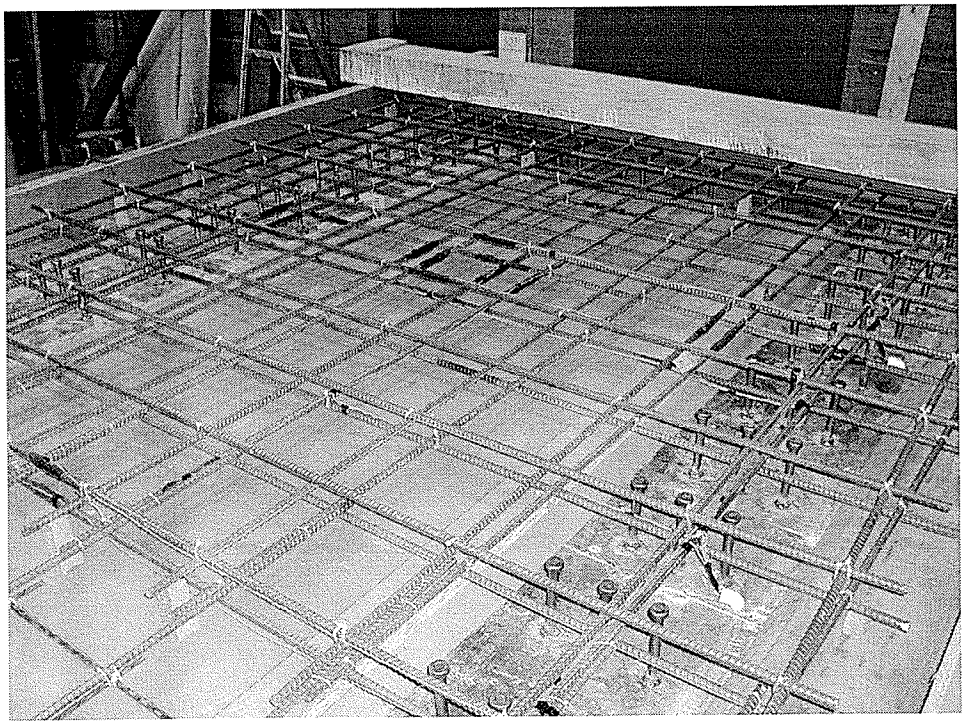

Fig. 4.7(a): Detail of steel reinforcement in Segment A

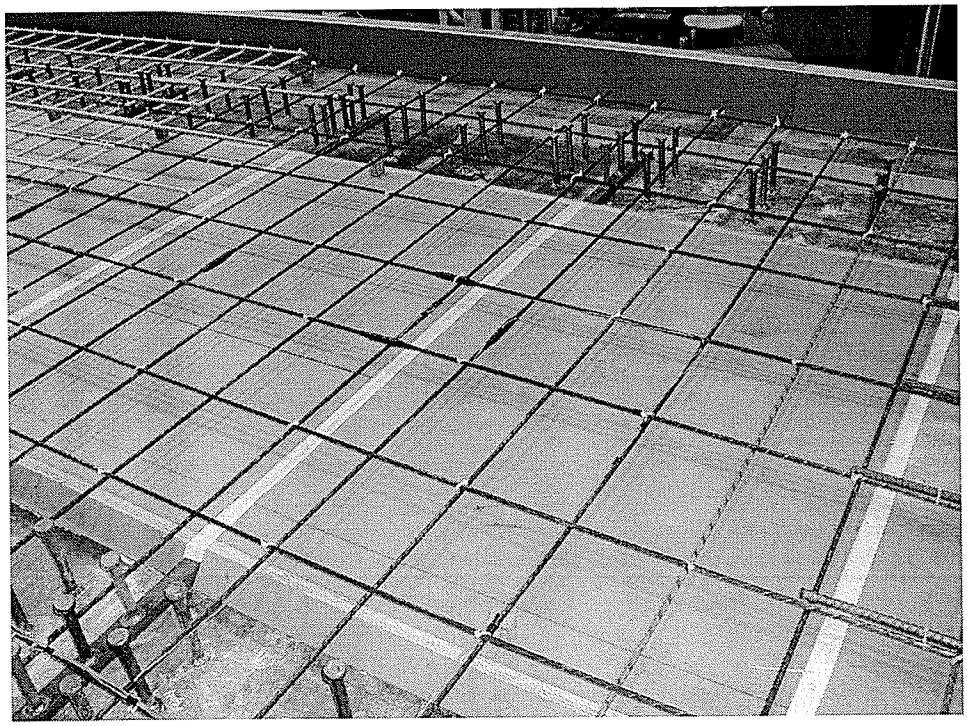

Fig. 4.7(b): Detail of CFRP-grid and steel straps in Segment B

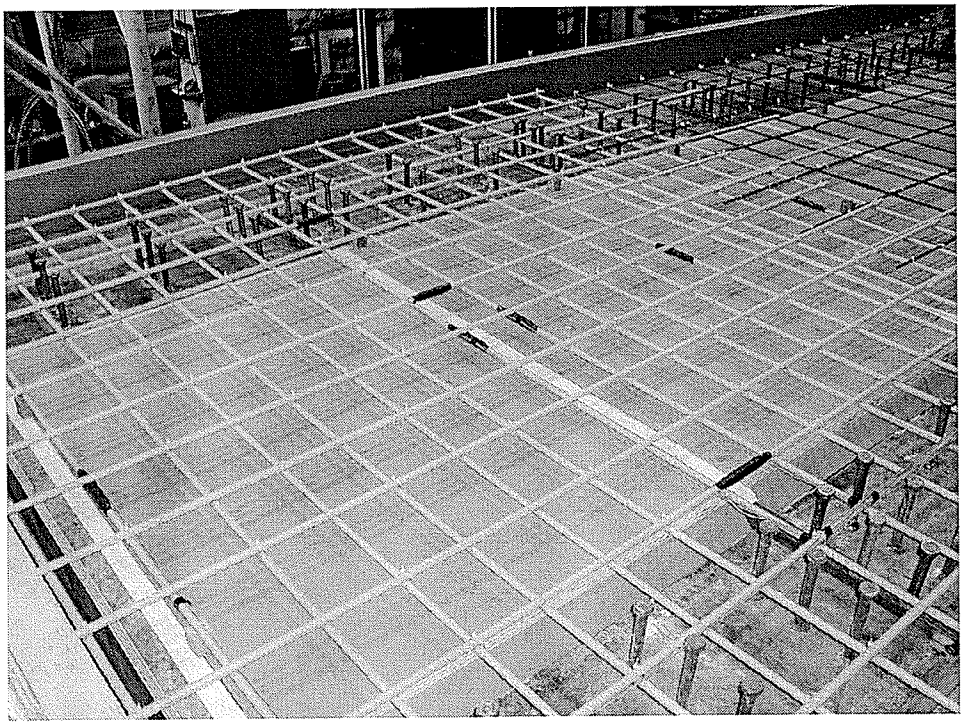

Fig.4.7(c): Detail of GFRP-grid and steel strap in Segment C

Once the formwork and placing of the reinforcement was completed, as shown in Fig. 4.6, the deck was ready to cast. The volume of the deck slab is more than the capacity of a standard truck, two batches of Grade-35 concrete were ordered. The mix proportions and properties are shown in Appendix A1. The plain concrete of batch 1 was poured into Segment A, as shown in Fig. 4.8 (a) and (b). Segments B and C were steel-free concrete deck slabs, to control shrinkage and thermal cracking 0.3% chopped polypropylene fibres by volume were mixed with the concrete. Fibres in the concrete mix reduce the workability significantly, thus it was recommended that superplasticizers be used to achieve the required workability. Once the fibre-reinforced concrete mix was compliant with ASTM C-1116, the concrete was poured into segments B and C, as shown in Fig. 4.9 and Fig. 4.10. Finally, the deck slab was cast, as shown in Fig. 4.11. During the casting of the deck slab, concrete cylinders

were cast for batch 1 and batch 2, with and without fibres. The test results are shown in Appendix A2.

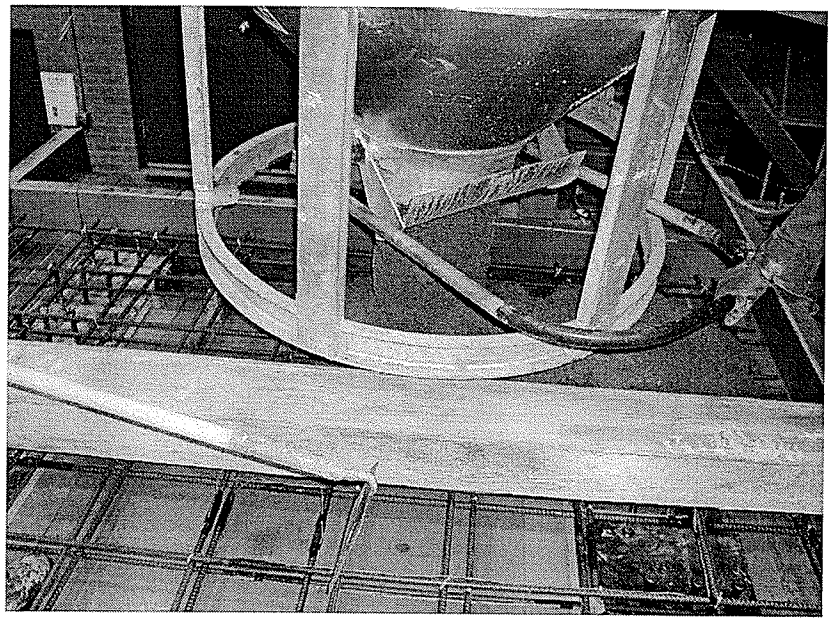

Fig. 4.8(a): Pouring of concrete

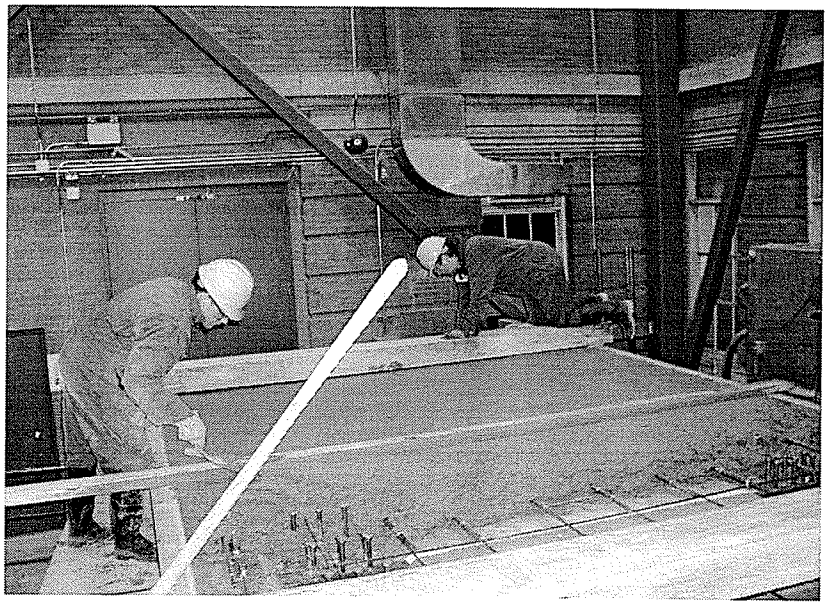

Fig. 4.8(b): Concreting of Segment A

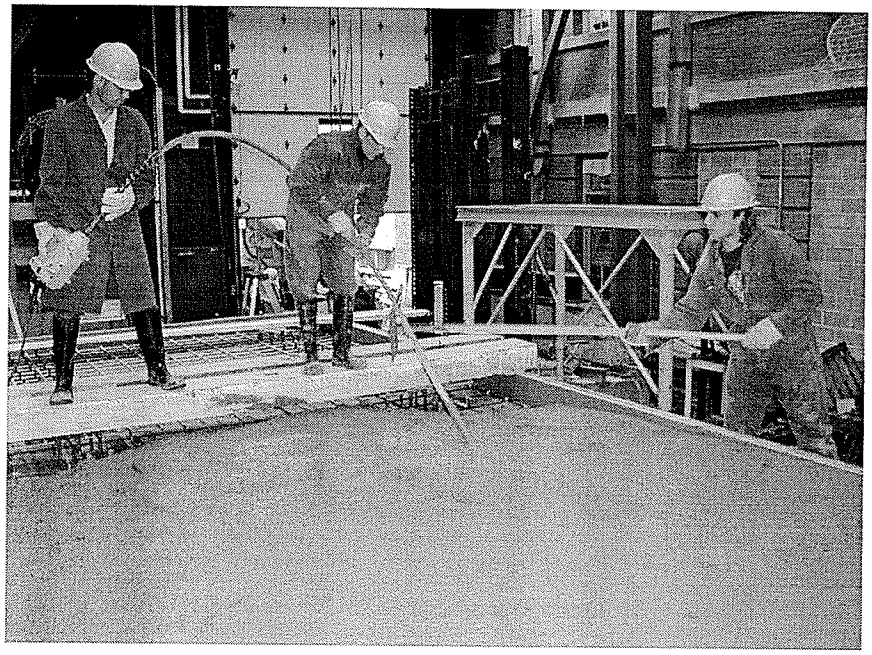

Fig. 4.9: Concreting of Segment B

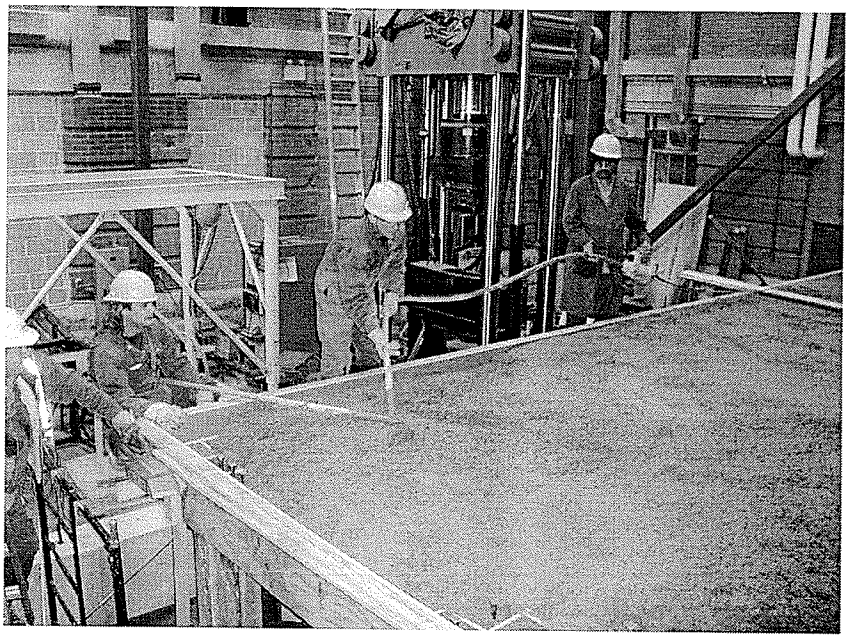

Fig. 4.10: Concreting of Segment C

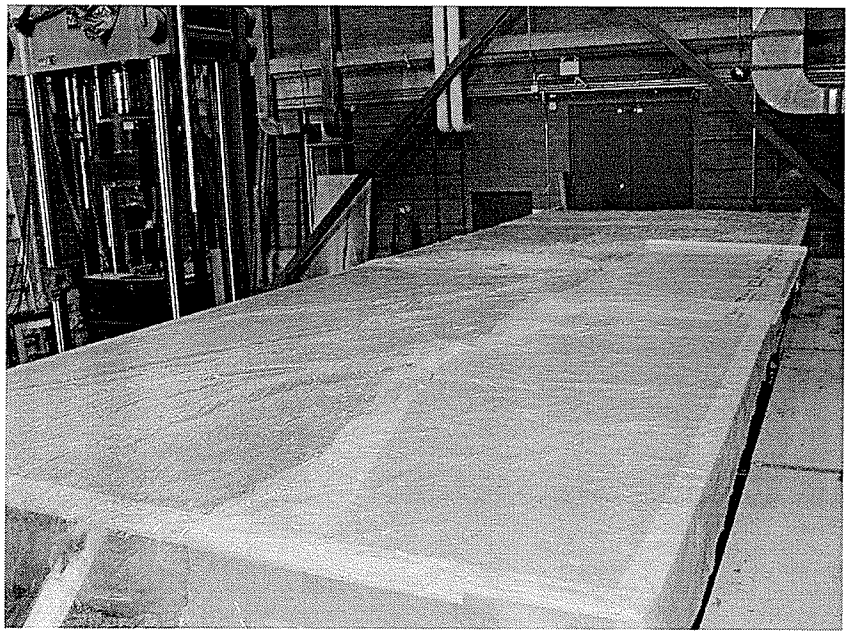

Fig. 4.11: Concrete deck slab after casting

4.3.2 Instrumentation for Concrete Bridge Deck Slab

The performance of the deck slab was monitored through a number of sensors, including linear variable displacement transducers (LVDTs), strain gauges, pi-gauges and linear motion transducer (LMT). The vertical deflection of the slab, midway between the girders, was measured with five LVDTs. In order to measure the deflection of the deck slab with respect to girders, the LVDTs were attached to steel beams resting directly above the center of the girders, as shown in Fig. 4.12. The performance of the steel straps was monitored by an electrical resistance strain gauge mounted at mid length. The performance of the internal steel reinforcement, the GFRP and CFRP bars, was measured by electrical resistance strain gauges that were mounted on some of the bars and placed in transverse and longitudinal directions. To measure the crack widths, pi-gauges were mounted midway between the girders, as

shown in Fig. 4.13. The outward movement of the girders due to arching action was measured by LMT under the applied cyclic load (Fig. 4.13).

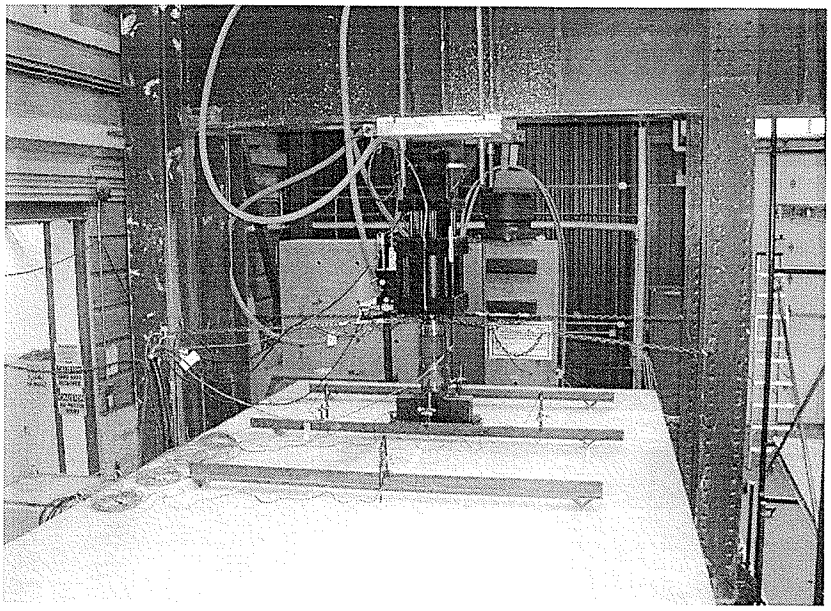

Fig. 4.12: Test setup and instrumentation

Fig. 4.13: Bottom view and instrumentation

4.3.3 Testing Detail of Concrete Bridge deck slab

The fatigue behaviour of the deck slab was monitored under cyclic loading. For Segment C, the load was applied at 245 kN (25 tonne), 490 kN (50 tonne) and 588 kN (60 tonne). For Segments A and B, the loads were applied at 245 kN (25 tonne) and 588 kN (60 tonne). The sine function was used to apply cyclic load. In each case, the load was applied through a hydraulic actuator with a load cell capacity of 1000 kN (102 tonne). The rectangular patch load measured 610 x 305 mm, with the latter dimension being along the girders. The test setup is shown in Fig. 4.12.

Chapter 5

Test Results of Pre-cast Concrete ArchPanel®

5.1 General

The full-scale specimen of pre-cast ArchPanel® with overall dimensions of 3000 x 4300 mm is shown in Fig. 4.1. The detailed description of ArchPanel® is given in Chapter 4. The fatigue behaviour of the steel-free concrete ArchPanel® was investigated under cyclic loading of various load levels of different magnitudes of 196 kN (20 tonne), 245 kN (25 tonne), 343 kN (35 tonne) and 490 kN (50 tonne) and the load was applied through a hydraulic actuator. The numbers of cycles are recorded by cycle counter on the MTS controller. A number of sensors were used to monitor the performance of the ArchPanel®, including linear variable displacement transducers (LVDTs), strain gauges and pi-gauges. At a 196 kN (20 tonne) cyclic load level, the ArchPanel® completed 300,000 cycles. After that the load was increased to 245 kN (25 tonne) and 500,000 cycles were completed without failure. Next the load was increased to 343 kN (35 tonne), at which level 74,000 cycles were completed without failure. Finally, a 490 kN (50 tonne) cyclic load was applied, and the ArchPanel® completed approximately 54,671 cycles at which point it failed.

The vertical deflection of the ArchPanel® was measured by LVDTs, as shown in Fig. 4.4. The ArchPanel® was designed entirely free of any internal tensile reinforcement and confined transversely by steel straps. In order to monitor the performance of the steel straps, a strain gauge was mounted at the mid point of the flat

surface of each strap. The strain response with an increasing number of cycles was measured under the applied cyclic load. The width of the longitudinal crack in the ArchPanel® was measured using pi-gauges.

The following test results are given in this chapter:

- Deflection of the ArchPanel® at 196 kN (20 tonne), 245 kN (25 tonne), 343 kN (35 tonne) and 490 kN (50 tonne) cyclic load levels (Section 5.2)
- Strain in the steel strap at 196 kN (20 tonne), 245 kN (25 tonne), 343 kN (35 tonne) and 490 kN (50 tonne) cyclic load levels (Section 5.3)
- Crack width at 245 kN (25 tonne), 343 kN (35 tonne) and 490 kN (50 tonne) cyclic load levels (Section 5.4)

5.2. Deflection behaviour in ArchPanel®

The load-deflection behaviour was monitored at the centre of the ArchPanel®, under the cyclic loads of 196 kN (20 tonne), 245 kN (25 tonne), 343 kN (35 tonne) and 490 kN (50 tonne), as shown in Fig. 5.1. The deflections, along with the increasing the number of cycles, are shown in Fig. 5.2. This figure does not show the deflection behaviour under 50 tonne cyclic load. The deflection under a 50 tonne cyclic load level is shown separately in Fig. 5.3 with number of cycles drawn separately in log scale. Fig. 5.3 demonstrated that the deflection increased smoothly up to 40,000 cycles under a 50 tonne cyclic load; after that, increase in the deflection was dramatic up until failure. Finally, the ArchPanel® failed after completing 54,671 cycles under a 50 tonne cyclic load.

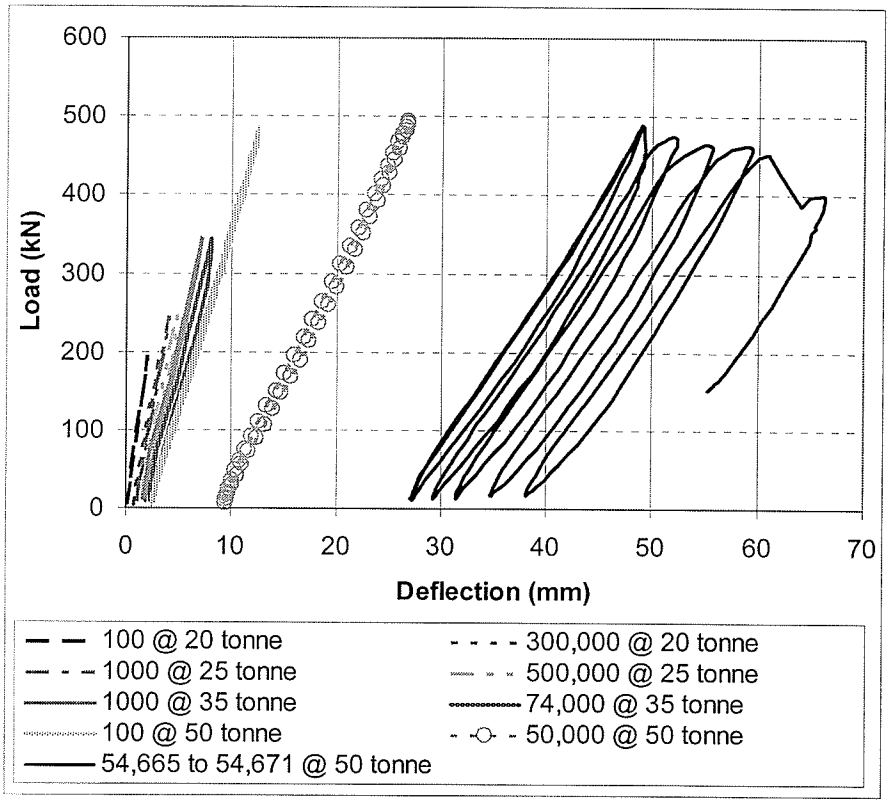

Fig. 5.1: Load–deflection behaviour under 20, 25, 35 and 50 tonne (ArchPanel®)

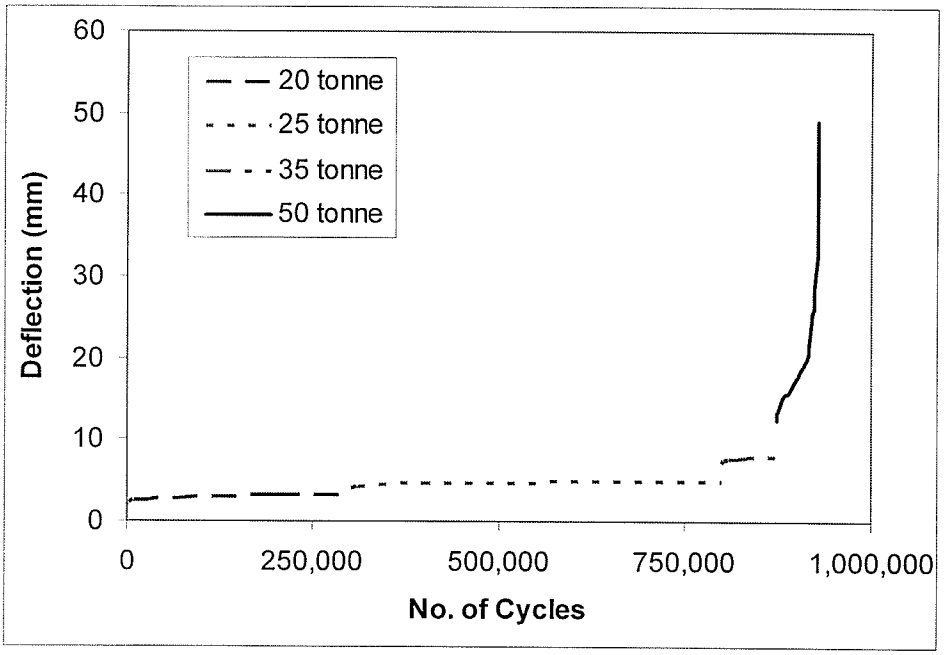

Fig. 5.2: Deflection behaviour under 20, 25, 35, and 50 tonne (ArchPanel®)

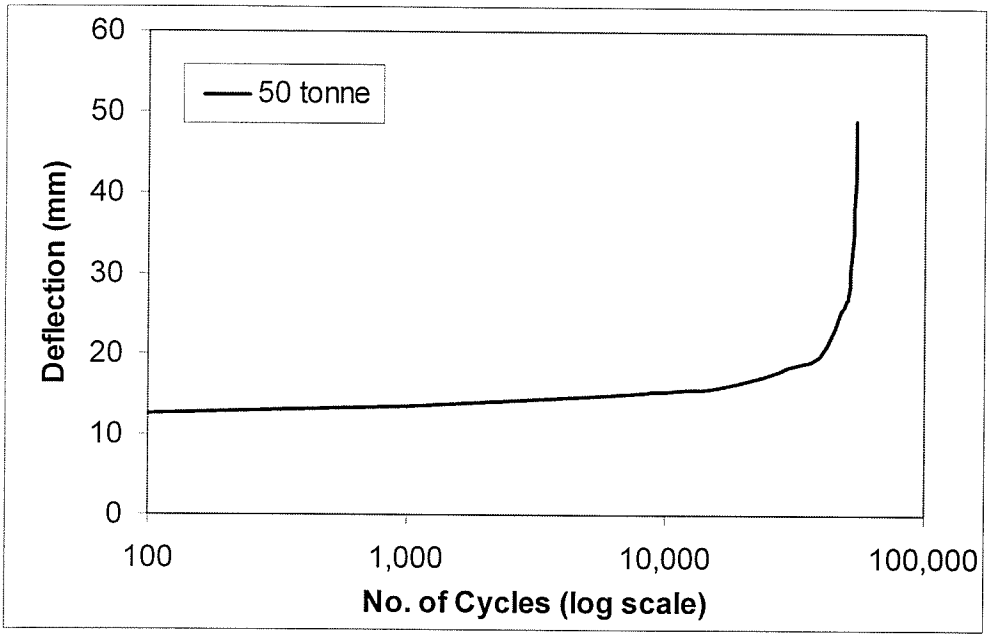

Fig. 5.3: Deflection behaviour under 50 tonne (ArchPanel®)

5.3. Strain in the steel strap behaviour in ArchPanel®

To monitor the performance of steel straps in the ArchPanel® as described earlier, an electrical resistance strain gauge was mounted at the mid-point of the flat surface of each strap. The strain response was reported under an applied cyclic load. The strain behaviour with an increasing number of cycles, under a 196 kN (20 tonne), 245 kN (25 tonne), 343 kN (35 tonne) and 490 kN (50 tonne) is shown in Fig. 5.4. This figure demonstrates that, under 20 tonne cyclic load, the ArchPanel® completed 300,000 cycles. At this point, the increase in the strain due to the applied cyclic load being increased from 20 to 25 tonne is apparent. It was also obvious that, when the ArchPanel® completed 800,000 cycles, a similar increase in the strain resulted from the increase in the applied cyclic load from 25 to 35 tonne. Similarly, when the ArchPanel® completed 874,000 cycles, a significant increase in the strain was observed due to the increase in applied cyclic load from 35 to 50 tonne. The strain behaviour under a 50 tonne cyclic load level cannot be clearly discerned from

Fig. 5.4. The strain behaviour under a 50 tonne cyclic load level is drawn separately in log scale (Fig. 5.5). These Figs. 5.4 and 5.5, show the trend is almost similar to the Figs. 5.2 and 5.3. This indicates that either strain or deflection can be use as an indicator of damage. As described earlier, the strain in strap and deflections with increasing number of cycles are measured under the applied cyclic load.

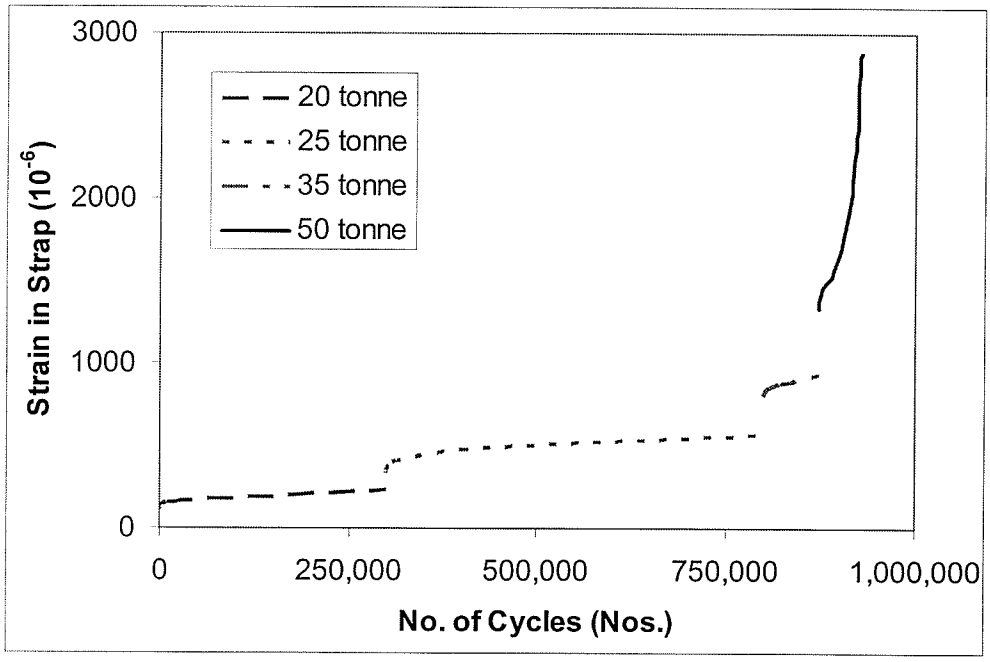

Fig. 5.4: Strain behaviour under 20, 25, 35 and 50 tonne (ArchPanel®)

5.4. Crack width behaviour in ArchPanel®

The width of the longitudinal crack in the ArchPanel® was measured using pi-gauges. The crack width behaviour with an increasing number of cycles under 245 kN (25 tonne), 343 kN (35 tonne) and 490 kN (50 tonne) load levels is shown in Fig. 5.6. This figure demonstrates that the crack width increased, when the ArchPanel® completed 800,000 cycles. This was due to the increase in the applied cyclic load from 25 to 35 tonne.

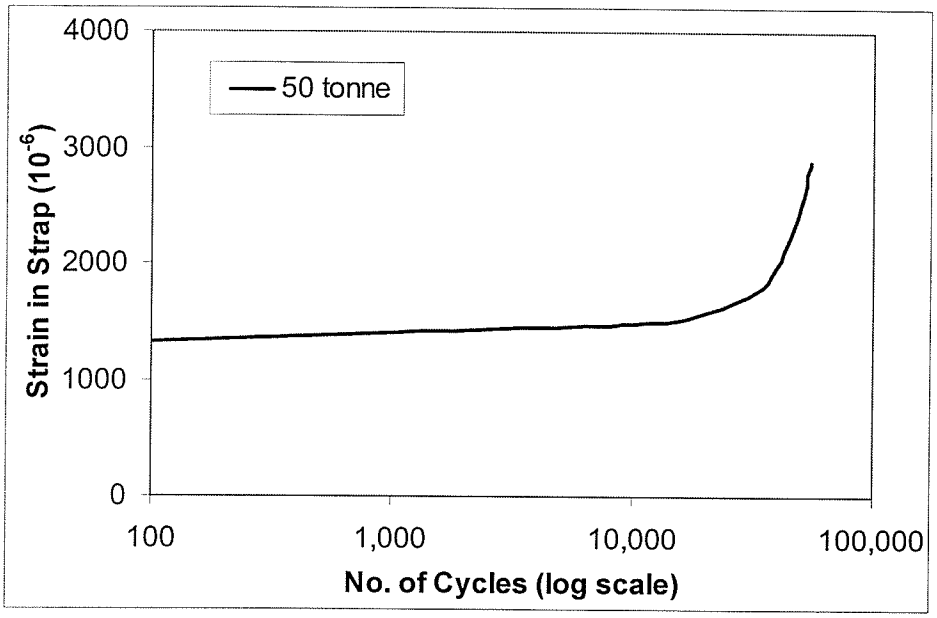

Fig. 5.5: Strain behaviour under 50 tonne (ArchPanel®)

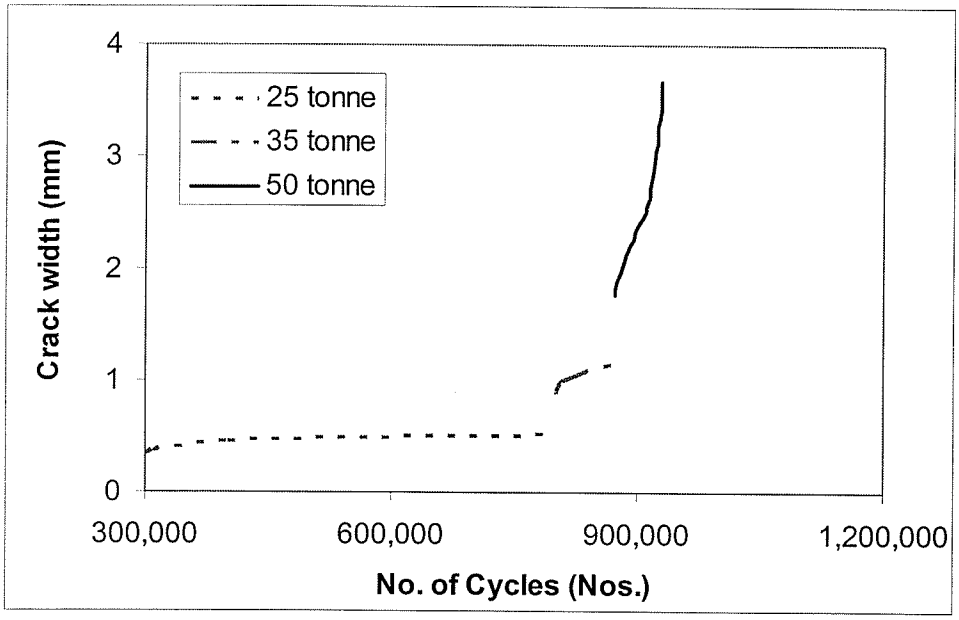

Fig. 5.6: Crack width behaviour under 25, 35, and 50 tonne (ArchPanel®)

Again a significant increase in crack width was found, when the applied cyclic load was increased from 35 to 50 tonne. This figure does not clearly show the crack width

behaviour under 50 tonne cyclic load level. The crack width behaviour with increasing number of cycles at a 50 tonne cyclic load level is drawn separately in log scale (Fig. 5.7). This figure also shows that this trend is similar to that observed for deflection and steel strap strain meaning that either crack width, deflection or steel strap strain can be used as an indicator of damage.

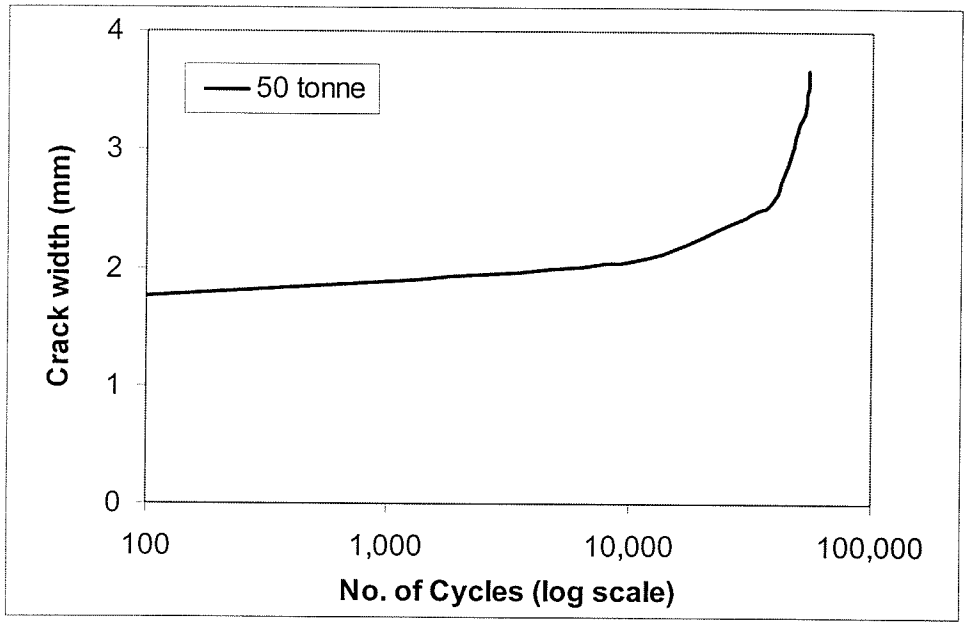

Fig. 5.7: Crack width behaviour under 50 tonne (ArchPanel®)

Chapter 6

Test Results of Cast-in-situ Concrete Deck Slab

6.1 General

The full-scale specimen of the cast-in-situ concrete bridge deck slab consisted of three segments with overall dimensions of 9000 x 3000 mm, as shown in Fig. 3.1. Segment C was tested first, followed by Segment A and Segment B. Segment C was a steel-free concrete deck slab with an internal GFRP crack control grid and external steel straps. Segment A was constructed using conventional design with steel reinforcement while Segment B was a steel-free concrete deck slab with an internal CFRP crack control grid and external steel straps. The experimental results from each test are given in the following sections.

6.2 Segment C (steel-free concrete deck slab with internal GFRP crack control grid and external steel straps)

Segment C is a second generation steel-free concrete deck slab containing an internal GFRP crack control grid and external steel straps, as shown in Fig. 3.4. Its fatigue behaviour was investigated under cyclic loading applied through a hydraulic actuator at load levels of 245 kN (25 tonne), 490 kN (50 tonne) and 588 kN (60 tonne). A number of sensors were used to monitor the performance of the deck slab, including linear variable displacement transducers (LVDTs), strain gauges, pi-gauges and linear motion transducers (LMTs).

The vertical deflection was measured by LVDTs, as shown in Fig. 4.14. The deflection of the structure can be used as an indicator of damage. The maximum response was measured at the center of the specimen deck slab. The strain in the steel straps and the GFRP rebar was measured by electrical resistance strain gauges. To monitor the performance of the GFRP rebar, strain gauges were mounted on some of the GFRP rebar and placed in the transverse and longitudinal directions, as shown in Fig. 4.9(c). To monitor the performance of the steel straps, a strain gauge was mounted on every steel strap, as shown in Fig. 4.15. The maximum strain was measured under the applied cyclic load. To measure the crack width of the deck slab, pi-gauges were used, as shown in Fig. 4.15. The crack width was recorded under the applied cyclic load. The deck slab under discussion was cast-in-situ on two steel girders. To achieve composite action, shear connectors were used. When loads are applied, the concrete has to crack to initiate the arching action and the steel girders try to move outward. To measure the outward movement of the steel girders, a linear motion transducer (LMT) was used under the applied cyclic load, as shown in Fig. 4.15.

The following test results of Segment C are discussed in this chapter.

1. Deflection of the deck slab at 245 kN (25 tonne), 490 kN (50 tonne) and 588 kN (60 tonne) cyclic load levels (Section 6.2.1)
2. Strains in the GFRP rebar and steel strap at 245 kN (25 tonne), 490 kN (50 tonne) and 588 kN (60 tonne) cyclic load levels (Section 6.2.2)
3. Crack width at 245 kN (25 tonne), 490 kN (50 tonne) and 588 kN (60 tonne) cyclic load levels (Section 6.2.3)

4. Outward movement of the girders at 245 kN (25 tonne), 490 kN (50 tonne) and 588 kN (60 tonne) cyclic load levels (Section 6.2.4)

The deck slab of Segment C was subjected to 1,000,000 cycles under an applied cyclic load of zero to 245 kN (25 tonne). No visible damage was observed under this load. Thus, the cyclic load range was increased to zero to 490 kN (50 tonne) and the deck slab was subjected to an additional 1,000,000 cycles. Although some deflection was observed, the deck slab was still far from failure. It was thus decided to increase the cyclic load range to zero to 588 kN (60 tonne). Finally, the deck slab failed after an additional 420,683 cycles under a cyclic load of zero to 588 kN (60 tonne).

6.2.1 Deflection behaviour in Segment C (GFRP)

The deflection at the center of the deck slab was recorded at different cycles under 245 kN (25 tonne), 490 kN (50 tonne) and 588 kN (60 tonne) load levels. The deflection corresponding to various cycles under these loads is shown in Fig. 6.1.The load-deflection results indicate a change in the stiffness of the structure with the increasing number of load cycles. Similar load-deflection behaviour has been reported by Selvadurai and Bakht (1995) and Youn and Chang (1998).

The deflection at the center of Segment C with the increasing number of cycles is drawn (Fig. 6.2). This figure shows the deflection behaviour under a 25, 50 and 60 tonne cyclic load. This graph also demonstrates that at 1,000,000 cycles there was an increase in deflection caused by the increase in loads

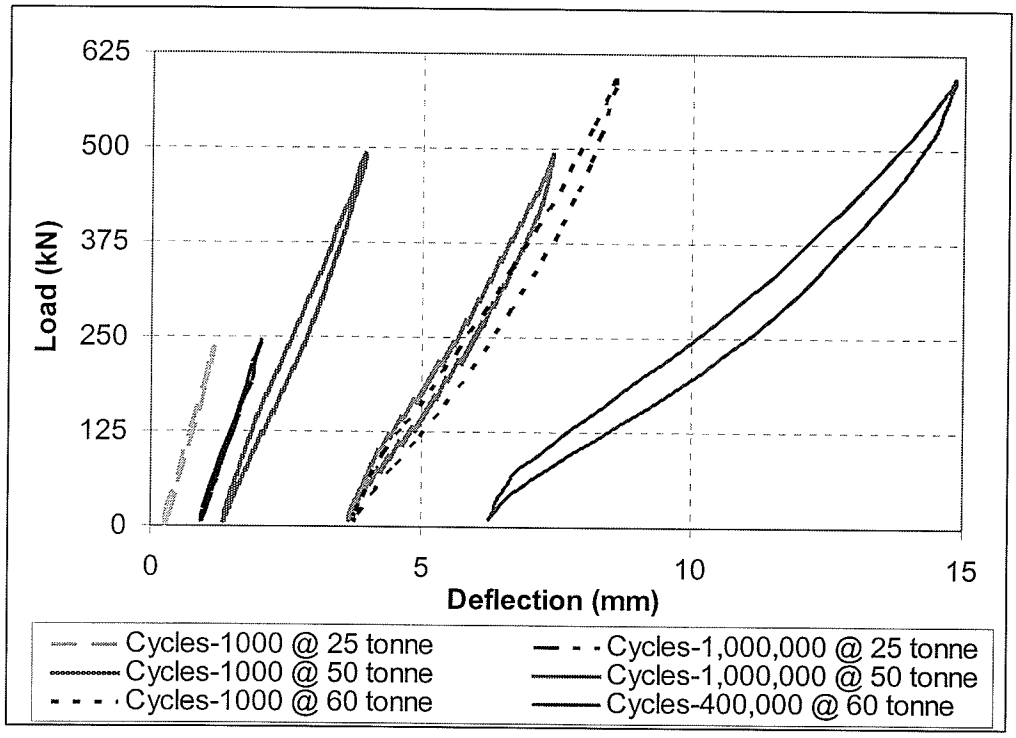

Fig. 6.1: Load-deflection behaviour under 25, 50 and 60 tonne (Segment C)

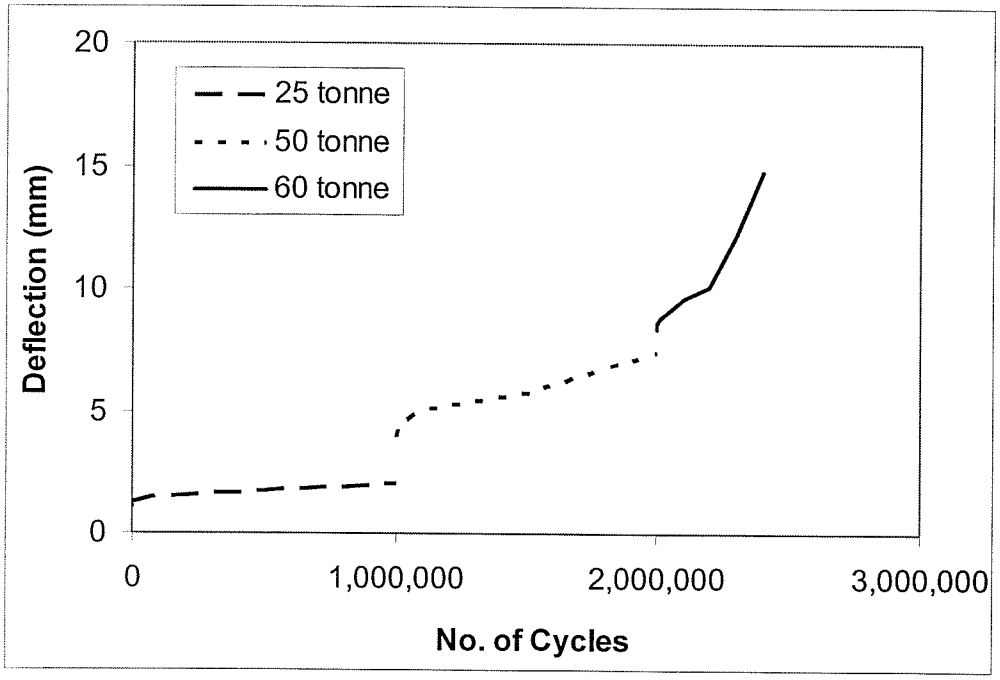

Fig. 6.2: Deflection behaviour under 25, 50 and 60 tonne (Segment C)

from 25 to 50 tonne. Similarly an increase in the deflection can be seen at 2,000,000 cycles caused by the increase in the loads from 50 to 60 tonne. At 60 tonne cyclic load, when the specimen deck slab completed 2,200,000 cycles, the increase in the deflection was suddenly increased. This was followed by punching shear failure at 2,420,683 cycles (Fig. 6.3).

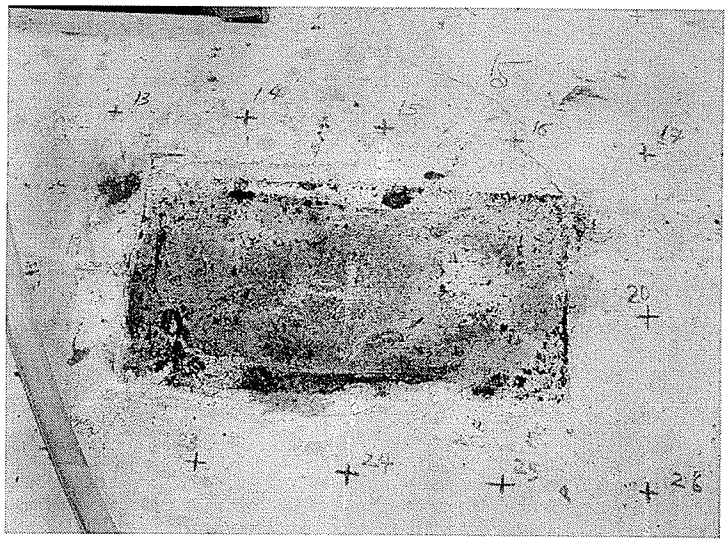

Fig. 6.3: Punching shear failure mode (Segment C)

To measure the profile of the deflection of the Segment C, five LVDTs were used, as shown in Fig. 4.14. This figure shows that the LVDTs were located at mid-span and on all four sides of the specimen deck slab on both the transverse and longitudinal centerline. The profiles of the deflection in the transverse and longitudinal directions with respect to the increasing the number of cycles are shown in Figs. 6.4 and 6.5 respectively. In the transverse direction, the center-to-center distance between the two steel girders was 2000 mm. The LVDTs were mounted at mid-span of Segment C and at 750 mm on either side of the mid-span, as shown in Fig. 4.14. The symmetric profile in the transverse direction was found to be as expected (Fig. 6.4). The distance

in the longitudinal direction was 3000 mm. The LVDTs were mounted at 600, 1500 and 3000 mm from the edge of the beam end. Due to the edge beam, less deflection was expected, as shown in Fig. 6.5.

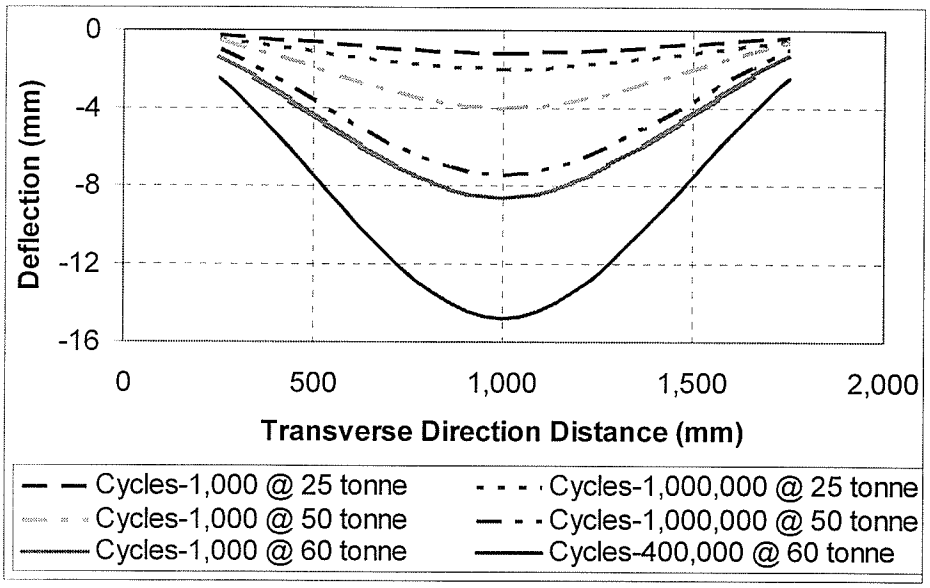

Fig. 6.4: Deflection profile of Segment C along transverse direction (Segment C)

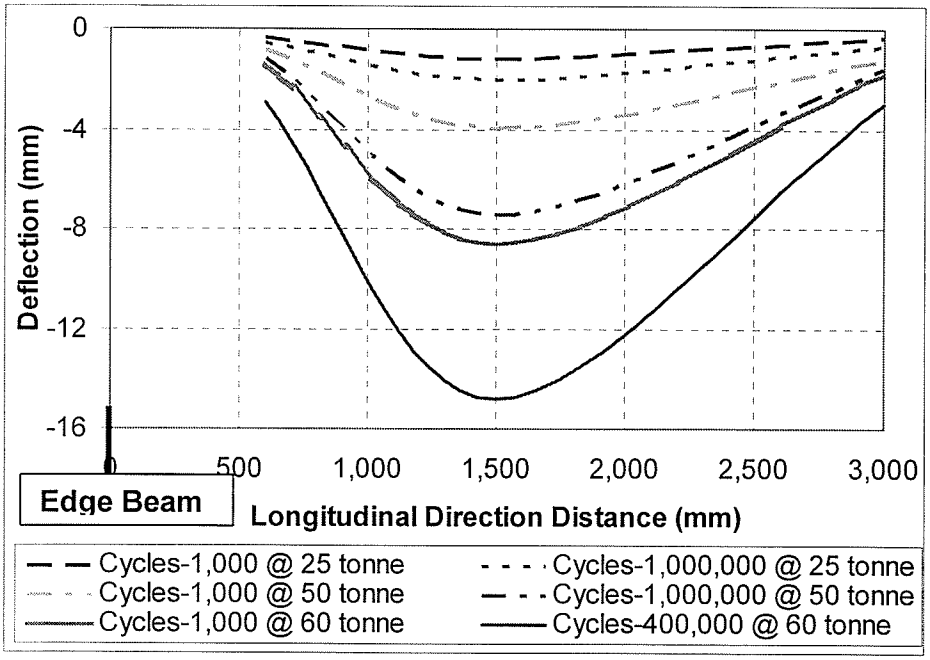

Fig. 6.5: Deflection profile of Segment C along longitudinal direction (Segment C)

6.2.2 Strain behaviour in Segment C (GFRP)

To monitor the performance of GFRP rebar and steel straps in Segment C, as described earlier, an electrical resistance strain gauge was mounted on every strap and some of the rebar in both the transverse and longitudinal directions. The maximum response was measured under the applied cyclic load. The strain behaviour of GFRP rebar with an increasing number of cycles under applied cyclic load is shown in Fig. 6.6(a). The initial strain versus the number of cycles from zero to 1000 cycles is shown in Fig. 6.6(b). Fig. 6.6(a) shows that the increase in the strain was gradual under a 25 tonne cyclic load up to 1,000,000 cycles. After that, the applied load was increased to 50 tonne. Under this increased load the strain increased significantly and finally, the GFRP bar ruptured, after the completion of 1,047,000 cycles. The profile of strains in the GFRP rebar along the longitudinal direction is shown in Fig. 6.7. This gives an idea of how the other GFRP rebar are performing in the deck slab.

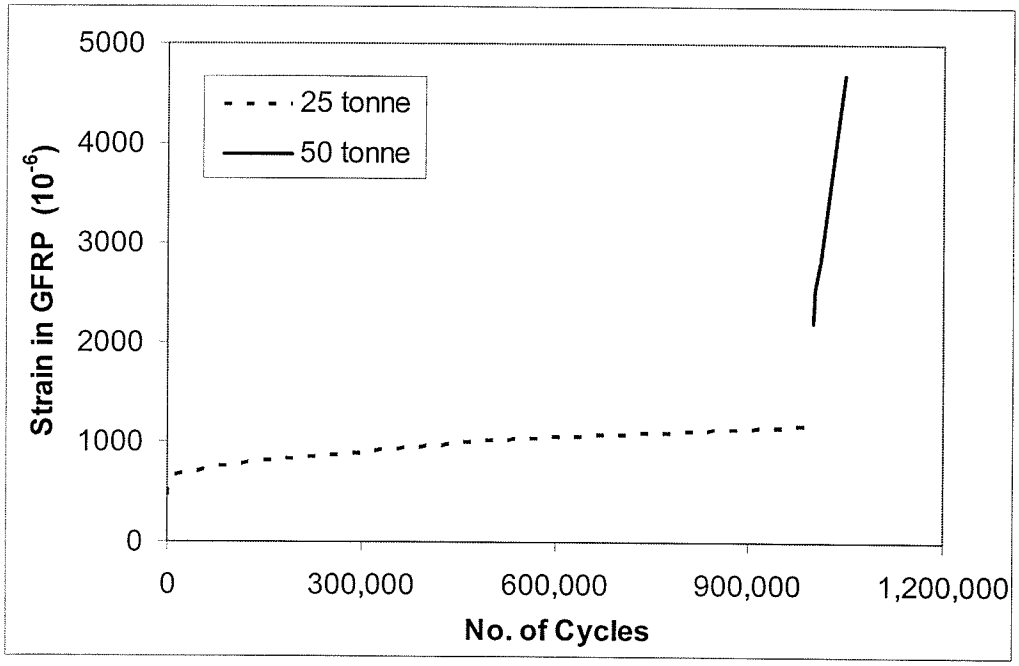

Fig. 6.6(a): Strain behaviour of GFRP rebar under 25 and 50 tonne (Segment C)

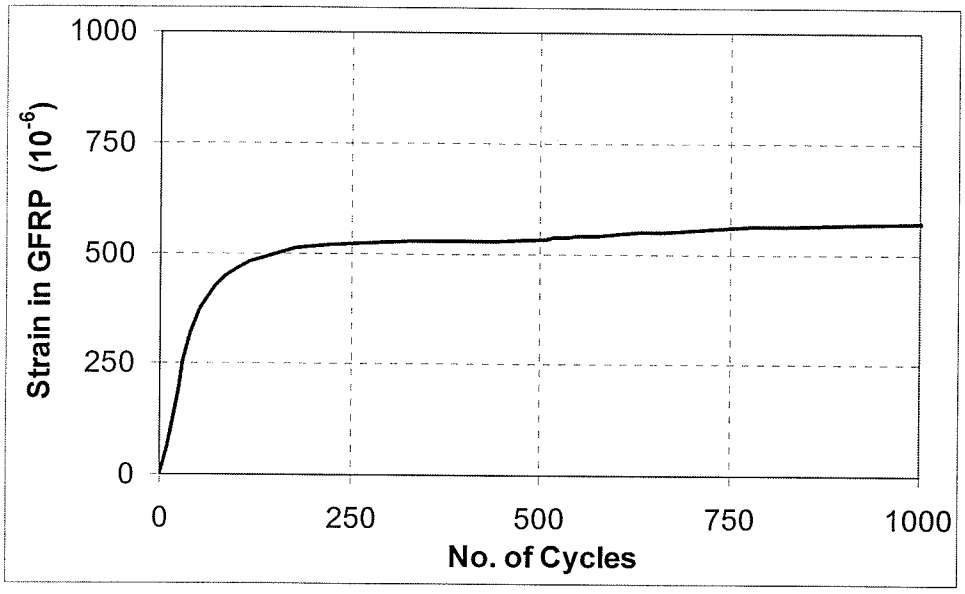

Fig. 6.6(b): Strain behaviour of GFRP rebar under 25 tonne (Segment C)

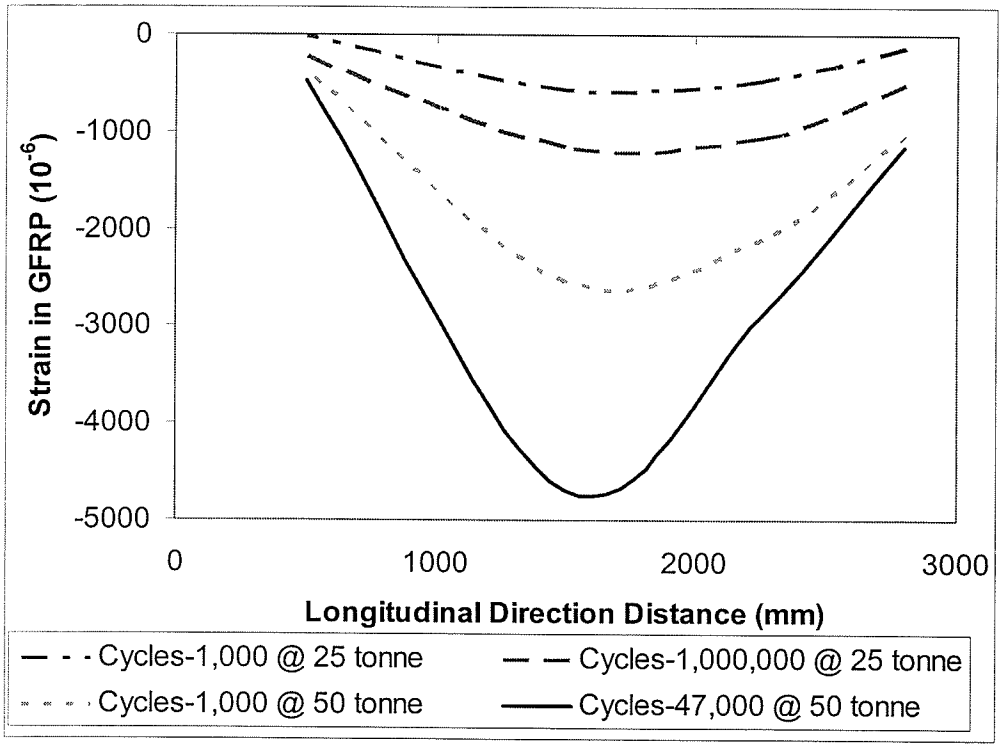

Fig. 6.7: Strain profile of GFRP rebar along longitudinal direction (Segment C)

The strain behaviour of steel strap with an increasing number of cycles under applied cyclic load is shown in Fig. 6.8(a). The initial strap strain versus the number of cycles from zero to 1000 is shown in Fig. 6.8(b). Fig. 6.8(a) shows that, when the deck slab completed 1,000,000 cycles, an increase in the strain appeared. This increase in the strap strain was due to the increased applied cyclic load from 25 to 50 tonne. Similar increase in strain was found in the deck slab, after the deck slab completed 2,000,000 cycles and the applied cyclic load was increased from 50 to 60 tonne. The trend shown in Fig. 6.8(a) is similar to that shown in Fig. 6.2. This indicates that either strain in the strap or deflection can be use as an indicator of damage.

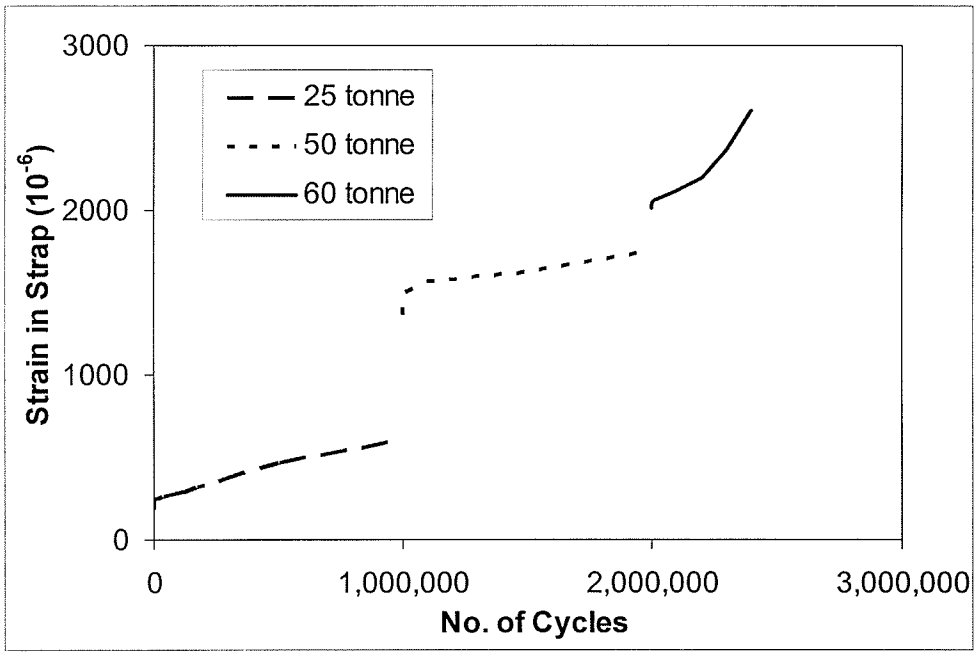

Fig. 6.8(a): Strain behaviour of steel strap under 25, 50 and 60 tonne (Segment C)

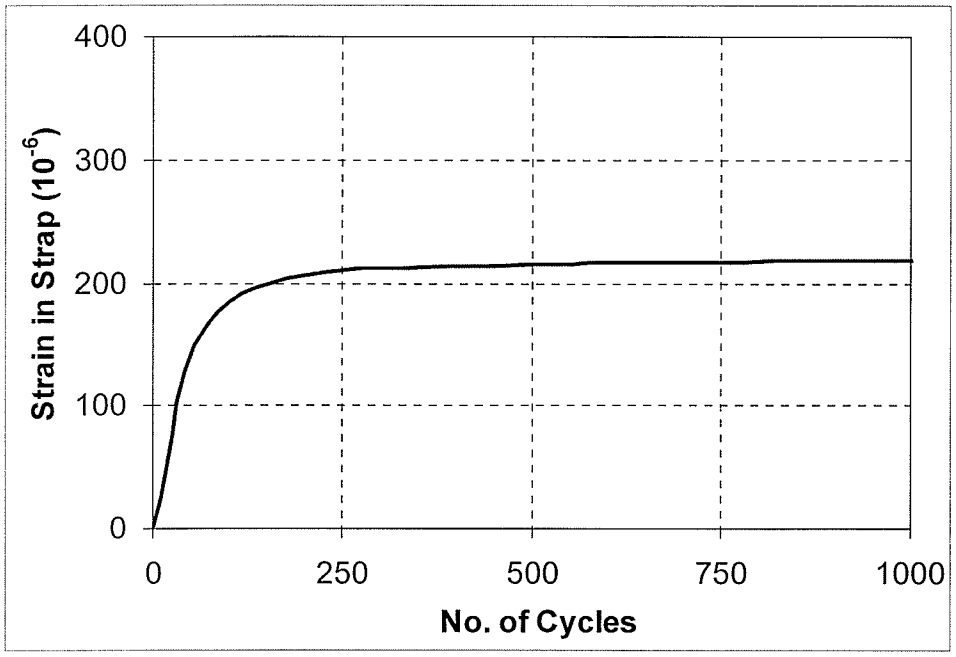

Fig. 6.8(b): Strain behaviour of steel strap under 25 tonne (Segment C)

6.2.3 Crack width behaviour in Segment C (GFRP)

The longitudinal crack width of Segment C under an applied load with an increasing number of cycles is shown in Fig. 6.9. This figure shows that, when the deck slab completed 1,000,000 cycles, the crack width increased, due to the increase applied cyclic load from 25 to 50 tonne. A similar increase in the crack width was found when the applied cyclic load was increased from 50 to 60 tonne. Fig. 6.9 shows that when deck slab reaches near to failure, a nickel appear on the curve and then sudden increase in the behaviour. Fig. 6.9 also shows that the trend is almost similar to that shown in Figs. 6.2 and 6.8(a). This indicates that either crack width, steel strap strain or deflection can be use as an indicator of damage.

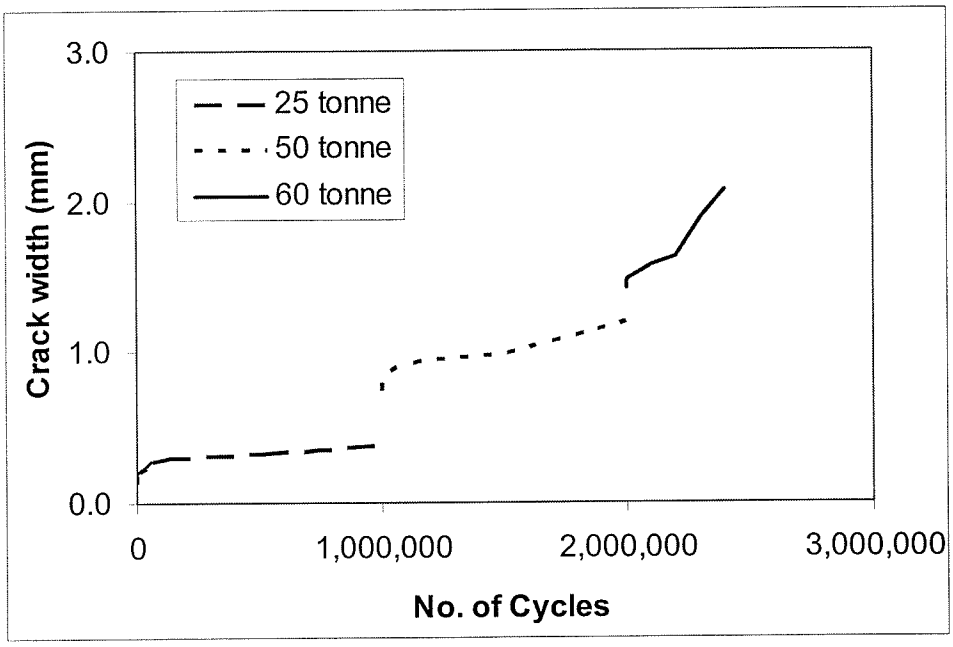

Fig. 6.9: Crack width behaviour under 25, 50 and 60 tonne (Segment C)

6.2.4 Outward movement of steel girders behaviour in Segment C (GFRP)

The outward movement of steel girders with an increasing number of cycles is shown in Fig. 6.10. This figure shows that when the deck slab completed 1,000,000 cycles, an increase in the outward movement of the girders occurred. This increase was due to the increase in the applied cyclic load from 25 to 50 tonne. A similar increase in the outward movement of the girders was found when deck slab completed 2,000,000 cycles, and the applied cyclic load was increased from 50 to 60 tonne. The trend shown in Fig. 6.10 is similar to that shown in Fig. 6.2, 6.8(a) and 6.9. As describe above, similar trends can be used as indicators of damage.

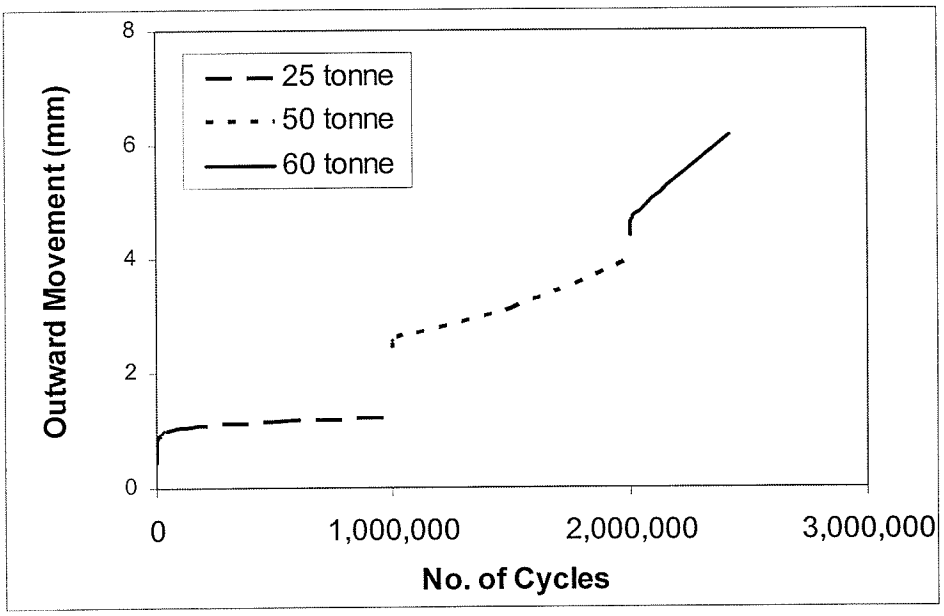

Fig. 6.10: Outward movement of girders behaviour under 25, 50 and 60 tonne (Segment C)

6.3 Segment A (conventional design with steel reinforcement)

Segment A is a conventional design reinforced concrete deck slab containing steel reinforcement, as shown in Fig. 3.2. Its fatigue behaviour was investigated under cyclic loading applied through a hydraulic actuator at load levels of 245 kN (25 tonne) and 588 kN (60 tonne). This Segment A, was not tested under 490 kN (50 tonne) cyclic load because Segment C tested under this load and it did not fail, even completed 1,000,000 cycles under 50 tonne load. Therefore it was decided to test the Segments A under cyclic load of 25 and 60 tonne load levels. A number of sensors were used to monitor the performance of the deck slab, including linear variable displacement transducers (LVDTs), strain gauges, pi-gauges and linear motion transducers (LMTs). The view of LVDTs and test setup for Segment A is shown in Fig. 6.11. The bottom view of Segment A, showing the Pi-gauge and LMT, is shown in Fig. 6.12.

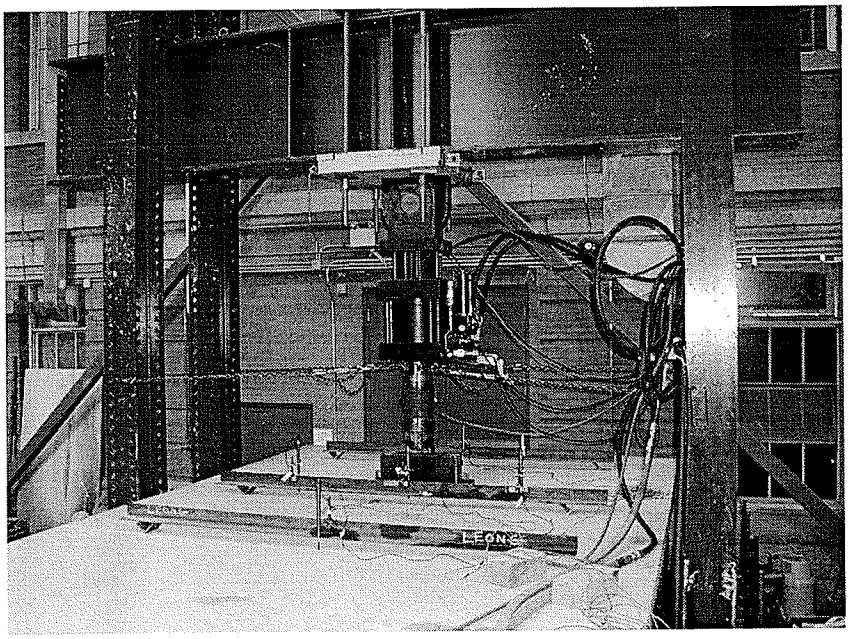

Fig. 6.11: View of LVDTs and test setup (Segment A)

The following test results of Segment A are discussed in this chapter.

1. Deflection of the deck slab at 245 kN (25 tonne) and 588 kN (60 tonne) cyclic load levels (Section 6.3.1)
2. Strains in the steel rebar at 245 kN (25 tonne) and 588 kN (60 tonne) cyclic load levels (Section 6.3.2)
3. Crack width at 245 kN (25 tonne) and 588 kN (60 tonne) cyclic load levels (Section 6.3.3)
4. Outward movement of the girders at 245 kN (25 tonne) and 588 kN (60 tonne) cyclic load levels (Section 6.2.4)

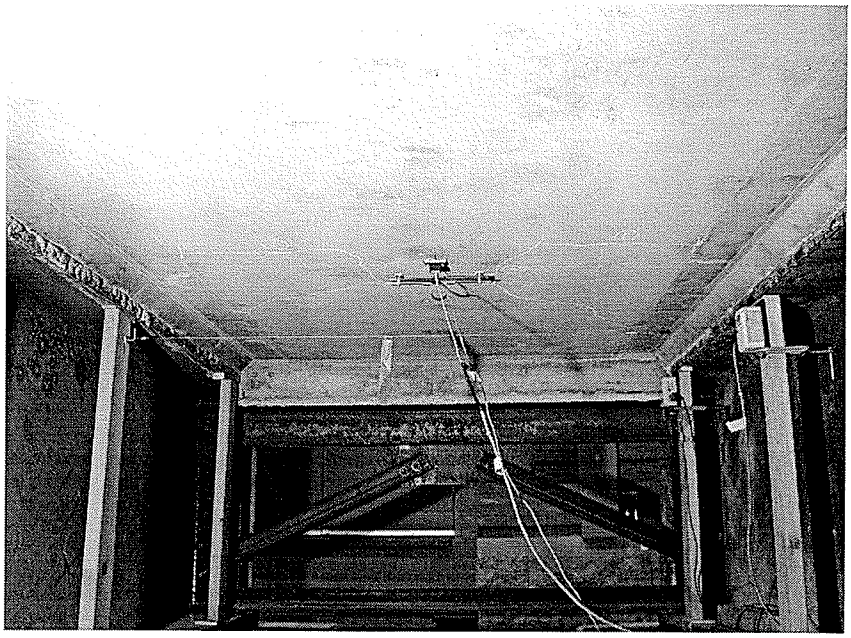

Fig. 6.12: View of the pi-gauge and LMT (Segment A)

The deck slab of Segment A was subjected to 1,000,000 cycles under an applied cyclic load of zero to 245 kN (25 tonne). No visible damage was observed under this load. Therefore, the cyclic load was increased and applied zero to 588 kN (60 tonne). The deck slab failed after an additional 23,162 cycles under a cyclic load of zero to 588 kN (60 tonne).

6.3.1 Deflection behaviour in Segment A (Steel)

The deflection at the center of the deck slab was recorded at different cycles under 245 kN (25 tonne) and 588 kN (60 tonne) load levels. The deflection of various cycles under these loads is shown in Fig. 6.13. The load-deflection results indicate a change in the stiffness of the structure with the increasing number of load cycles. Similar load-deflection behaviour has been reported by Selvadurai and Bakht (1995) and Youn and Chang (1998).

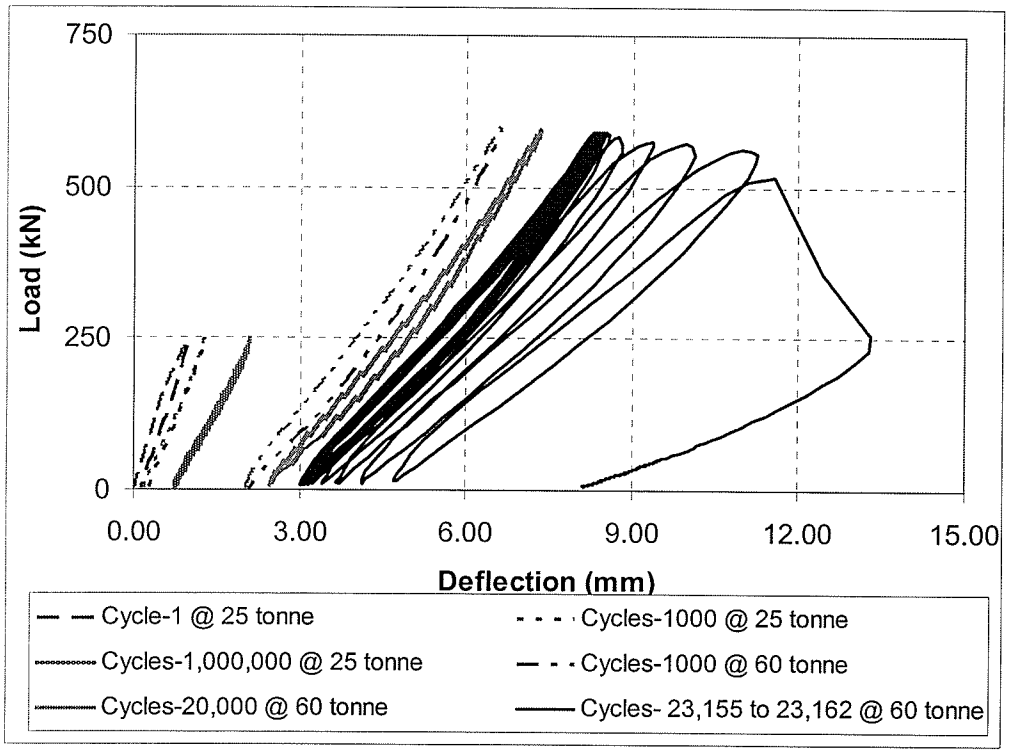

Fig. 6.13: Load-deflection behaviour under 25 and 60 tonne (Segment A)

The deflection along with the increasing number of cycles was measured at the center of the Segment A, as shown in Fig. 6.14. This figure shows the complete deflection behaviour with the increasing number of cycles, but the behaviour under 60 tonne cyclic load is not clearly shown. The deflection behaviour under 60 tonne load level is shown in Fig. 6.15.

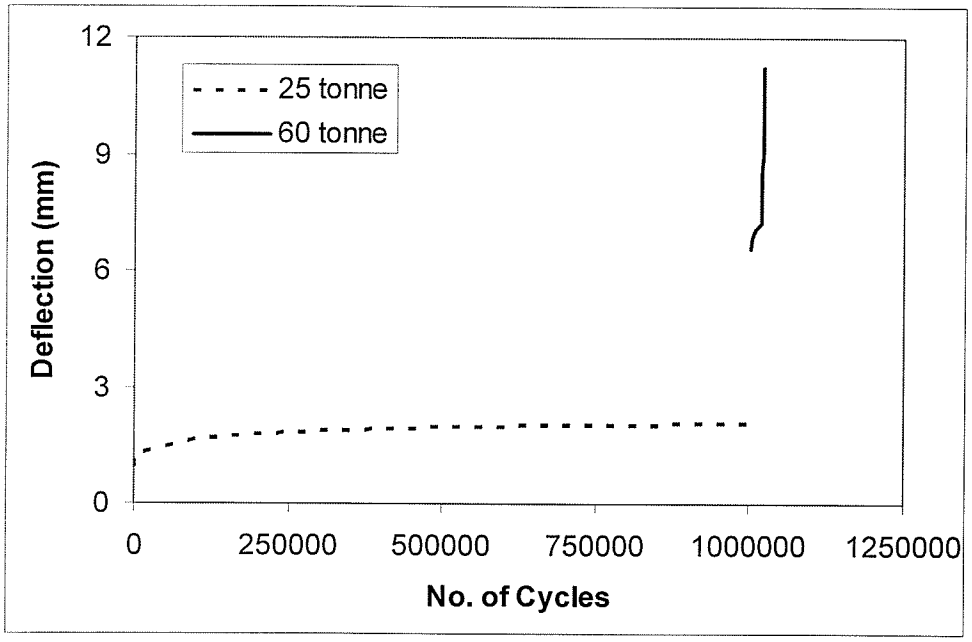

Fig. 6.14: Deflection behaviour under 25 and 60 tonne (Segment A)

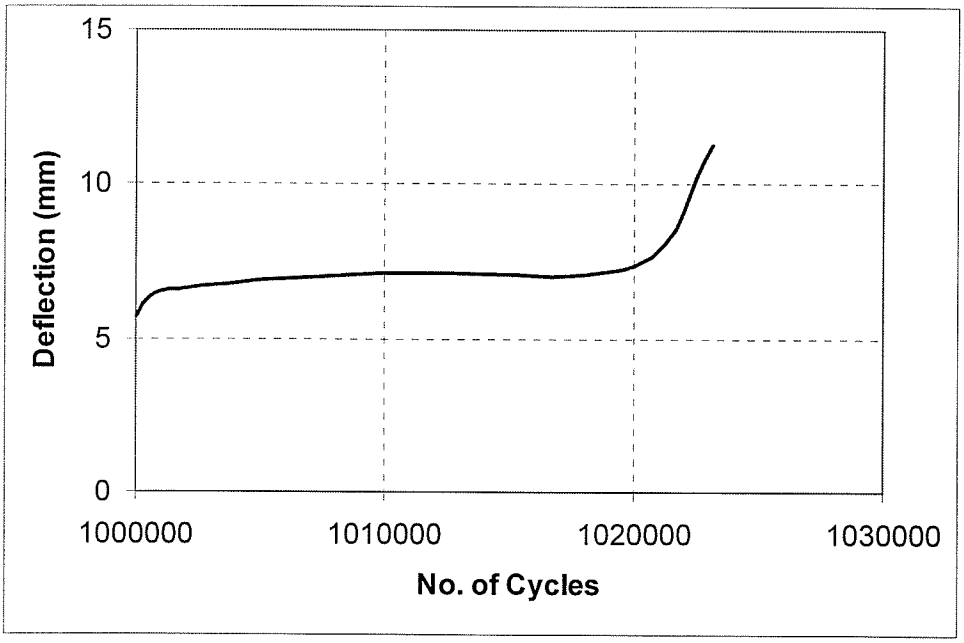

Fig. 6.15: Deflection behaviour under 60 tonne (Segment A)

Fig. 6.14 demonstrates that the significant increase in the deflection, when specimen deck slab completed 1,000,000 cycles. This increased in the deflection due to the increase in the applied cyclic load 25 to 60 tonne. Fig. 6.15 shows clearly that after the specimen deck slab completed 1,020,000 cycles, the deflection increased abruptly, followed by punching shear failure at 1,023,162 cycles (Fig. 6.16).

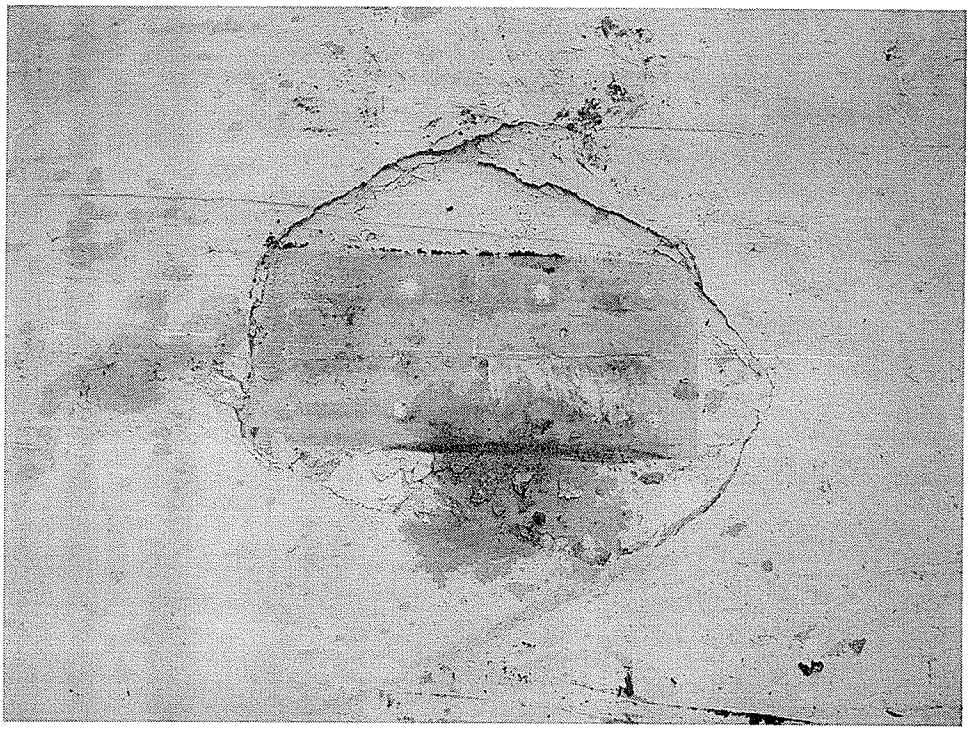

Fig. 6.16: Punching shear failure mode (Segment A)

To measure the profile of the deflection of the Segment A, five LVDTs were used, as shown in Fig. 6.11. This figure shows that the LVDTs were located at mid-span and on all four sides of the specimen deck slab on both the transverse and longitudinal centerline. The profiles of the deflection in the transverse and longitudinal directions with respect to the increasing the number of cycles are shown in Fig. 6.17 and Fig. 6.18 respectively. In the transverse direction, the center-to-center distance between

the two steel girders was 2000 mm. The LVDTs were mounted at mid-span of Segment A and at 750 mm on either side from mid-span, as shown in Fig. 6.11. The symmetric profile in the transverse direction was found, and it was as expected (Fig. 6.17). The distance in the longitudinal direction was 3000 mm. The LVDTs were mounted at 600, 1500 and 3000 mm from the edge of the beam end. The deflection on one side was smaller as expected due to the edge beam, (Fig. 6.18).

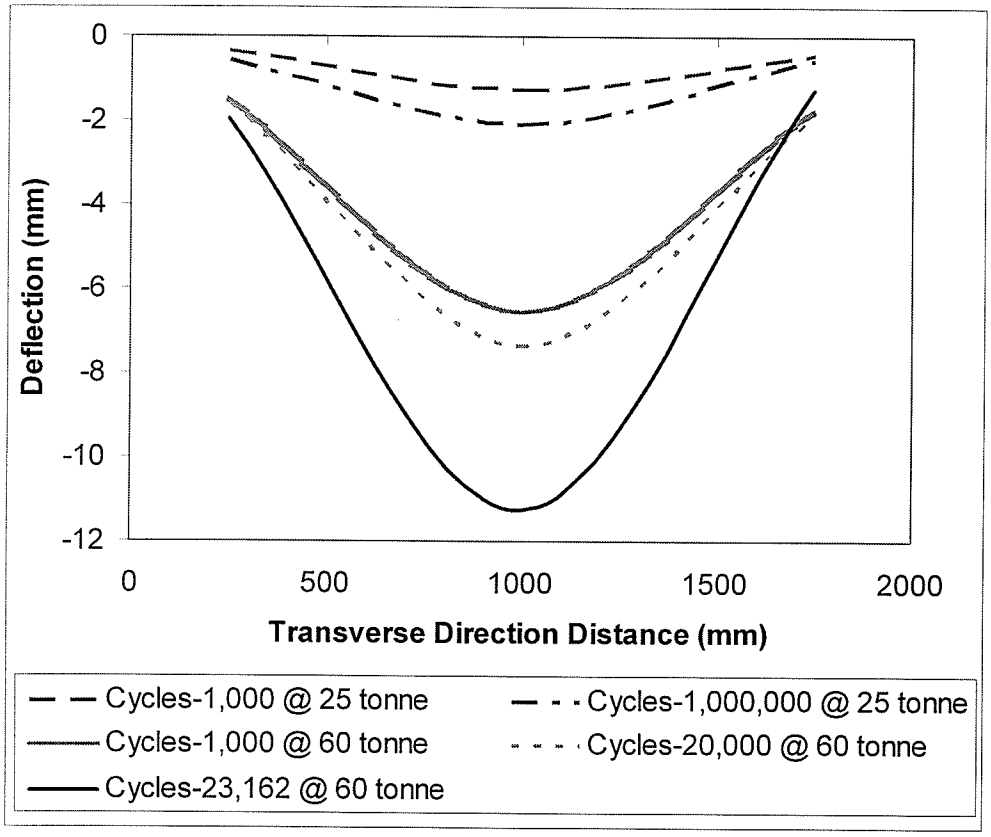

Fig. 6.17: Deflection profile along transverse direction at different no. of cycles (Segment A)

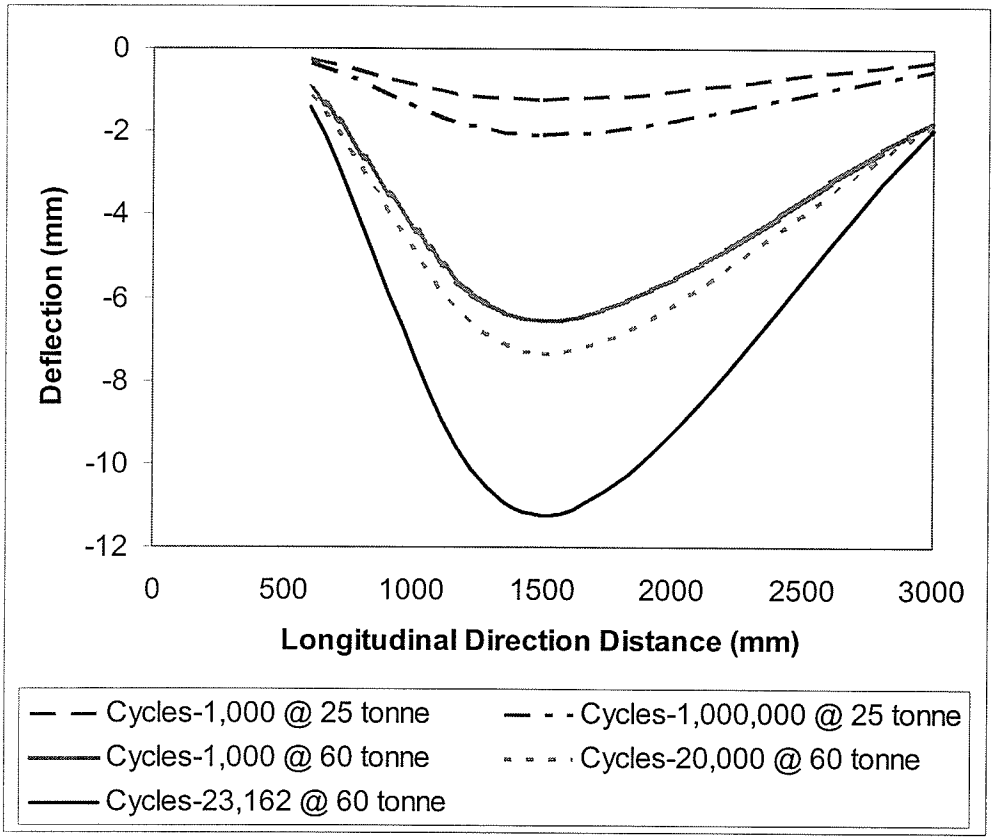

Fig. 6.18: Deflection profile along longitudinal direction at different no. of cycles (Segment A)

6.3.2 Strain behaviour in Segment A (Steel)

To monitor the performance of steel rebar in Segment A, an electrical resistance strain gauge was used on some of the steel rebar in both the transverse and longitudinal directions. The maximum response was measured under the applied cyclic load. The strain behaviour of bottom transverse rebar under applied cyclic loads is shown in Fig. 6.19. This figure is not clearly shown the strain behaviour under 60 tonne cyclic load. The strain behaviour under 60 tonne cyclic load is shown in Fig. 6.20. The strain profile of bottom transverse rebar along longitudinal direction of different number of cycles at 25 and 60 tonne cyclic load are shown in Fig. 6.21.

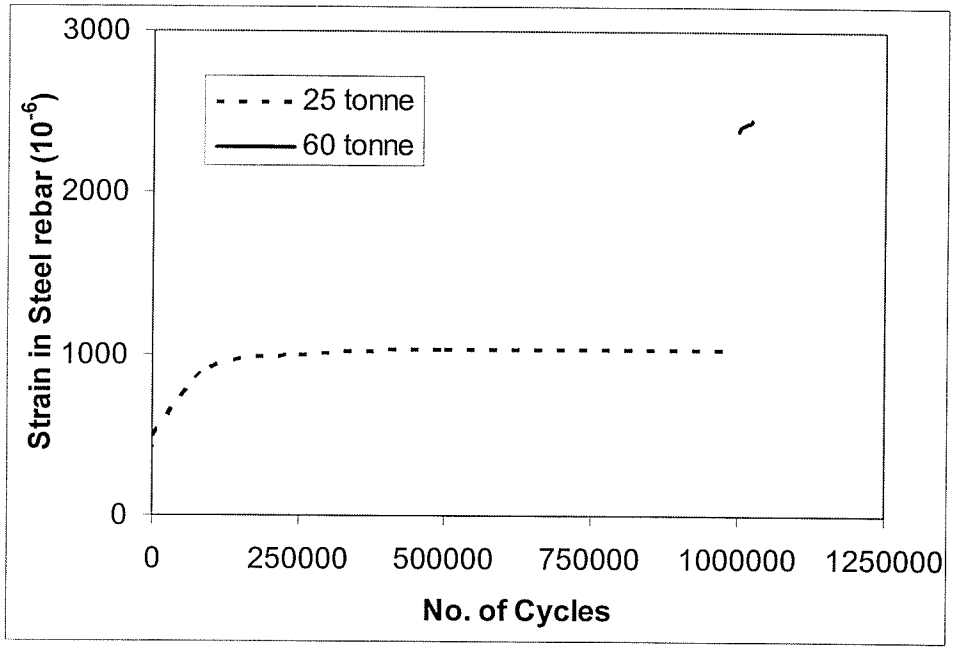

Fig. 6.19: Strain behaviour from bottom transverse rebar under 25 and 60 tonne (Segment A)

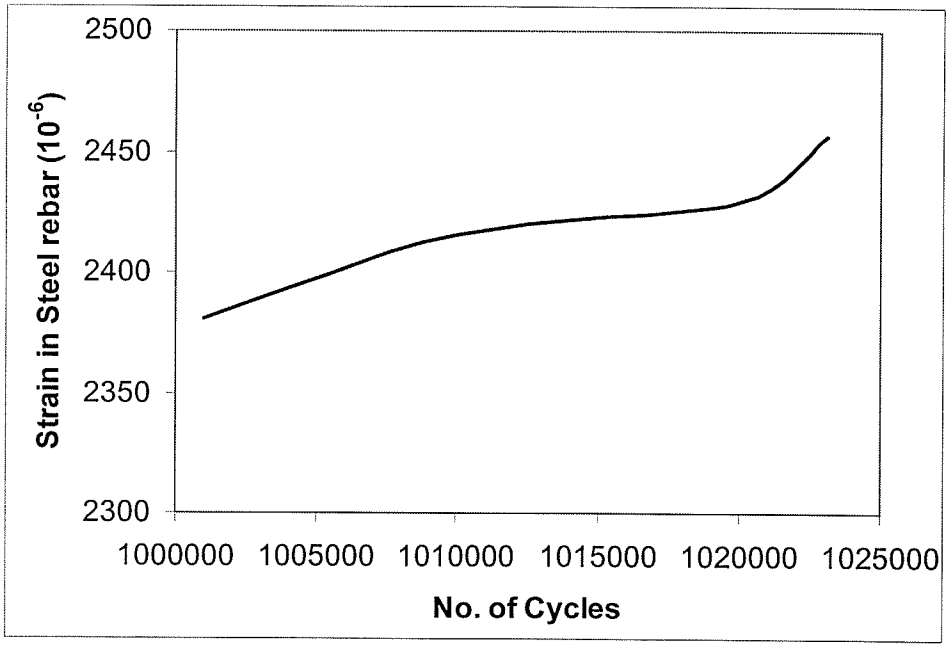

Fig. 6.20: Strain behaviour under 60 tonne (Segment A)

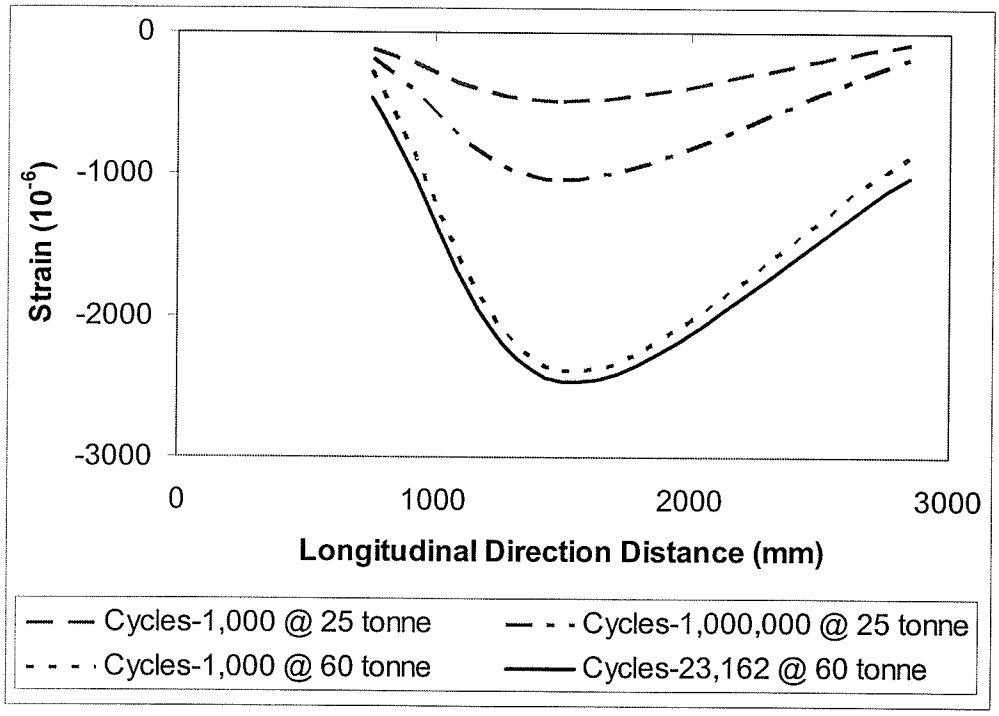

Fig. 6.21: Strain profile from bottom transverse rebar along longitudinal direction (Segment A)

6.3.3 Crack-width behaviour in Segment A (Steel)

The crack width behaviour with increasing number of cycles is shown in Fig. 6.22. This figure is not shown clearly the crack width behaviour under 60 tonne cyclic load. The crack width behaviour under 60 tonne cyclic load is shown in Fig. 6.23. These figures shown the trend is almost similar to the deflection behaviour of Segment A. These similar trends demonstrate that either crack width or deflection can be used as an indicator of damage. According to ISIS Canada Design Manual No. 3 (2001) and ACI 440.1 (2001), if the crack width is lower than 0.5 mm, then the structural member satisfies the serviceability limit. The specimen deck slab achieved the maximum crack width of 0.37 mm under a 25 tonne cyclic load after completing

1,000,000 cycles. This is clearly less than the serviceability limit of 0.5 mm and the specimen deck slab demonstrated that it has satisfied the serviceability criterion.

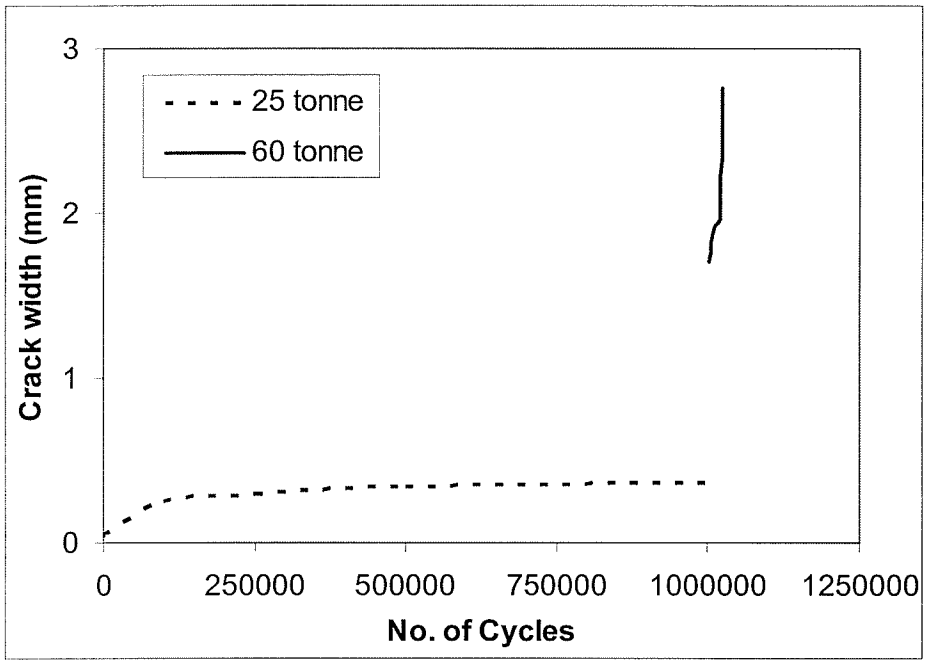

Fig. 6.22: Crack width behaviour under 25 and 60 tonne (Segment A)

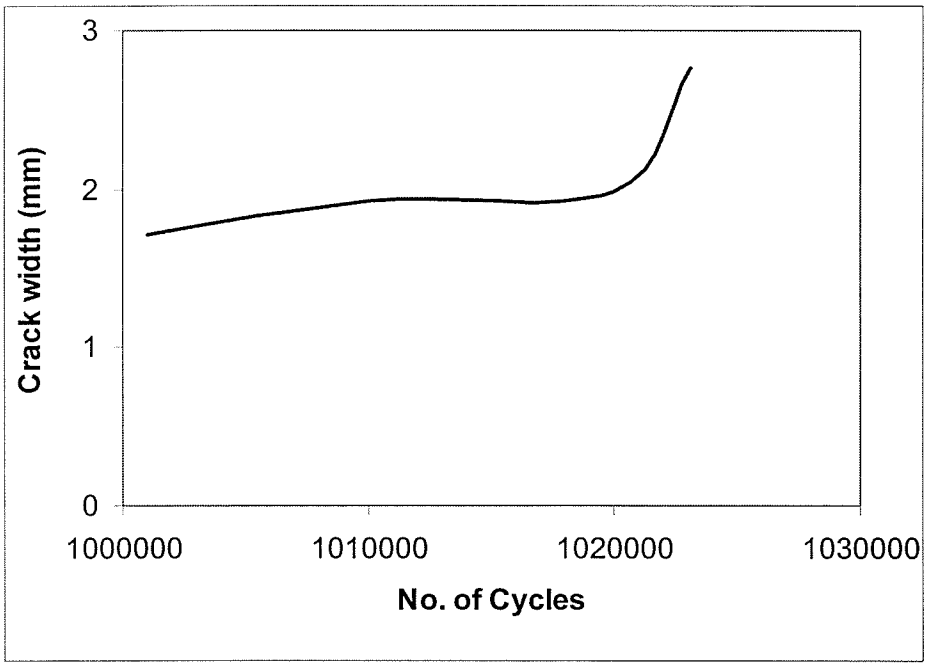

Fig. 6.23: Crack width behaviour under 60 tonne (Segment A)

6.3.4 Outward movement of steel girders behaviour in Segment A (Steel)

To monitor the outward movement of the girders of Segment A, an LMT was used, as shown in Fig. 6.12. The maximum outward movement of steel girders with an increasing number of cycles was measured under an applied load, as shown in Fig. 6.23. However this figure does not clearly depict the behaviour of outward movement of steel girders under 60 tonne cyclic load. This outward movement of steel girders under 60 tonne load is shown in Fig. 6.25. These figures clearly demonstrate that the outward movement of the girders increases continuously until failure occurs.

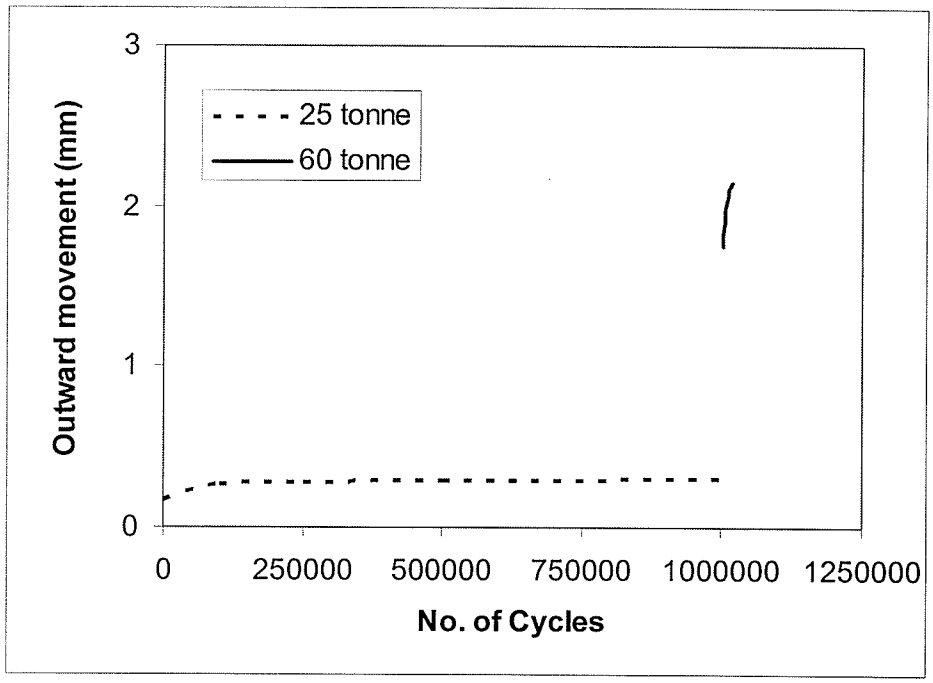

Fig. 6.24: Outward movement of girders behaviour under 25 and 60 tonne (Segment A)

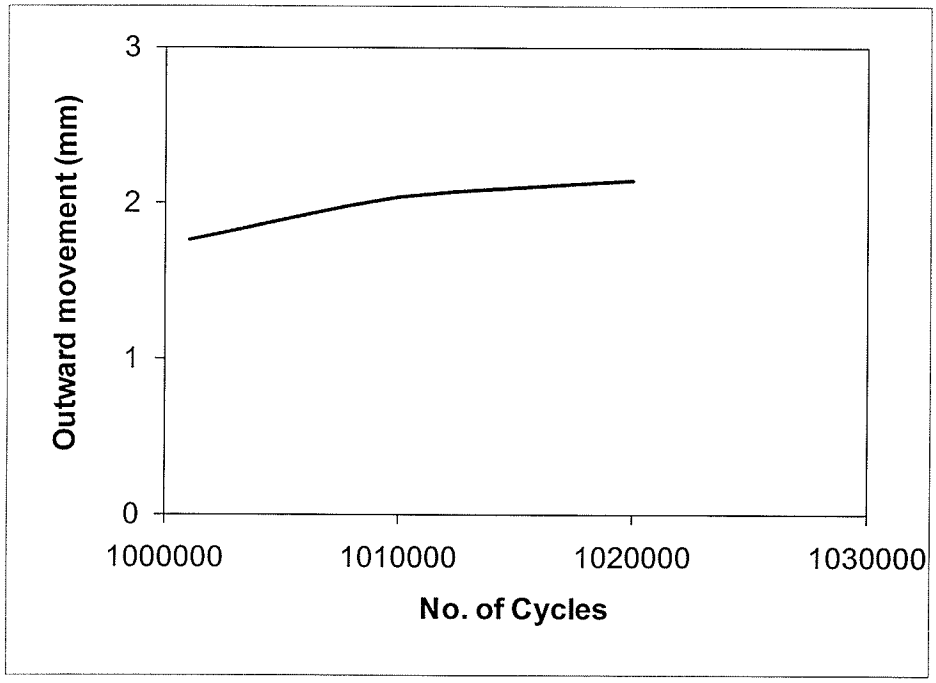

Fig. 6.25: Outward movement of girders behaviour under 60 tonne (Segment A)

6.4 Segment B (steel-free concrete deck slab with internal CFRP crack control grid and external steel straps)

Segment B is a second generation steel-free concrete deck slab containing an internal CFRP crack control grid and external steel straps, as shown in Fig. 3.3. Its fatigue behaviour was investigated under cyclic loading applied through a hydraulic actuator at load levels of 245 kN (25 tonne) and 588 kN (60 tonne). This Segment B, was not tested under 490 kN (50 tonne) cyclic load because Segment C tested under this load and it did not fail, even completed 1,000,000 cycles under 50 tonne load. Therefore it was decided to test the Segment B under cyclic load of 25 and 60 tonne load levels. A number of sensors were used to monitor the performance of the deck slab, including linear variable displacement transducers (LVDTs), strain gauges, pi-gauges and linear motion transducers (LMTs). The view of LVDTs and test setup for Segment B is shown in Fig. 6.26. The bottom view of Segment B, showing the instrumentation is

shown in Fig. 6.27. The deck slab of Segment B was subjected to 1,000,000 cycles under an applied cyclic load of zero to 245 kN (25 tonne). No visible damage was observed under this load. Therefore, the cyclic load was increased by applying a load of zero to 588 kN (60 tonne). The deck slab failed after an additional 198,863 cycles under this load.

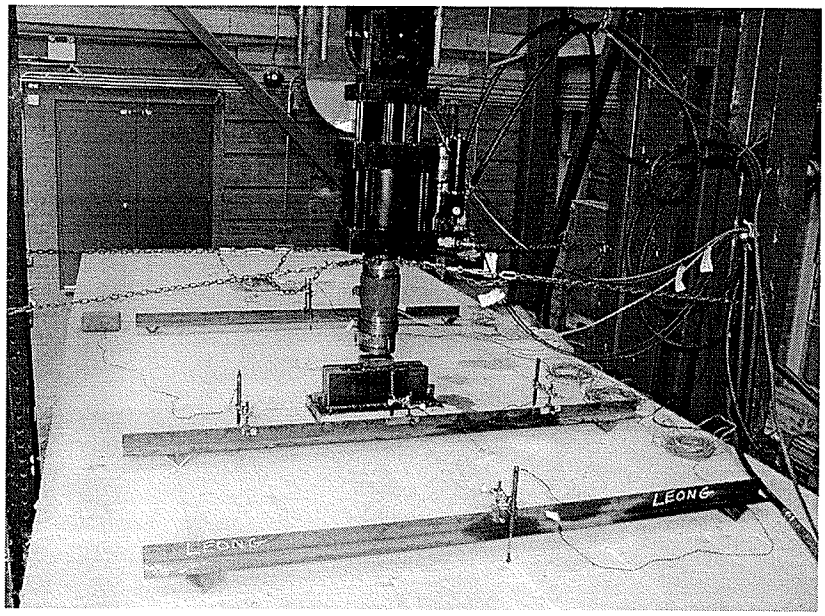

Fig. 6.26: View of LVDTs and test setup (Segment B)

The following test results of Segment B are discussed in this chapter.

1. Deflection of the deck slab at 245 kN (25 tonne) and 588 kN (60 tonne) cyclic load levels (Section 6.4.1)
2. Strains in the CFRP rebar and steel strap at 245 kN (25 tonne) and 588 kN (60 tonne) cyclic load levels (Section 6.4.2)
3. Crack width at 245 kN (25 tonne) and 588 kN (60 tonne) cyclic load levels (Section 6.4.3)

4. Outward movement of the girders at 245 kN (25 tonne) and 588 kN (60 tonne) cyclic load levels (Section 6.2.4)

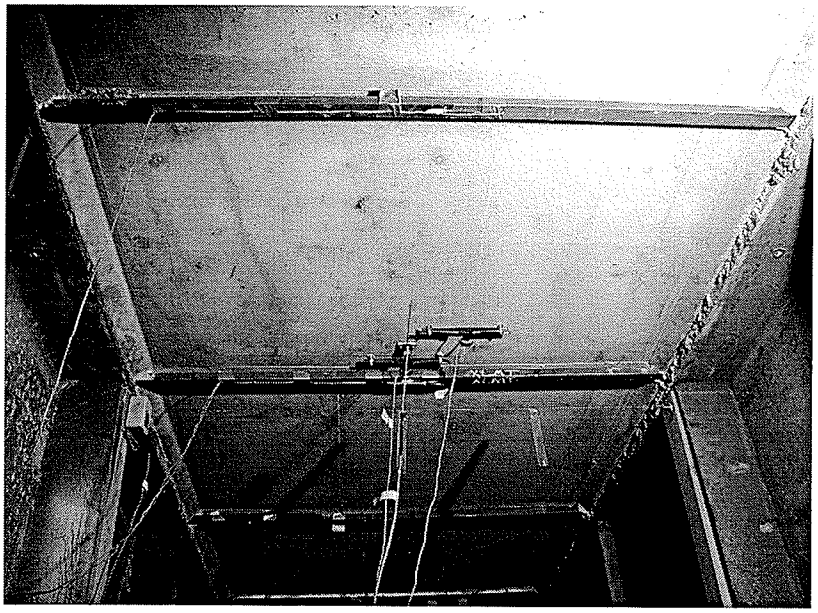

Fig. 6.27: Bottom view of Segment B and instrumentation (Segment B)

6.4.1 Deflection behaviour in Segment B (CFRP)

The deflection at the center of the deck slab was recorded at different cycles under 245 kN (25 tonne) and 588 kN (60 tonne) load levels. The deflection of various cycles under these loads is shown in Fig. 6.28. the load-deflection results indicate a change in the stiffness of the structure with the increasing number of load cycles. Similar load deflection behaviour has been reported by Selvadurai and Bakht (1995) and Youn and Chang (1998).

The deflection along with the increasing number of cycles was measured at the center of the Segment B (Fig. 6.29). However from this figure the behaviour under 60 tonne

cyclic load is not clearly shown. The deflection behaviour under 60 tonne load level is shown in Fig. 6.30. Fig. 6.29 demonstrates that deflection was increasing smoothly up to the 1,000,000 cycles. At this level, the cyclic load had been increased to 60 tonne. Fig. 6.29 clearly shows that the increased applied cyclic load resulted in a significant increase in deflection. Fig. 6.30 depicts clearly that at a 60 tonne cyclic load level the rate of increase in deflection was slow up to 1,100,000 cycles. After that the increase in deflection was rapid up to 1,150,000 cycles. The increase in the deflection continued until failure corresponding to 1,198,863 cycles. Fig. 6.30 suggest that there are three mechanism, first at low load the longitudinal cracks develop, as the load increases the radial cracks formed and gradually migrate to the top surface of the slab, finally just before failure shear cracks develop. Punching shear failure occurs, when inclined shear cracks forms the upper surface of the punch cone. The failure mode was determined the punching shear, as shown in Fig. 6.31.

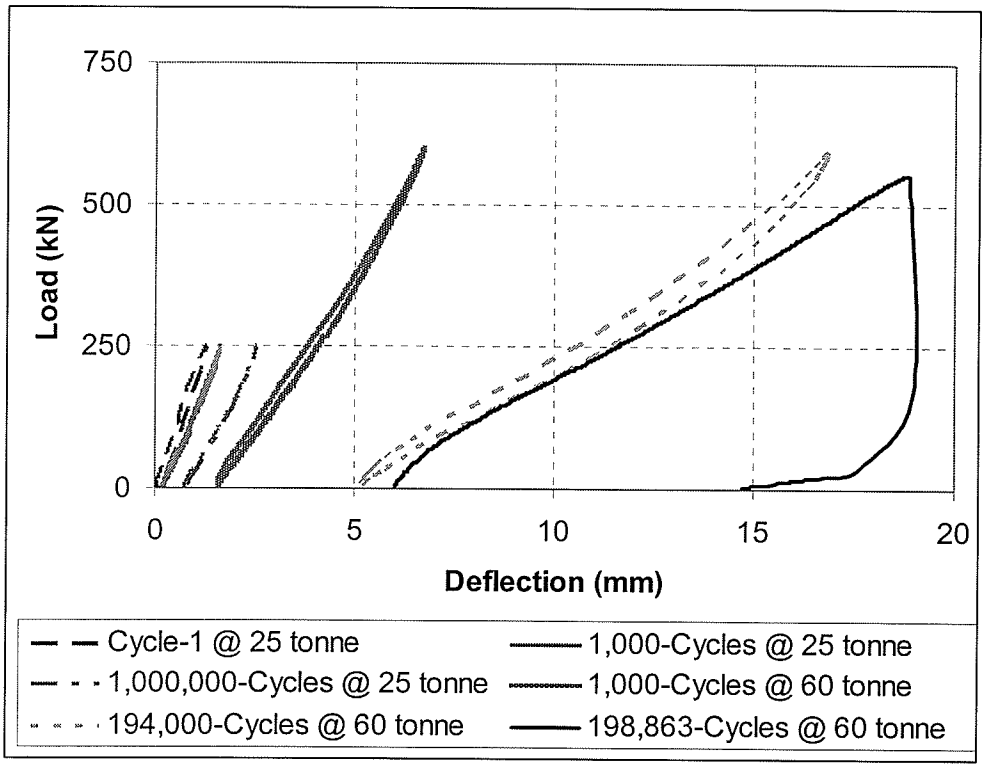

Fig. 6.28: Load-deflection behaviour under 25 and 60 tonne (Segment B)

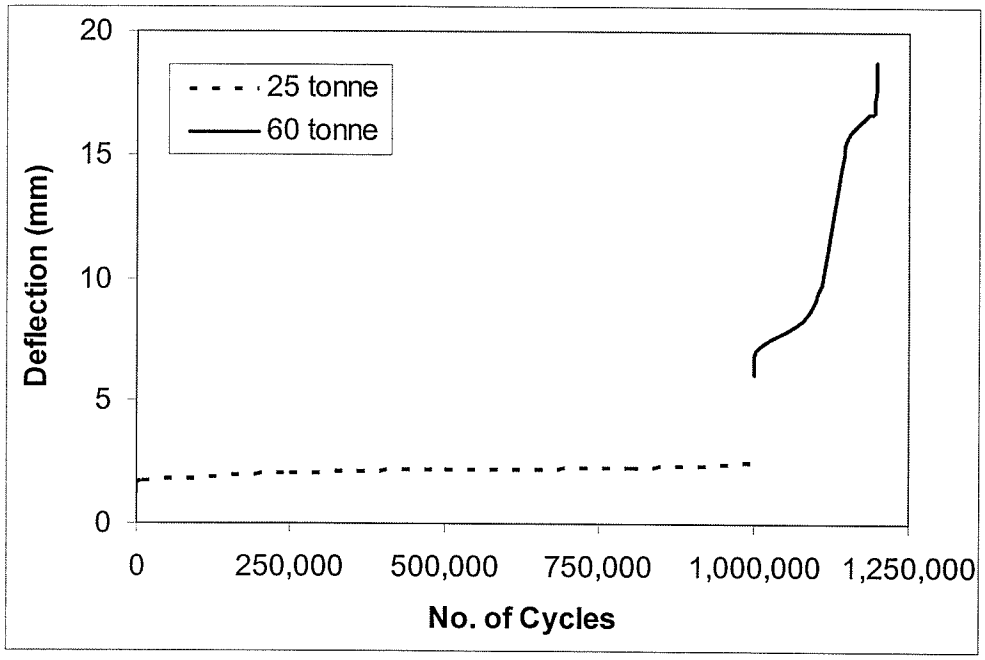

Fig. 6.29: Deflection behaviour under 25 and 60 tonne (Segment B)

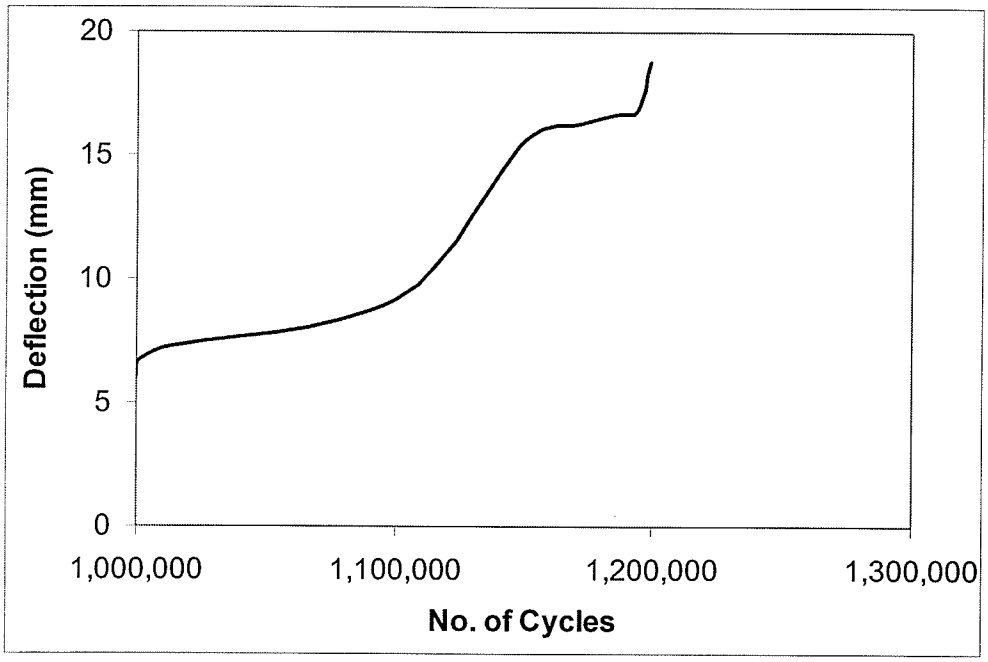

Fig. 6.30: Deflection – No. of cycles behaviour at 60 tonne load level (Segment B)

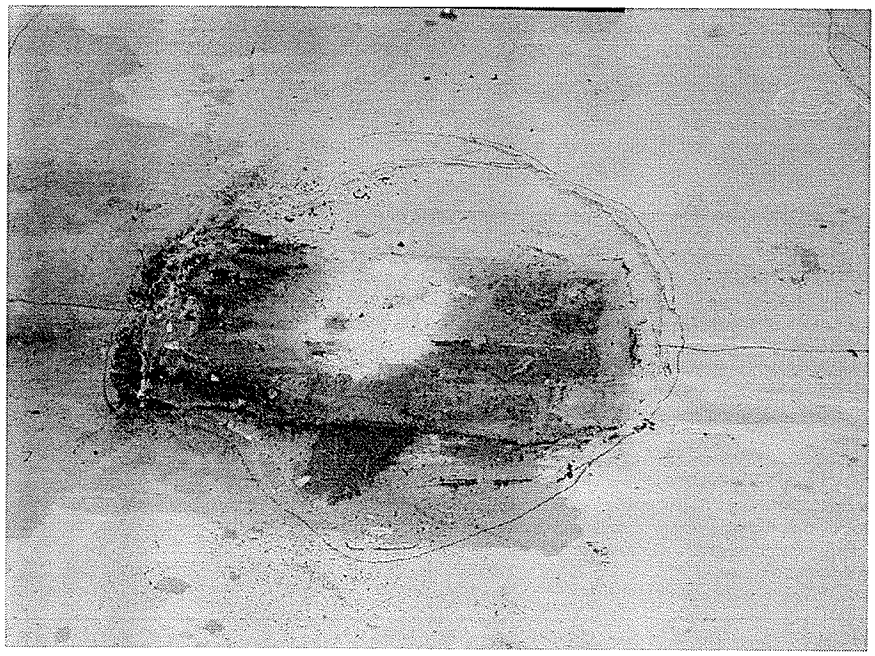

Fig. 6.31: Punching shear failure mode (Segment B)

To measure the profile of the deflection of the Segment B, five LVDTs were used (Fig. 6.26). This figure depicts that the LVDTs located at mid-span and on all four sides of the deck slab on both the transverse and longitudinal centerline. The profiles of the deflection in the transverse and longitudinal directions with respect to an increasing the number of cycles are shown in Fig. 6.32 and Fig. 6.33 respectively. In the transverse direction, the center-to-center distance between the two steel girders was 2000 mm. The LVDTs were mounted at mid-span of Segment B and at 750 mm on either side from the mid-span (Fig. 6.26). The deflection profile in the transverse direction was symmetric as expected (Fig. 6.32). The distance in the longitudinal direction was 3000 mm. The LVDTs were mounted at the mid-span of Segment B and at 1500 mm on either side of the mid-span (Fig. 6.32). The deflection profile in the longitudinal direction was determined and found to be reasonably symmetric within the experimental error (Fig. 6.33).

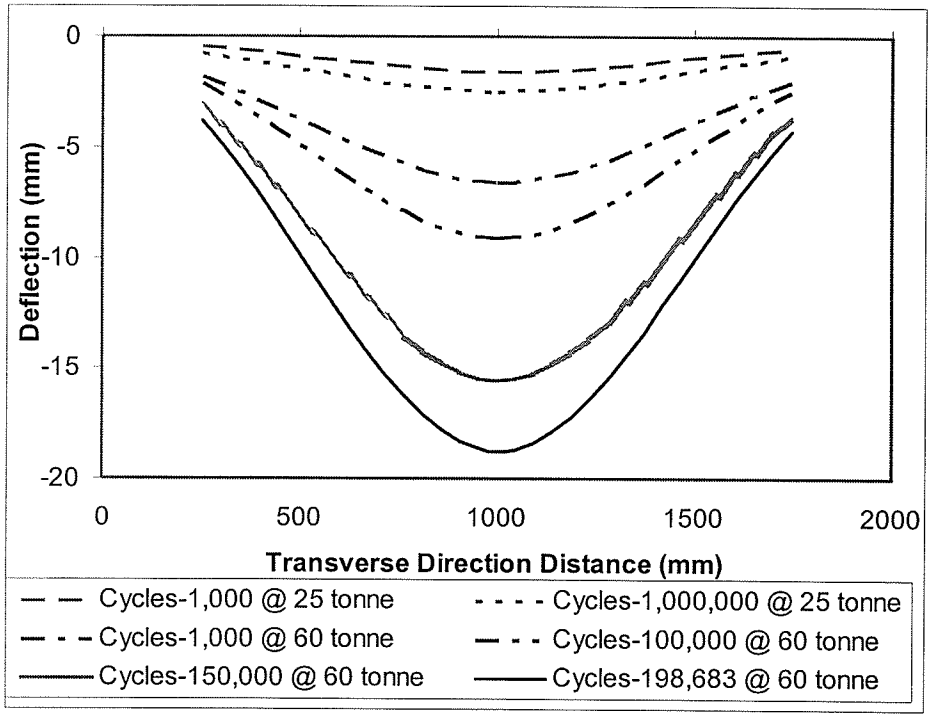

Fig. 6.32: Deflection profile along transverse direction (Segment B)

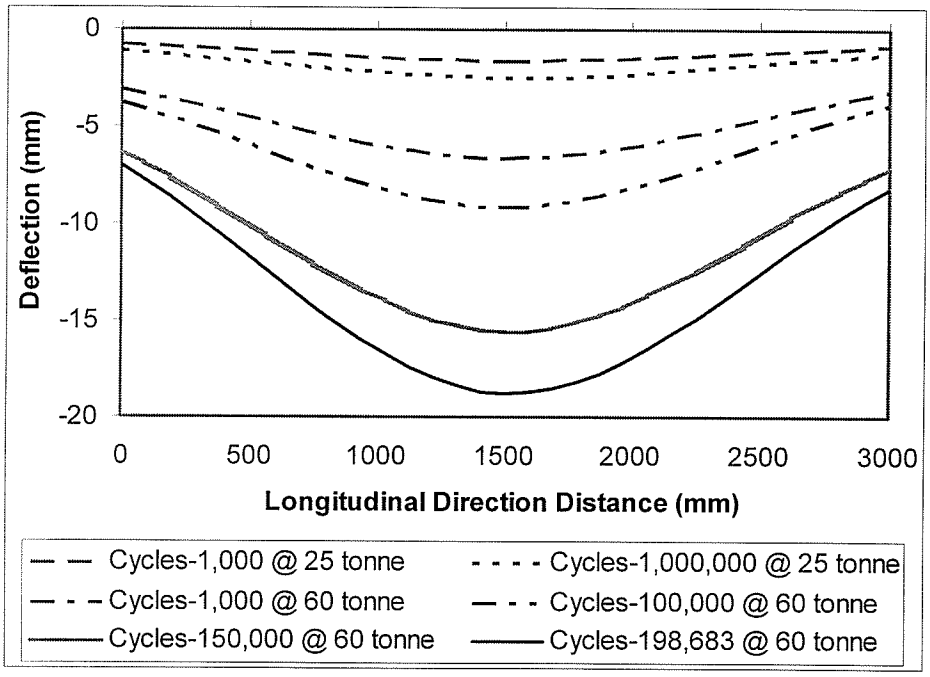

Fig. 6.33: Deflection profile along longitudinal direction (Segment B)

6.4.2 Strain behaviour in Segment B (CFRP)

To monitor the performance of the CFRP rebar and steel straps in Segment B, an electrical resistance strain gauge was mounted on every strap and on some of the rebar in both the transverse and longitudinal directions. The maximum response was measured under an applied cyclic load. The strain on the transverse rebar with increasing number of cycles under an applied cyclic load is shown in Fig. 6.34. However, this figure does not clearly show the behaviour under a 60 tonne load level. This strain behaviour under a 60 tonne cyclic load is shown in Fig. 6.35. Figures 5.6, 6.2 and 6.35 indicated that the behaviour is stabilised until nickel then rapid increase in the behaviour and finally failure occurs. The strain profile of the transverse rebar along the longitudinal direction under 25 and 60 tonne cyclic loads are shown in Fig. 6.36. The strain on the steel strap with the increasing number of cycles under an

applied cyclic load is shown in Fig. 6.37. Fig. 6.37 demonstrates that the trend is almost similar to the deflection behaviour as shown in Fig. 6.29. This indicates that either the strain in the strap or the deflection can be used as an indicator of damage.

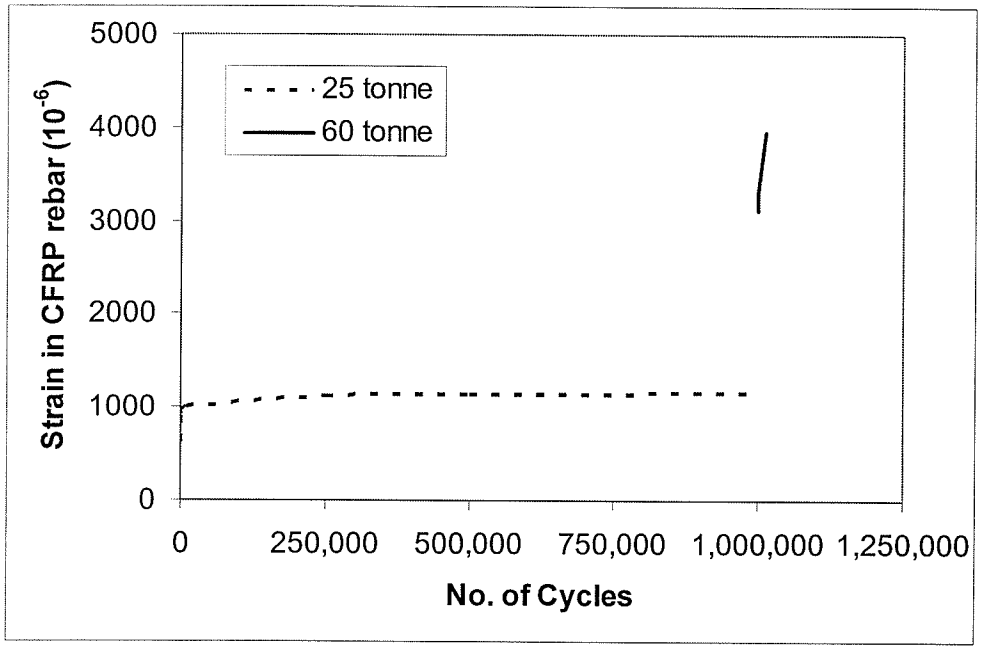

Fig. 6.34: Strain behaviour of CFRP rebar under 25 and 60 tonne (Segment B)

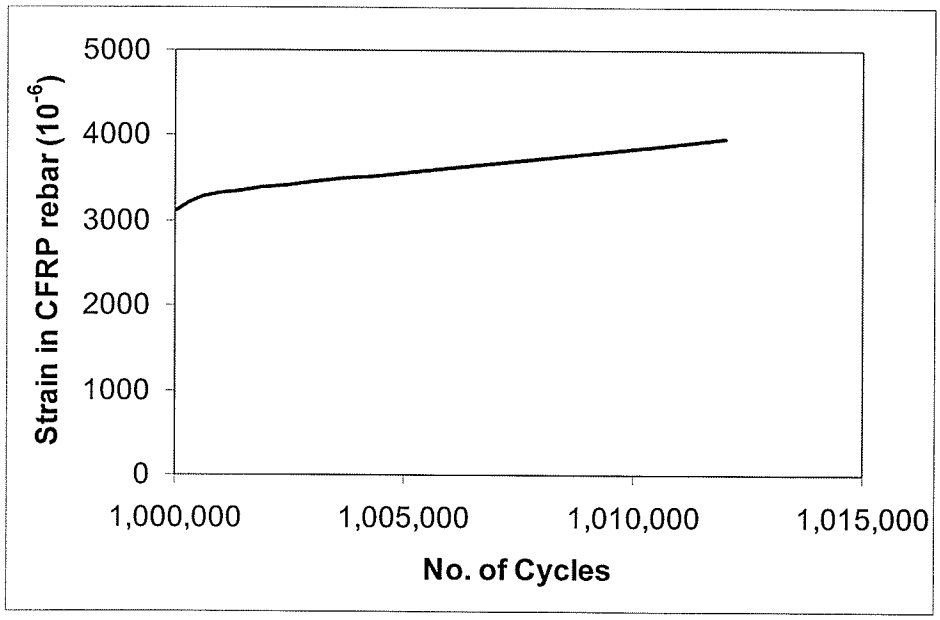

Fig. 6.35: Strain behaviour of transverse CFRP rebar under 60 tonne (Segment B)

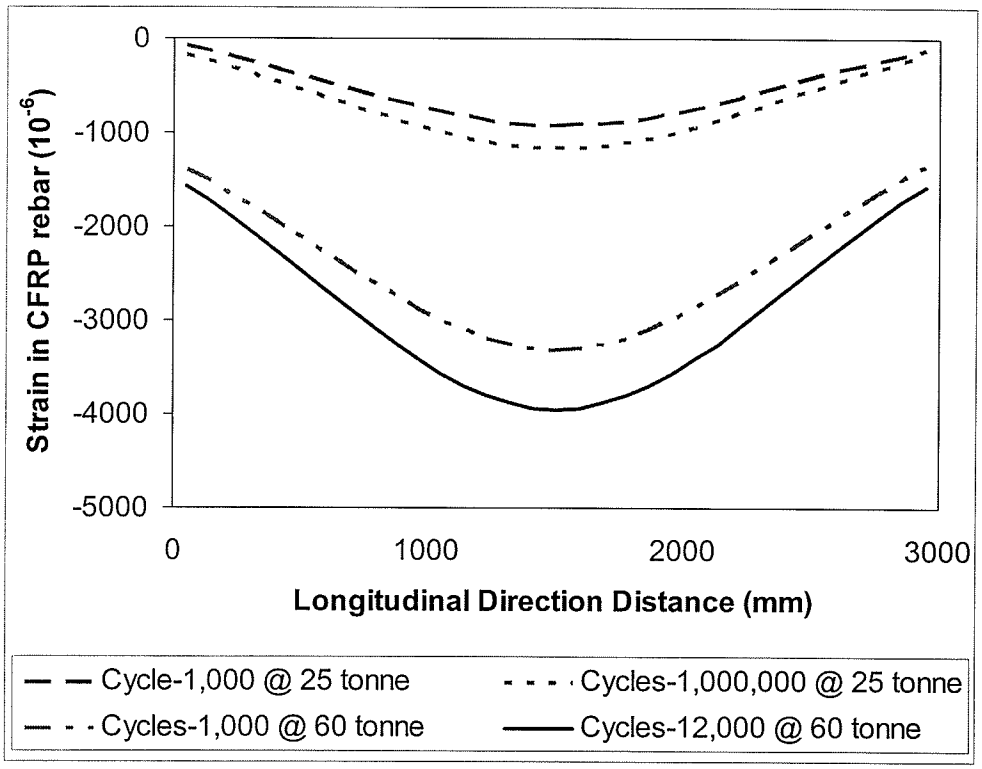

Fig. 6.36: Strain profile of transverse CFRP rebar under 25 and 60 tonne (Segment B)

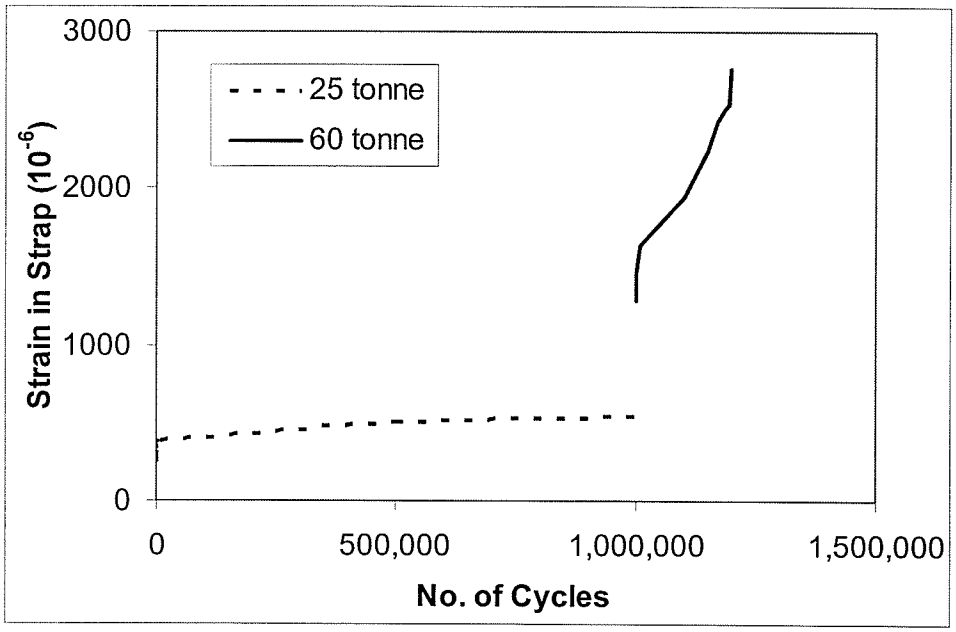

Fig. 6.37: Strain behaviour of the steel strap under 25 and 60 tonne (Segment B)

6.4.3 Crack-width behaviour in Segment B (CFRP)

To measure the crack width of Segment B, pi-gauges were used under an applied load (Fig. 6.27). The crack width behaviour with the increasing the number of cycles at 25 and 60 tonne cyclic load levels are shown in Fig. 6.38. However, this figure does not show the crack width behaviour under 60 tonne. The crack width behaviour under a 60 tonne load level is shown separately in Fig. 6.39. These figures demonstrate that trend is almost similar like deflection behaviour as shown in Figs. 6.29 and 6.30. This indicates that either the crack width or the deflection can be used as an indicator of damage. ACI Committee 440.1 (2001) reported that FRP rods are corrosion resistant; therefore the maximum crack-width limitation can be relaxed, but excessive crack width is undesirable for aesthetic and other reasons that can damage or promote the deterioration of structural concrete.

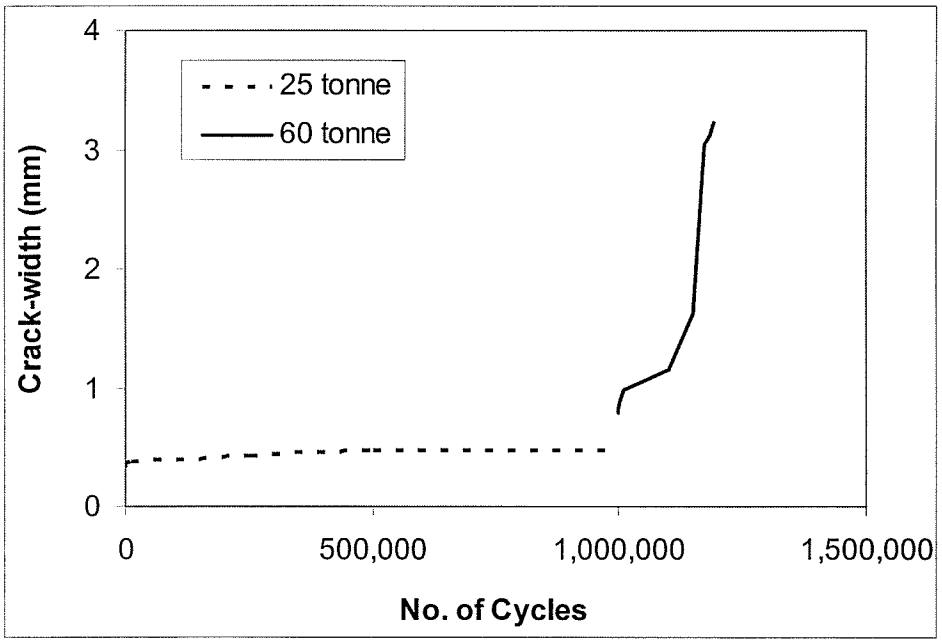

Fig. 6.38: Crack-width behaviour under 25 and 60 tonne (Segment B)

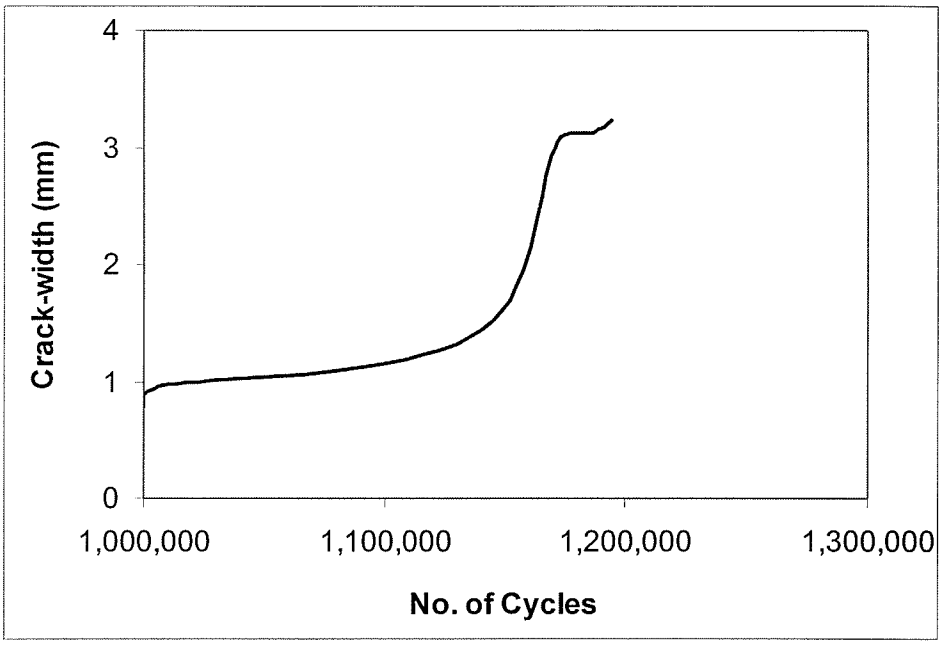

Fig. 6.39: Crack-width behaviour under 60 tonne (Segment B)

6.4.4 Outward movement behaviour in Segment B (CFRP)

To monitor the outward movement of the girders in Segment B, an LMT was used (Fig. 6.27). The outward movement of steel girders with an increasing number of cycles was measured under an applied load, as shown in Fig. 6.40. However, this figure does not clearly show the behaviour under 60 tonne. The outward movement of girders behaviour under a 60 tonne is shown in Fig. 6.41. These figures clearly demonstrate that the trend is shown identical to that shown in the crack width. This means that similar trends can be used as indicators of damage.

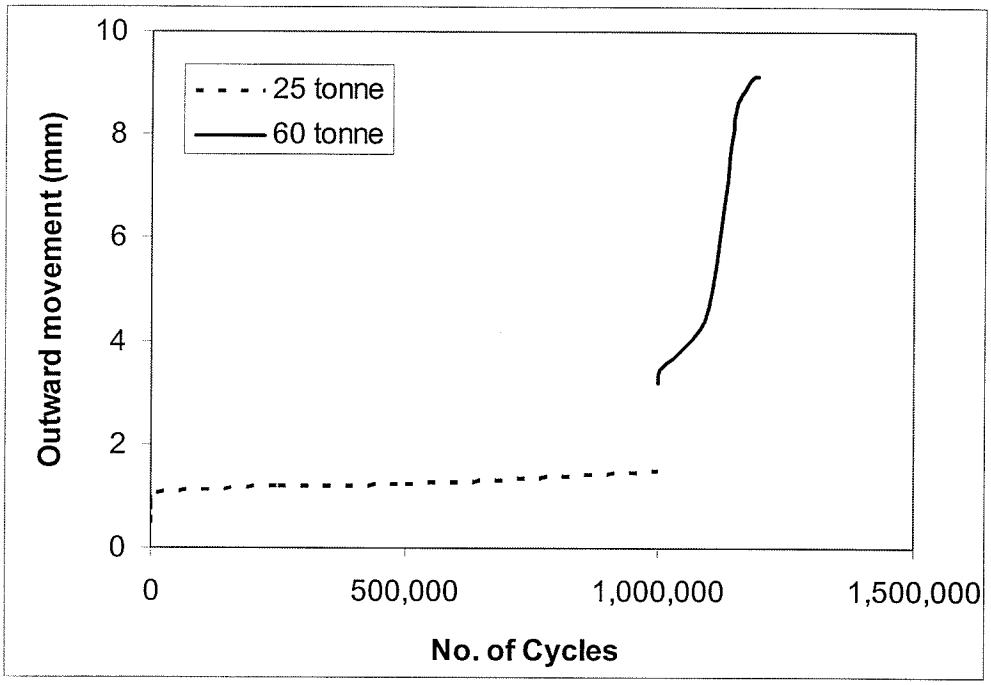

Fig. 6.40: Outward movement of girders behaviour under 25 and 60 tonne (Segment B)

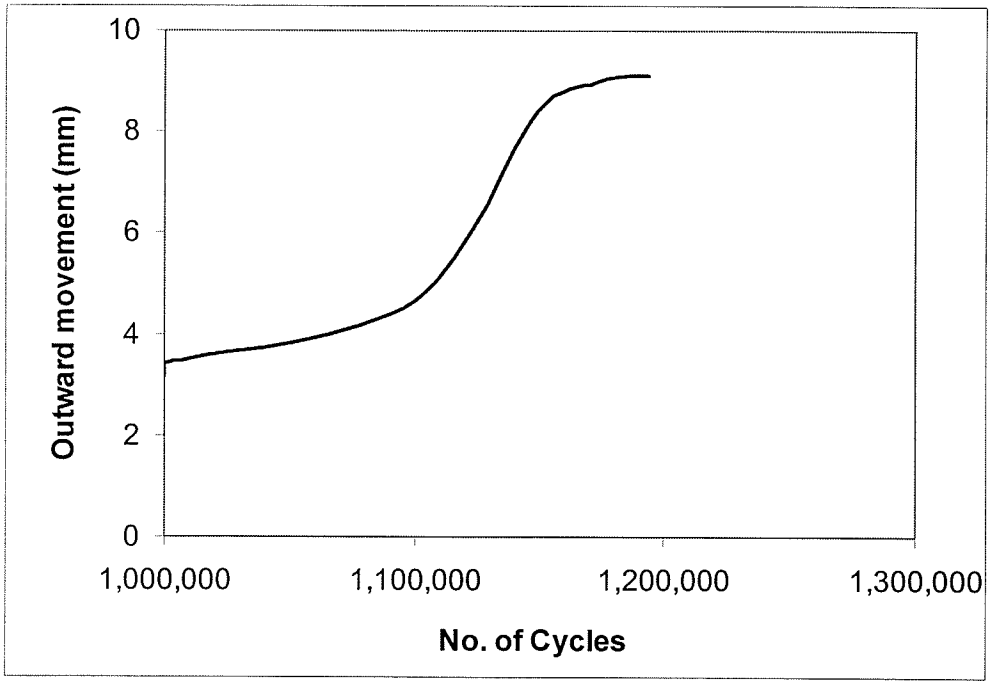

Fig. 6.41: Outward movement of girders behaviour under 60 tonne (Segment B)

6.5 Fatigue Performance Comparison of Segments A, B and C

The fatigue performance of all three segments A, B and C was compared under a 245 kN (25 tonne) and 588 kN (60 tonne) load levels for deflection, strain, and crack width are discussed in this chapter.

1. Deflection comparison of segments A, B and C under a 245 kN (25 tonne) and 588 kN (60 tonne) load levels (Section 6.5.1)
2. Strain comparison of segments A, B and C under a 245 kN (25 tonne) and 588 kN (60 tonne) load level (Section 6.5.2)
3. Crack width comparison of segments A, B and C under a 245 kN (25 tonne) and 588 kN (60 tonne) load levels (Section 6.5.3)

6.5.1 Deflection comparison of Segments A, B and C

The deflection comparison of segments A, B and C along with the increasing number of cycles under a 25 tonne load levels is drawn in log scale (Fig. 6.42). This Fig. 6.42 demonstrates that, the deflections of all three segments A, B and C are comparable. The maximum deflection was approximately 2 mm, when all segments A, B and C completed 1,000,000 cycles under a cyclic load of peaked to 25 tonne. Segment C was tested under a cyclic load of 50 tonne and completed another 1,000,000 cycles and the deflection was found approximately 7.43 mm (Fig. 6.43). Segments A and B were not tested under a cyclic load of 50 tonne. Thus to make the comparison between the segments correction in deflection was applied. The deflection value at 100 cycles under a cyclic load zero to 50 tonne was deducted from the deflection value at 1,000,000 cycles under a cyclic load of zero to 25 tonne (Fig. 6.44). The deflection comparison of all segments A, B and C under a cyclic load of zero to 60 tonne is

drawn in log scale (Fig. 6.45). This Fig. 6.45 depicts that all segments achieved the comparable deflection.

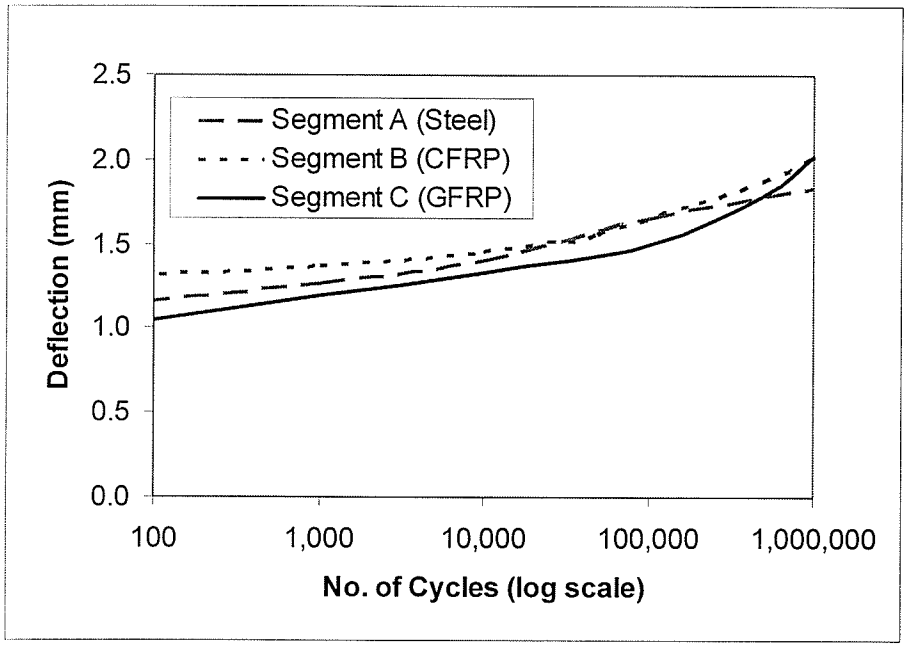

Fig. 6.42: Deflection behaviour of segments A, B and C under 25 tonne

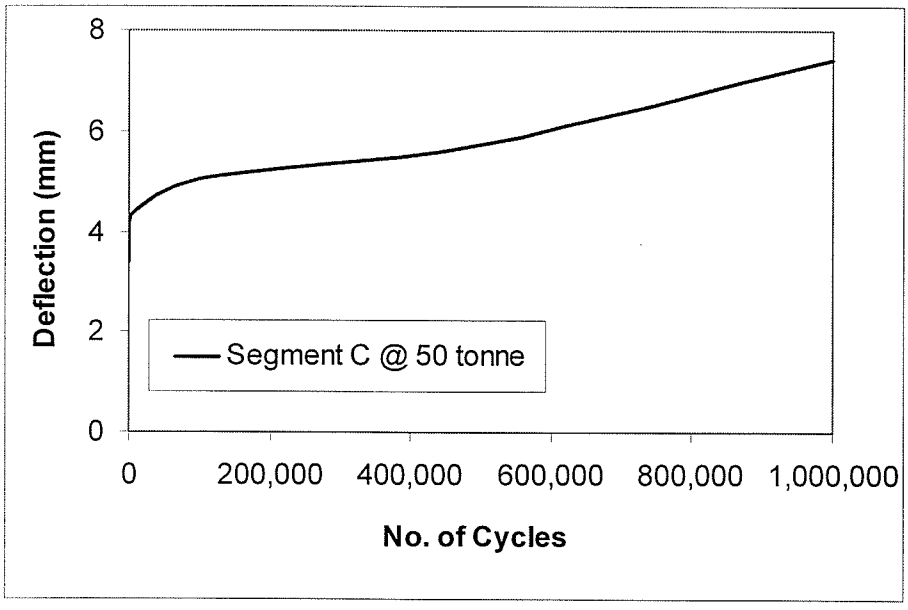

Fig. 6.43: Deflection behaviour of Segment C under 50 tonne

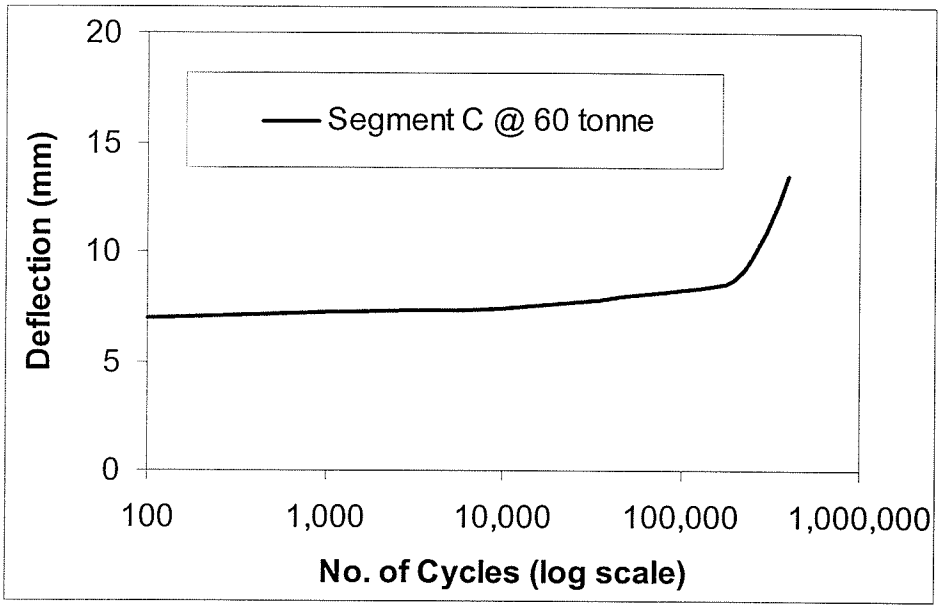

Fig. 6.44: Deflection behaviour of Segment C under 60 tonne

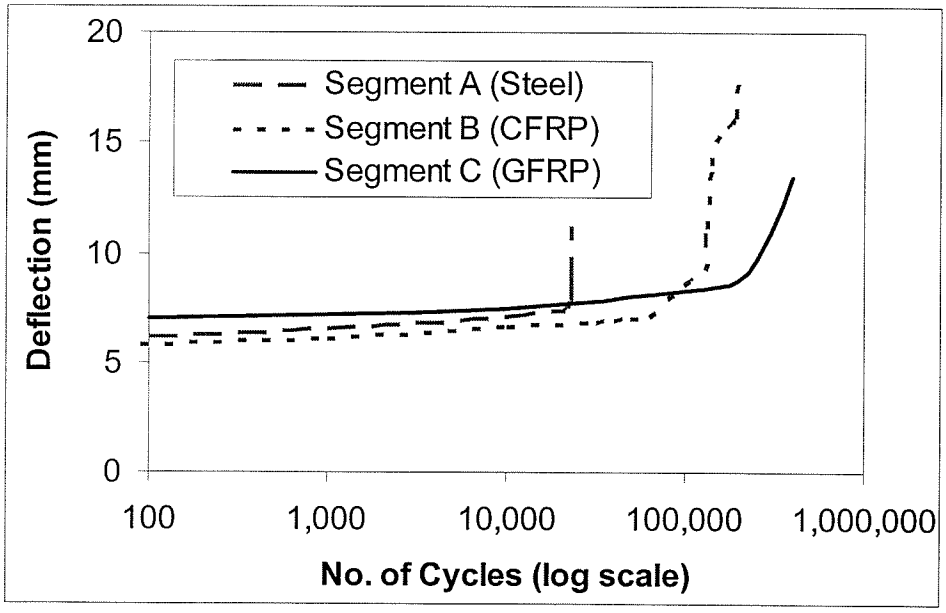

Fig. 6.45: Deflection behaviour of segments A, B and C under 60 tonne

6.5.2 Reinforcement and steel strap strain comparison of segments A, B and C

The strain comparison of segments A, B and C along with the increasing number of cycles under a cyclic load peaked to 25 and 60 tonne is drawn in log scale (Figs. 6.46(a), 6.46(b) and 6.47). These figures demonstrate that, the strain values of all three segments are lower than 1200 (10^{-6}). Thus all three segments A, B and C satisfied the serviceability criterion. Fig. 6.47 clearly indicates that CFRP and GFRP achieved the strain values approximately 1200 (10^{-6}), which are less than serviceability strain 2000 (10^{-6}). Thus the area of CFRP and GFRP can be reduced up to 40%.

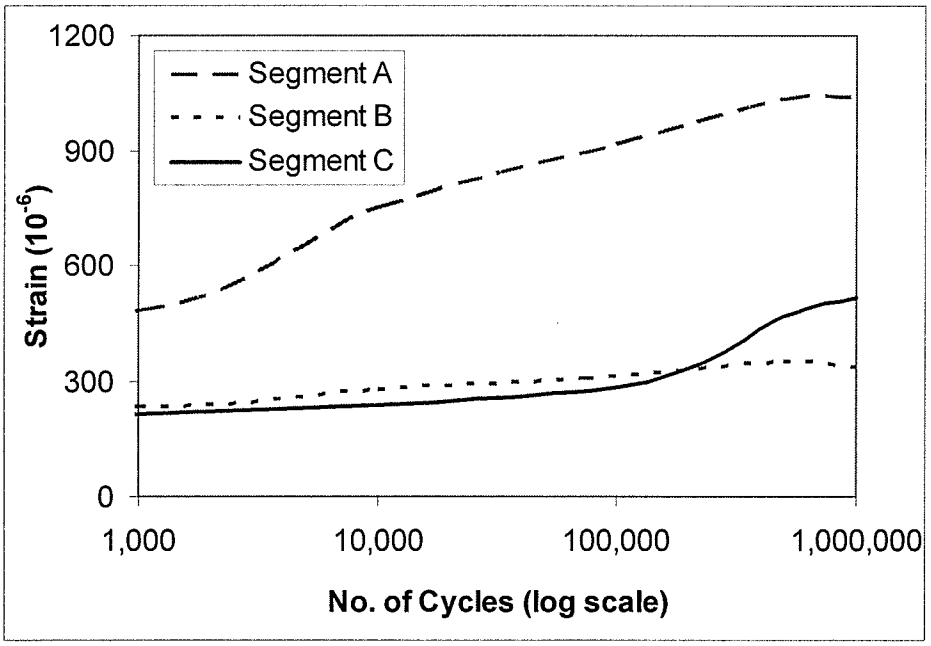

Fig. 6.46(a): Steel reinforcement (Segment A) and steel strap strain (Segments B & C) behaviour under 25 tonne

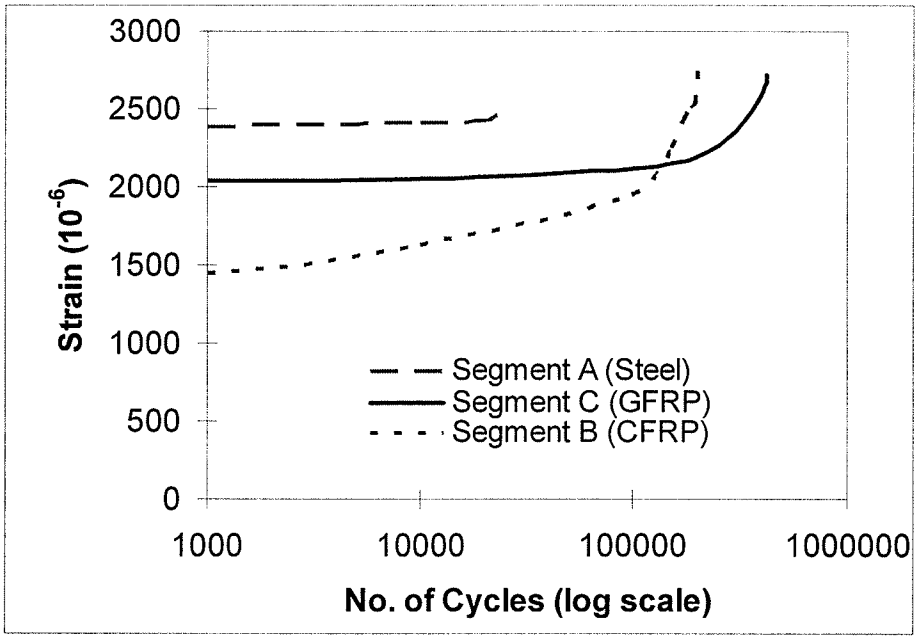

Fig. 6.46(b): Steel reinforcement (Segment A) and steel strap strain (Segments B & C) behaviour under 60 tonne

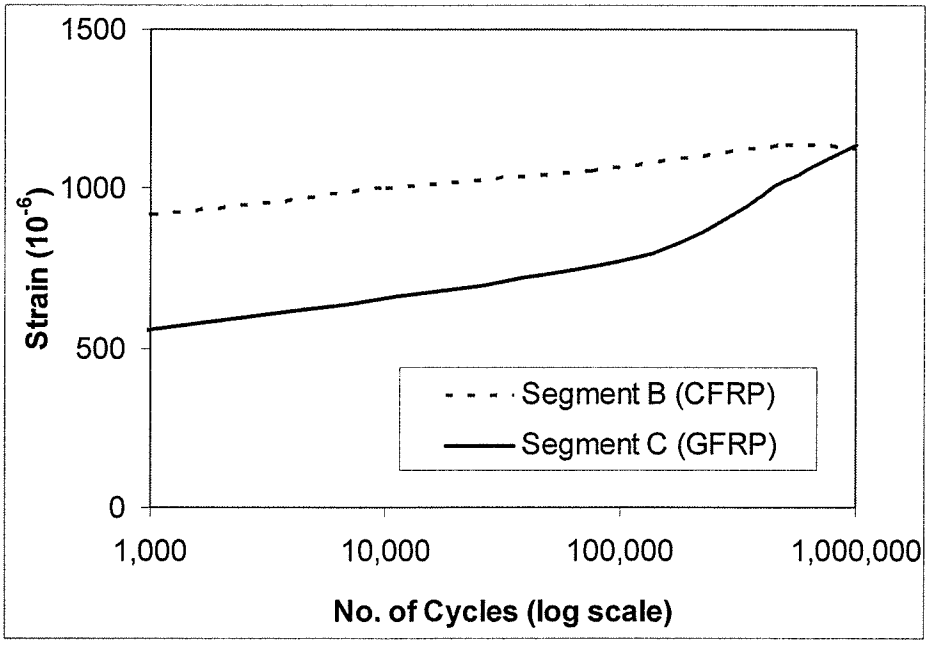

Fig. 6.47: Strain behaviour of CFRP and GFRP under 25 tonne

6.5.3 Crack width comparison of segments A, B and C

The crack widths comparison of segments A, B and C along with the increasing number of cycles under a 25 tonne load levels is drawn in log scale (Fig. 6.48). This Fig. 6.48 demonstrates that, the crack widths of all three segments A, B and C are comparable and less than the serviceability limit (0.5 mm). The maximum crack width was found approximately 0.4 mm, when all segments A, B and C completed 1,000,000 cycles under a cyclic load peaked to 25 tonne. Thus all three segments satisfied serviceability criterion. Segment C was tested under a cyclic load peaked to 50 tonne and completed another 1,000,000 cycles and the crack width was found approximately 0.94 mm (Fig. 6.49). The crack width comparison of all segments A, B and C under a cyclic load peaked to 60 tonne is drawn in log scale (Fig. 6.50). This Fig. 6.50 depicts that, the crack widths of segments B and C are less than 1 mm and comparable up to the 100,000 cycles. Segment A has a crack width of approximately 2 mm at approximately 20,000 cycles.

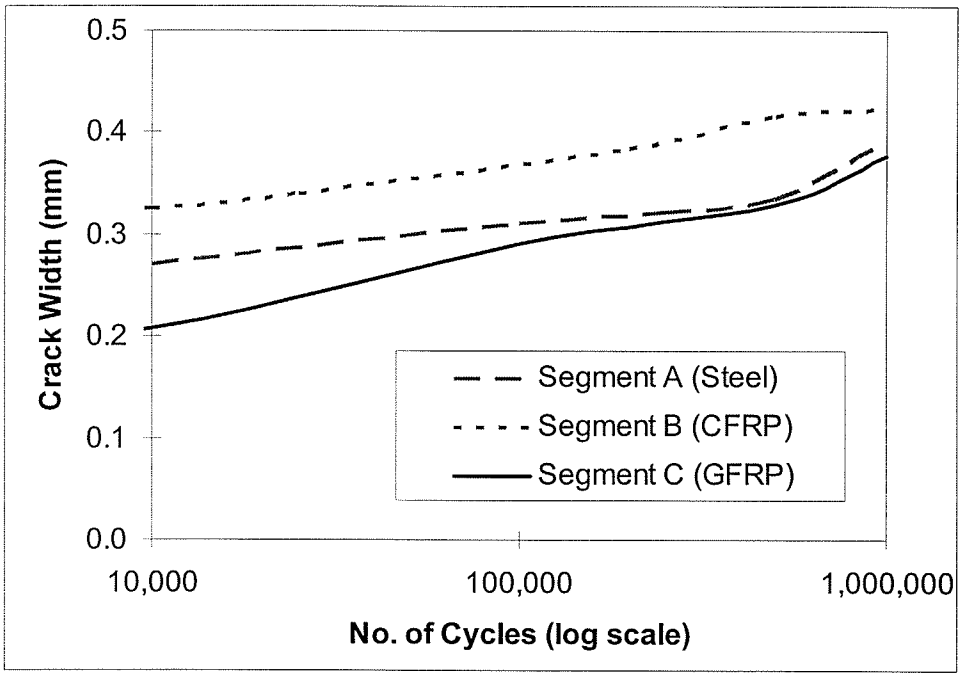

Fig. 6.48: Crack width behaviour of segments A, B and C under 25 tonne

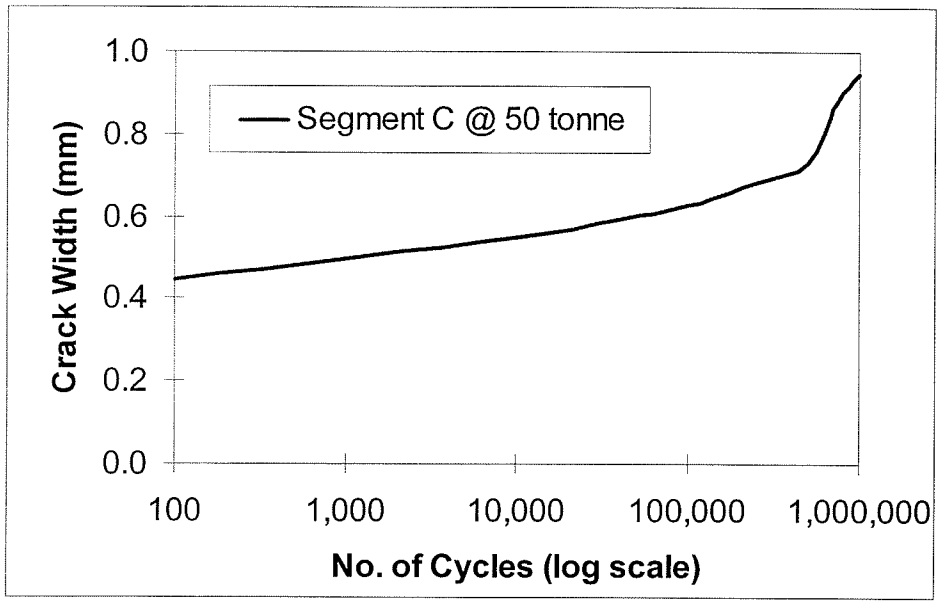

Fig. 6.49: Crack width behaviour of Segment C under 50 tonne

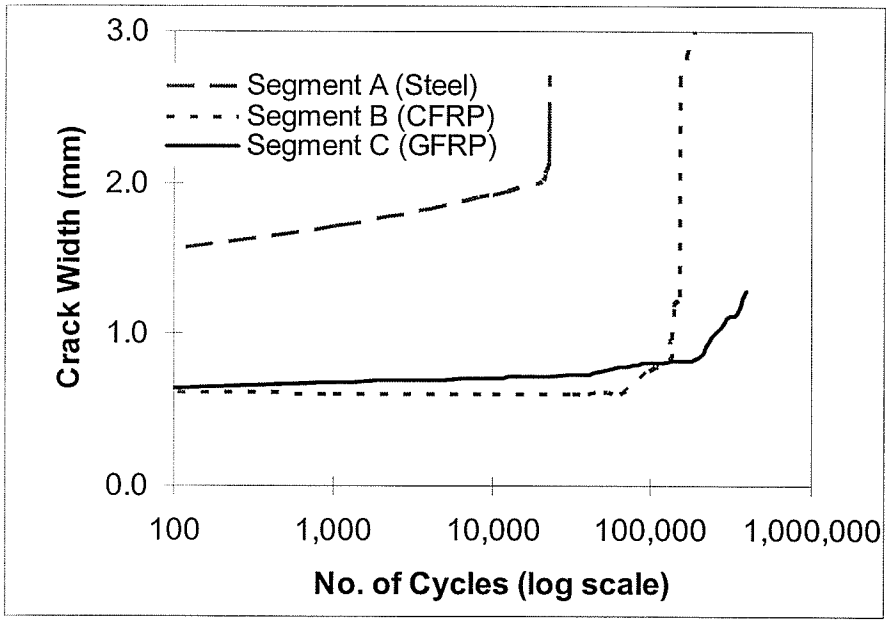

Fig. 6.50: Crack width behaviour of segments A, B and C under 60 tonne

Chapter 7

Estimate of the Fatigue Strength of Steel-Free Deck Slab

7.1 General

The goal of this research is to develop P-N Curves that can estimate the fatigue strength of steel-free concrete bridge deck slabs. In this regard, tests were conducted on an ArchPanel® to understand the fatigue behaviour and to modify the Matsui's P-N Curve. Also, full-scale deck slabs with steel reinforcement, CFRP grid with steel straps and GFRP grid with steel straps were tested under cyclic loading and their fatigue behaviour investigated. Based on the test results, P-N Curves were developed and a method for estimating the fatigue strength of concrete deck slabs is suggested.

7.2 Modifying Matsui's P-N Curve

Matsui et al. (2001) developed a P-N relationship based on rolling wheel tests applied to full-scale reinforced and un-reinforced deck slabs. Their conclusions are quantified by the following expression:

$$\log(P/P_s) = -0.07835\log(N) + \log(1.52) \qquad (7.1)$$

Where,

P = applied cyclic load,

P_s = static failure load and

N = number of cycles.

Above Eq. 7.1 gives P/Ps greater than 1.0 for N smaller than about 500. Matsui contends that this equation is valid only for N greater than 10,000.

As discussed in Chapter 5 of this report, the non-composite ArchPanel® was tested under a cyclic loading of 50 tonne. The ArchPanel® was tested in Dalhousie University and the static ultimate capacity was found 77.6 tonne. The test results showed that the ArchPanel® failed after completing 54,671 cycles under a 50 tonne (490 kN) cyclic load. Based on these test results, Eq. 7.1, was modified as follows:

$$P / P_u = 1.0 - \ln(N) / 30 \tag{7.2}$$

where,

P = applied cyclic load,

P_u =static failure load and

N = number of cycles.

Equations 7.1 and 7.2 are plotted in Fig. 7.1. This figure demonstrates that, for N greater than 10,000 cycles, the results from both equations are comparable. The modified Eq. 7.2, also gives the correct result for N = 1, when $P/P_u = 1$.

After testing the ArchPanel®, full-scale bridge deck slabs were tested under cyclic loading to investigate fatigue behaviour. As discussed in Chapters 3 and 4, the specimen deck slab had overall dimensions of 9000 x 3000 mm, and was divided into three segments (A, B and C). Segment A was designed according to CHBDC (2000) Section 8, while segments B and C were designed according to CHBDC (2000) Section 16 and make use of the principle of a steel-free concrete deck slab that is confined transversely by steel straps.

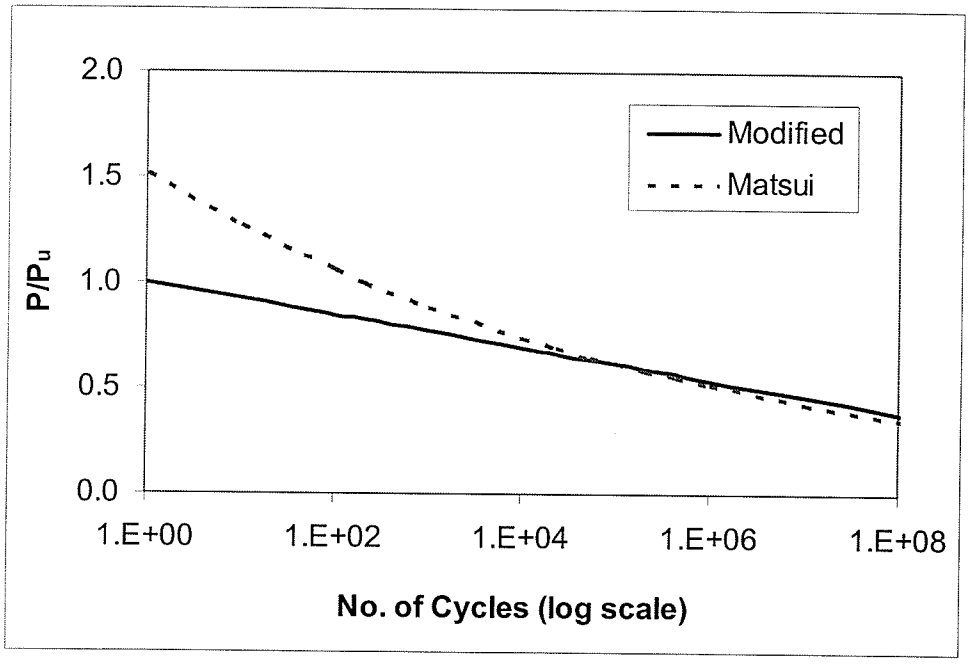

Fig. 7.1: Comparison of P-N curves

According to Eq. 7.2, all three deck slabs were expected to fail under a 60 tonne (590 kN) cyclic load using the ultimate capacity of a deck slab computed according to the PUNCH Program to be approximately 117.8 tonne. According to Eq. 7.2 the number of cycles expected at failure for segments A, B and C is approximately 2,470,335 cycles. From the test results, it was learned that segments A, B and C failed after completing 23,162, 198,863 and 420,684 cycles, respectively, under a 60 tonne (590 kN) cyclic load. Thus Eq. 7.2 does not predict the number of cycles at failure accurately. All three segments were designed to have almost the same ultimate capacity, but from experimental results, it was apparent all three panels behaved differently under fatigue. This was due to the fatigue resistance of each material. Segment C with a GFRP crack control grid had the highest fatigue resistance, followed by Segment B with a CFRP crack control grid, then Segment A with steel

reinforcement. Based on the experimental results, Eq. 7.2, once again was modified as follows:

$$P / P_s = 1.0 - \ln(N) / M \tag{7.3}$$

where,

M = 30 for ArchPanel®

M = 26.5 for internal GFRP grid and external steel strap

M = 25 for internal CFRP grid and external steel strap

M = 20.5 for steel reinforcement

According to Eq. 7.3, the fatigue strength of the ArchPanel® and bridge deck slabs can be predicted by using Eq. 7.3 and the charts shown in Fig. 7.2.

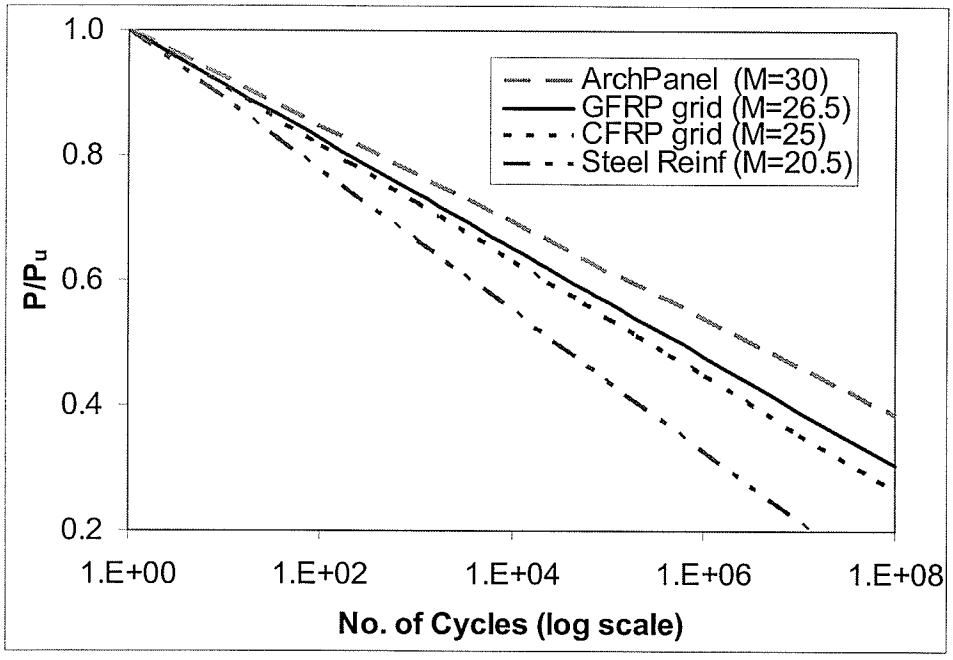

Fig. 7.2: P-N curves for ArchPanel® and bridge deck slabs

7.3 Estimate Equivalent Number of Cycles at Two Load Levels

In the absence of a more reliable relationship, Eq. 7.3 can be used to determine the equivalent number of cycles at different load levels. Using the first cumulative damage theory created by Minor (1945) or the linear damage rule. The hypothesis asserts that the damage fraction at any load level is linearly proportional to the ratio of the number of cycles of operation to the total number of cycles that would produce failure at that load level:

$$D_i = \frac{n_i}{N_i} \tag{7.4}$$

If P_1 and P_2 are two different wheel loads, n_1 and n_2 are the corresponding number of cycles of P_1 and P_2, respectively; so that the two loads have the same damaging effect ($D_1 = D_2$) and N_1 and N_2 are the limiting number of cycles corresponding to P1 and P2, respectively then ;

$$\frac{n_1}{N_1} = \frac{n_2}{N_2} \tag{7.5}$$

Thus,

$$n_2 = n_1 \frac{N_2}{N_1} \tag{7.6}$$

Leting,

$$R_i = \frac{P}{P_u} \tag{7.7}$$

Then, according to Eq. 7.3, R_1, R_2 becomes:

$$R_1 = 1.0 - \ln(N_1)/M \tag{7.8}$$

$$R_2 = 1.0 - \ln(N_2)/M \tag{7.9}$$

According to Eq. 7.8 and Eq. 7.9, N_1, N_2 becomes:

$$N_1 = e^{(1.0-R_1)M} \tag{7.10}$$

$$N_2 = e^{(1.0-R_2)M} \tag{7.11}$$

Substitute the values of N_1, N_2 and

$$n_2 = n_1 \frac{e^{(1.0-R_2)M}}{e^{(1.0-R_1)M}} \tag{7.12}$$

$$n_2 = n_1 e^{(R_1-R_2)M} \tag{7.13}$$

Therefore, the equivalent number of cycles at two load levels can be calculated using Eq. 7.13.

7.4 Recommended Approach for Fatigue

7.4.1 Background

If for an ArchPanel® it is assumed that M=30, in Eq. 7.13, and R_i is the ratio of applied cyclic load to ultimate static load, then Eq. 7.13 can be written as:

$$\frac{n_2}{n_1} = e^{30(\frac{P_1-P_2}{P_u})} \tag{7.14}$$

Where P_1, P_2 are load levels with n_1, n_2 cycles to failure respectively, and P_u is the ultimate static load. In Eq. 7.14, letting $P_1 = P_u$ and $n_1 = 1$, and letting P_2 and n_2 become the general quantities P and n, then Eq. 7.14 will become:

$$n = e^{30(\frac{P_u-P}{P_u})}$$

(7.15)

and for convenience, recast this to the power of 10 as:

$$n = 10^{13(\frac{P_u - P}{P_u})} \tag{7.16}$$

$$n = 10^{13(1-\frac{P}{P_u})} \tag{7.17}$$

Using log with base 10, Eq. 7.17 becomes:

$$\log_{10} n = 13(1 - \frac{P}{P_u}) \tag{7.18}$$

Using Eq. 7.18, the number of cycles (n) for applied load to ultimate load (P/P_u) are plotted with the natural scale for (P/P_u) and the logarithmic scale for (n), it depicts a straight line, as shown in Fig. 7.3.

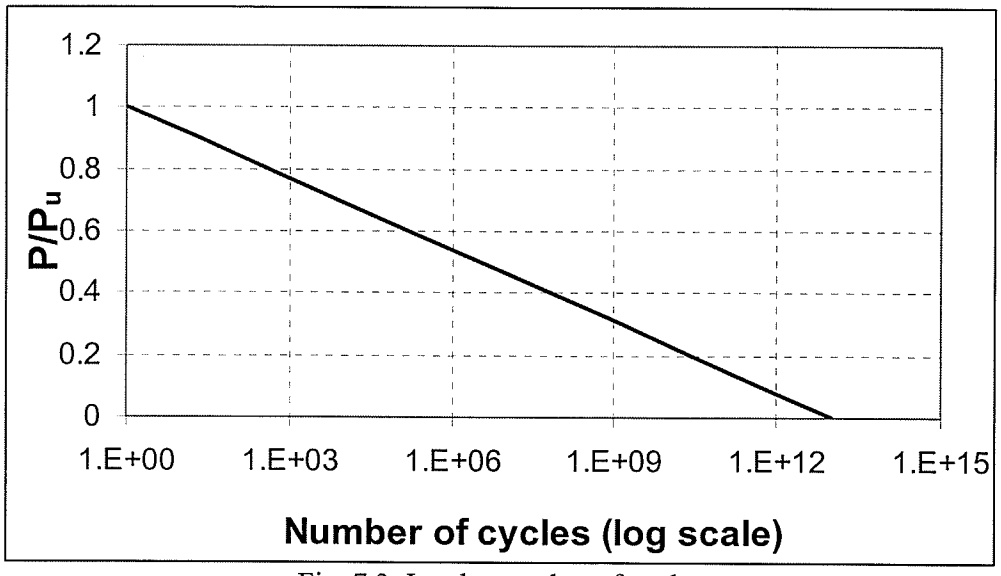

Fig. 7.3: Load – number of cycles

Fig. 7.3 demonstrates that this relationship gives a finite value of n = 1.1E+13 at P = 0 instead of an infinite one; nevertheless, the form is potentially very useful as explained below. If the assumed number M=30 in Eq. 7.13 is changed to say M=21 then the number 13 in Eq. 7.18 would become approximately 9 and a different straight line would result.

7.4.2 Suggested Method

This study suggested to use any static load–deflection curve (Fig. 7.4), it is reasonable, at load level (P), to consider the increase of deflection (δ_u-δ_p), which occurs during the fatigue loading. It is also reasonable to assume that the rate of increase of permanent set is related to the initial deflection (δ_p). It is then necessary to look at the functions of [(δ_u-δ_p) / δ_p] as possibilities. Normally the complete curve of load–deflection is not available, so it is necessary to consider instead the function of [(P_u-P) / P]. Note that this differs from the form of Eq. 7.15 because it now has (P) as the denominator, not (P_u). This makes the following a necessary consideration:

$$n = 10^{C(\frac{P_u - P}{P})^{\alpha}} \tag{7.19}$$

$$\log_{10} n = C(\frac{1}{\left(\frac{P}{P_u}\right)} - 1)^{\alpha} \tag{7.20}$$

$$n = 10^{C(\frac{1}{\left(\frac{P}{P_u}\right)} - 1)^{\alpha}} \tag{7.21}$$

The advantages of Eq. 7.21 are:

(i) It satisfies the condition when, $P=P_u$ and $N=1$

(ii) when, $P \rightarrow 0$ and $N=\infty$

(iii) The presence of two parameters, (C and α) mean that two other points on the fatigue curve can be satisfied. Thus, it is potentially a good curve–fitting relationship.

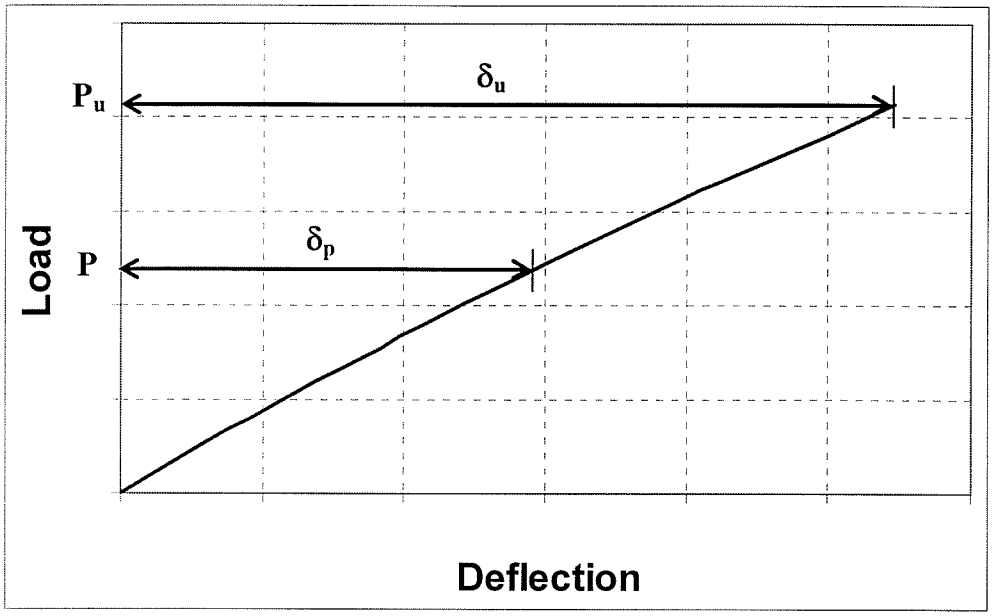

Fig. 7.4: Load – deflection curve

7.4.3 Numerical Example

Suppose that $P = 0.5\ P_u$ and $n = 10^6$ cycles, then according to Eq. 7.20, C = 6.

Suppose also that $P = (2/3)\ P_u$ and n = 16,000 cycles, then again from Eq. 7.20:

$$4.2 = 6(1/2)^{\alpha}$$

$\alpha = 0.5$ (approximately).

Thus Eq. 7.21 will become;

$$n = 10^{\sqrt[6]{\frac{1}{(\frac{P}{P_u})}-1}} \tag{7.22}$$

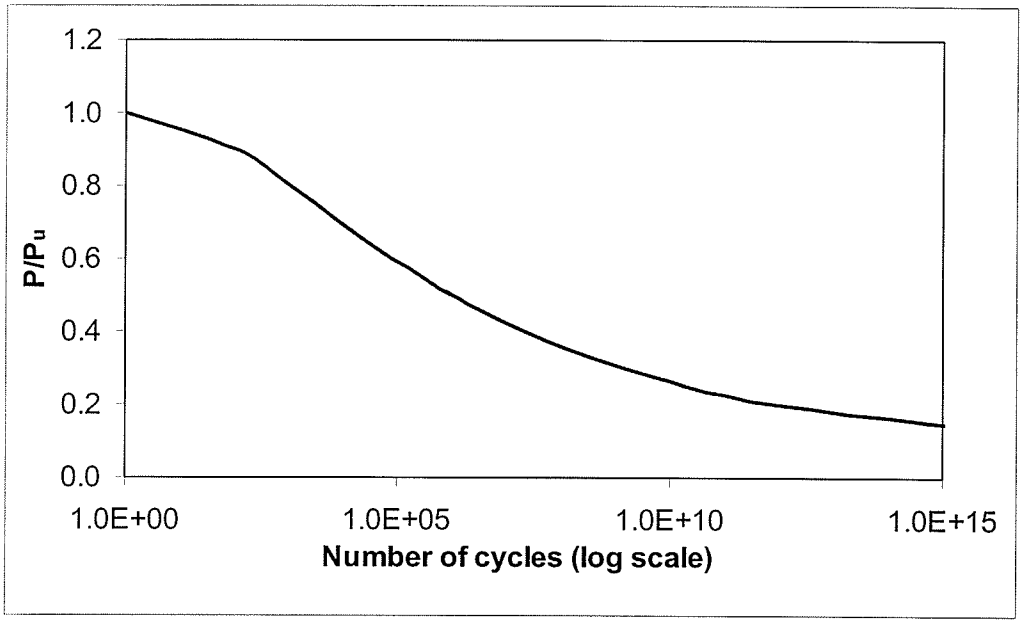

Fig. 7.5: Load–number of cycles of suggested method

Using Eq. 7.22, the number of cycles (n) for applied load to ultimate load (P/P_u) is shown in Fig. 7.5. This figure demonstrates that the relationship gives an infinite value at P=0 instead of finite one, and also that behaviour is non-linear compared to the linear behaviour shown in Fig. 7.3.

7.5 Estimate Fatigue Strength of Segment C

Segment C of the steel-free concrete deck slab containing a GFRP crack control grid and steel strap was tested under cyclic loading to investigate fatigue behaviour. At a 60 tonne cyclic load level, the Segment C failed after completing 420,683 cycles. The deflection with an increasing number of cycles under a 60 tonne cyclic load is shown

in Fig. 7.6. Using the trend line function in Excel demonstrates that the best fitting curve was polynomial in the order of 2 with an accuracy of approximately 99%. The details of the test results have been shown in Chapter 6. The suggested method described previously in Section 7.4 shows that the two parameters C and α are based on a fatigue curve. The fatigue curve of Segment C (Fig. 7.6) is a polynomial in the order of 2. Thus the value of $\alpha = 1/2$ (where α = 1/order of polynomial) and according to Eq. 7.20, C = 5.735. Once the values of C and α are known then, according to Eq. 7.21, the number of cycles with respect to applied load can be calculated (Fig. 7.7). Thus, by using Fig. 7.7 the fatigue strength of Segment C at various load levels can be predicted.

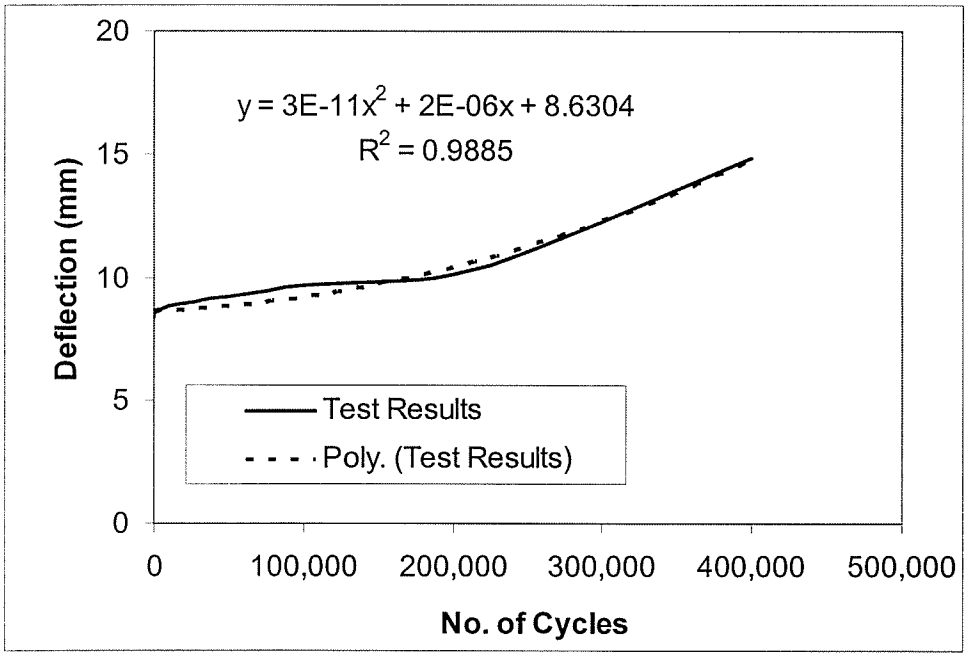

Fig. 7.6: Fatigue curve of Segment C

7.6 Estimate Fatigue Strength of Segment B

Segment B of the steel-free concrete deck slab containing CFRP crack control grid and steel strap was tested under cyclic loading to investigate fatigue behaviour. At a 60 tonne cyclic load level, the Segment B failed after completing 198,862 cycles. The deflection with an increasing the number of cycles under a 60 tonne cyclic load is shown in Fig. 7.8. Using the trend line function from Excel, the best fitting curve was

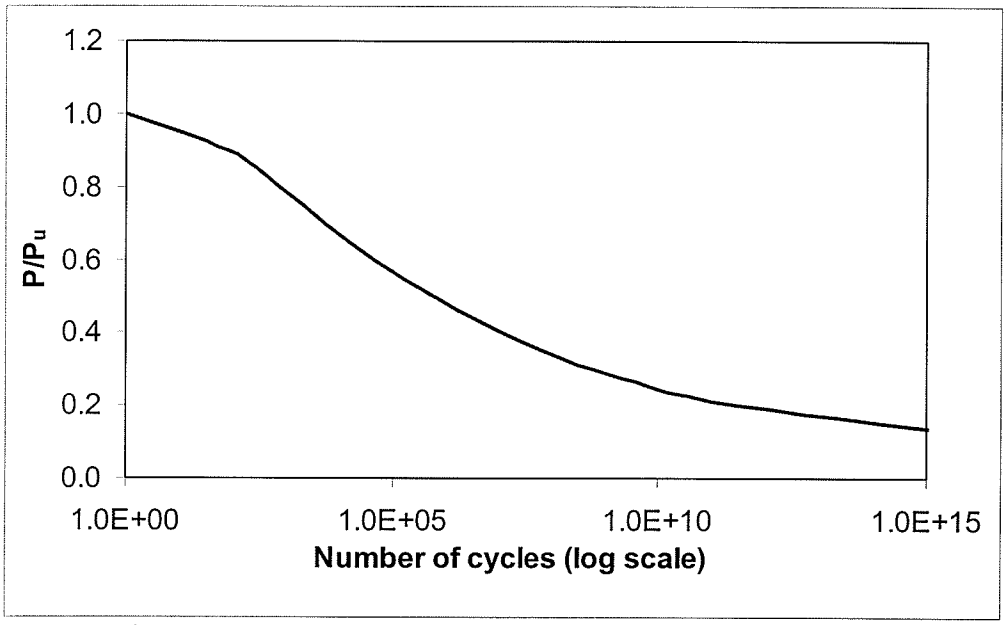

Fig. 7.7: P-N Curve for Segment C to estimate fatigue strength

polynomial in the order of 2 with an accuracy of approximately 97% can be demonstrated. The details of the test results are shown in Chapter 6. The suggested method described in Section 7.4.2 shows that the two parameters C and α are based on a fatigue curve. The fatigue curve of Segment B (Fig. 7.8) is a polynomial in the order of 2. Thus the value of $\alpha = 1/2$ (where α = 1/order of polynomial). According to Eq. 7.20, C = 5.405. Once the values of C and α, are known then, according to Eq. 7.21, the number of cycles (n) with respect to applied load can be calculated

(Fig. 7.9). Using the values shown in Fig. 7.9, the fatigue strength of Segment B at various load levels can be estimated.

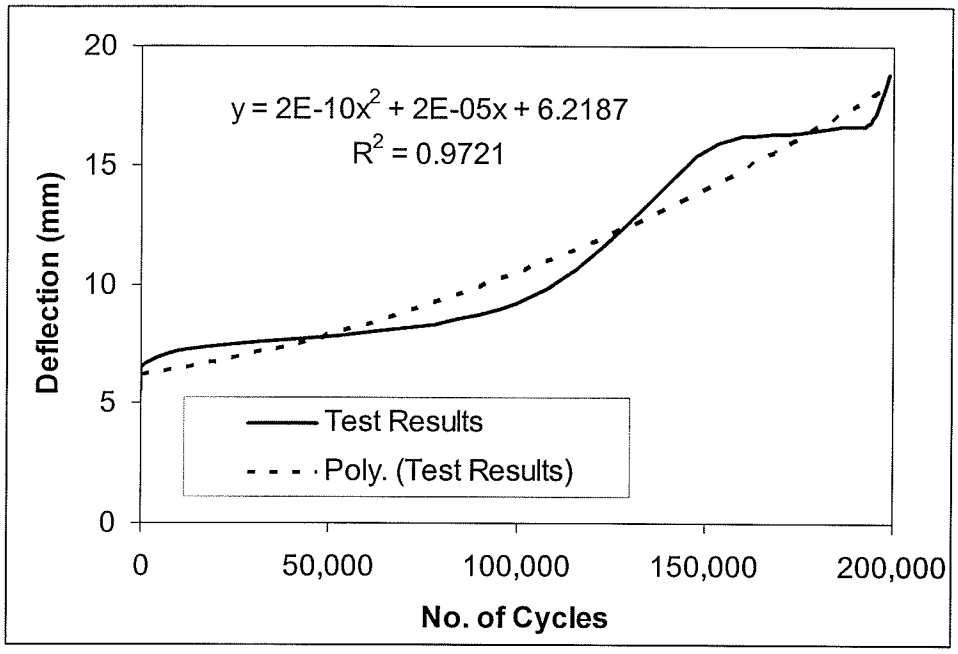

Fig. 7.8: Fatigue curve for Segment B

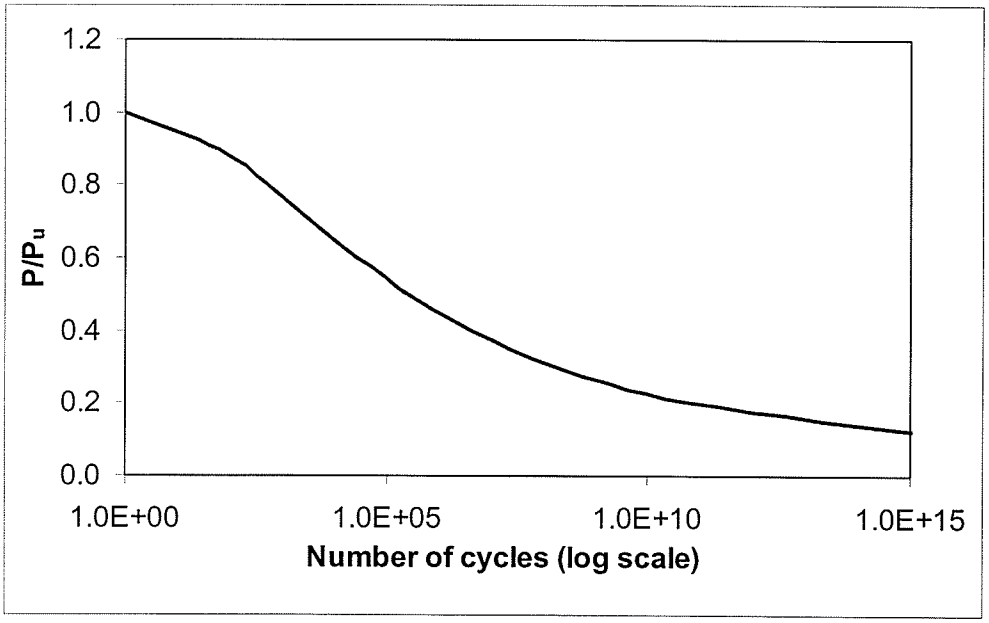

Fig. 7.9: P-N curve for Segment B to estimate fatigue strength

7.7 Fatigue Strength of Steel-free Concrete Bridge Deck Slab

From the limited test results described in Sections 7.5 and 7.6, a fatigue curve of a steel-free concrete bridge deck slab with an approximate polynomial of the order of 2 (α=0.5) and a constant C was developed approximately equal to 5.737 and 5.405 for segments C and B, respectively. In the absence of the fatigue curve, α=0.5 and C=5.0 (conservatively) can be used, and the Eq. 7.21 can be written as:

$$n = 10^{C\left(\frac{1}{\left(\frac{P}{P_u}\right)}-1\right)^{\alpha}} \tag{7.23}$$

For GFRP $C = 5.737$ and $\alpha = 0.5$

For CFRP $C = 5.405$ and $\alpha = 0.5$

Therefore, estimating the fatigue strength of a steel-free concrete bridge deck slab can be calculated using Eq. 7.23. According to Eq. 7.23, the number of cycles (n) for applied load to ultimate load (P/P_u) can be estimated (Fig. 7.10).

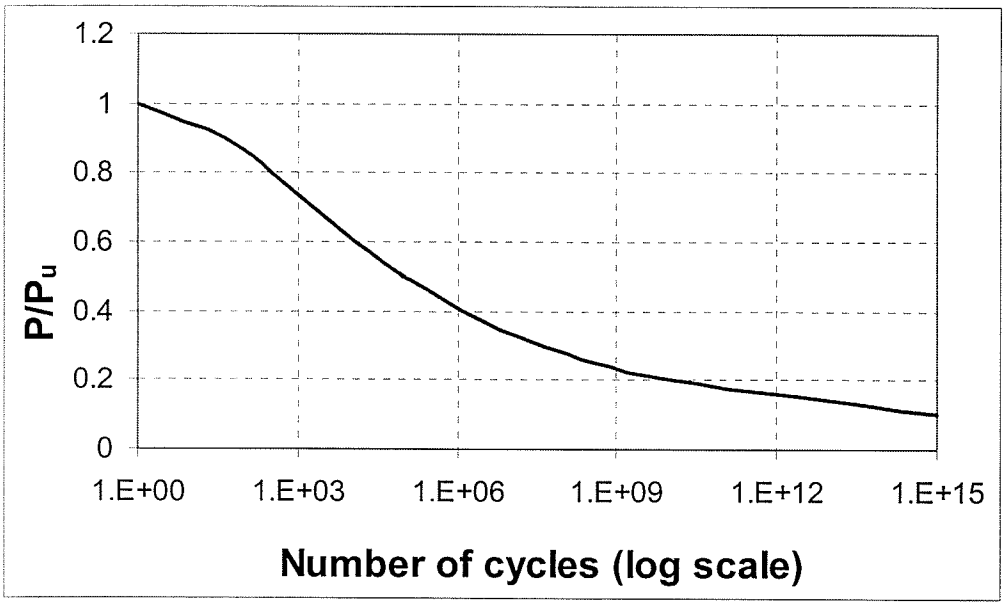

Fig. 7.10: P-N Curve for steel-free concrete bridge deck slab

Chapter 8

Conclusions and Recommendations

8.1 Conclusions

Based on test results and investigation, the following conclusions can be drawn:

- Experimental results of the ArchPanel® show that fatigue damage induced at 20 and 25 tonne load levels are within permissible limits, therefore satisfying the serviceability criterion.
- The ArchPanel® failed after completing 54, 671 cycles under a 50 tonne cyclic load. The deflection, strain and crack width experimental results of the ArchPanel® under a 50 tonne cyclic load showed similar trends indicating that either deflection, strain, or crack width can be used as an indicator of damage.
- The experimental results from the testing of the ArchPanel® were used to modify Matsui's P-N curve.
- Three slabs (segments A, B and C) of a full-scale bridge deck were tested under a 25 tonne cyclic load, completed 1,000,000 cycles. The experimental results for segments A, B and C indicated that the deflections were approximately 2 mm, and the crack widths were approximately 0.4 mm, the crack width is lower than the serviceability limit (0.5 mm). The strain values of steel reinforcement in Segment A, steel straps in Segment B and C and CFRP reinforcement in Segment B and GFRP reinforcement in Segment C

were lower than the 1200 (10^{-6}) which satisfied the serviceability limit. Thus all three segments A, B and C satisfied the serviceability criterion.

- Test results of Segment B and C under 25 tonne cyclic load indicated that, CFRP and GFRP rebar reached a maximum strain of approximately 1200 (10^{-6}), which is the 60% of the service limit. Thus the area of either CFRP or GFRP can be reduced by up maximum of 40%.
- All three segments failed under a cyclic load, which peaked at 60 tonne. Segment A failed after completing 23,162 cycles; Segment B failed after completing 198, 863; and Segment C failed after completing 420,682 cycles. These results show that deck slabs having the same thickness but confined differently have significantly different fatigue resistance. The tests indicated that Segment A had the least favourable fatigue resistance, whereas segments B and C had the most favourable fatigue resistance. Segment C, with an internal GFRP grid and external steel strap, provided the best fatigue resistance for a bridge deck slab.
- A modified P-N curve was developed on the basis of the results from the ArchPanel. However this curve did not estimate the fatigue strength of segments A, B and C accurately, because of the varying fatigue resistance of each material. Based on the experimental results segments A, B and C, the modified P-N curve was further modified and a variable constant, M, was introduced to account for the type of reinforcement. Thus,

  M = 30 for ArchPanel®

  M = 26.5 for internal GFRP grid and external steel strap

  M = 25 for internal CFRP grid and external steel strap

  M = 20.5 for steel reinforcement

This modified P-N curve can be used to estimate the fatigue strength of slabs.

- Based on the limited experimental results and fatigue curves, a simple theoretical model was proposed to estimate the fatigue strength of steel-free concrete bridge deck slabs. The suggested method has two parameters: C and α, that depend upon the fatigue behaviour of the slab. In the absence of a fatigue curve, α=0.5 and C=5.0 (conservatively) can be used to estimate the fatigue strength of steel-free concrete bridge deck slabs. Refinements of the model are to be expected as additional fatigue test data on steel-free concrete bridge deck slabs become available.
- The second generation steel-free concrete deck slabs reinforced with a hybrid system of internal FRP grid and external steel straps eliminates corrosion completely from the deck slab.
- The presence of an FRP grid in the second generation steel-free concrete deck slab reduces the chances of the development of cracks.
- Test results of the second generation steel-free concrete deck slab showed similar trends indicating that deflection, strain or crack width can be used as indicators of fatigue damage in concrete deck slabs.
- Finally, the hybrid system consisting of internal a GFRP grid and an external steel strap results in an efficient, economical, and corrosion-free second generation steel-free concrete bridge deck slab that satisfies the serviceability, ultimate and fatigue limit states criterion.

8.2 Recommendations for Future Research

Recommendations for future research include investigating the static and fatigue behaviour of steel-free concrete deck slabs by measuring the crack width, deflection, strap strain and outward movement of girders in the following cases:

- Without a FRP-grid;
- Increasing spacing between the girders;
- Reducing GFRP-grid to a maximum of 40%.

Also, refinement of a theoretical model of fatigue strength of steel-free concrete bridge deck slab, is needed.

Determine the damage mechanism and fatigue mechanism, by using ultrasonic monitoring or perhaps micro analysis of materials.

References

AASHTO (1998) *LRFD Bridge Design Specifications*, American Association of State Highway and Transportation Officials, Washington, D.C.

ACI 440.1R-01 (2001) "Guide for the Design and Construction of Concrete Reinforced With FRP Bars". Reported by ACI Committee 440.

Bakht, B. and Agarwal, A.C. (1995) "Deck Slab of Skew Girder Bridges", Canadian Journal of Civil Engineering, Vol. 22(3): 514-523.

Bakht, B. and Lam, C. (2000) "Behaviour of Transverse Confining System for Steel-Free Deck Slabs," ASCE Journal of Bridge Engineering, 5(2): 139-147.

Bakht, B. and Markovic, S. (1986) "Accounting for Internal Arching in Deck Slab Design". Journal of the Institution of Engineers (India), Vol. 67(CII): 18-25.

Bakht, B. and Mufti, A.A. (1998) "Five Steel-Free Bridge Deck Slabs in Canada", Journal of the International Association for Bridge and Structural Engineering (IABSE), Vol. 8(3): 196-200.

Bakht, B. and Selvadurai, A. P. S. (1996) "Performance of Steel-Free Deck Slab under Simulated Wheel Loads", Proceedings: 2nd Annual Conference on Advance Composite Materials in Bridges and Structures, Montreal, pp. 767-776.

CHBDC, 2000, "Canadian Highway Bridge Design Code", Canadian Standards Association International, Toronto, ON.

CISC Handbook of Steel Construction, 7th Edition (2000)

Dorton, R.A., Holowka, M. and King, J.P.C. (1977) "The Connestego River Bridge Design and Testing", Canadian Journal of Civil Engineering, Vol. 4(1):18-39.

Hewitt, B.E. and Batchelor, B. (1975) "Punching Shear Strength of Restrained Slabs", ASCE, Journal of the Structural Division, 101(STP9): 1837-1853.

ISIS Canada Design Manual #3 (2001) "Reinforcing Concrete structures with Fibre Reinforced Polymers", Winnipeg, MB.

Khanna, O.S., Mufti, A.A. and Bakht, B. (2000) "Experimental Investigation of the Role of Reinforcement in the Strength Of Concrete Deck Slabs", Canadian Journal of Civil Engineering, Vol.27(3): 475-480.

Kinnunen, S., and Nylander, H. (1960) "Punching of Concrete Slab without Shear Reinforcement", Transactions of the Royal Institute of Technology, Stockholm, Sweden, No. 158.

Limaye, N. V. (2004) "Steel-Free Bridge Decks Under Cyclic Loading: A Study of Crack Propagation and Strength Degradation," Doctor of Philosophy Thesis, DalTech-Dalhousie University, Halifax, Nova Scotia, Canada.

Marzouk, H. and Hussein, A. (1991) "Punching Shear Analysis of Reinforced High-Strength Concrete Slabs", Canadian Journal of Civil Engineering, Vol. 18: 954-963.

Matsui, S. and Tei, K. (2001) "Researches and Japanese Developments on Highway Bridge Slabs and Contribution of Wheel Running Machines", Proceedings, Third International Conference on Concrete under Severe Conditions, Vancouver, B.C. Vol. 1: 992-1008

Matsui, S., Tokai, D., Higashiyama, H. and Mizukoshi, M. (2001) "Fatigue Durability of Fibre Reinforced Concrete Decks under Running Wheel Load", Proceedings Third International Conference on Concrete Under Severe Conditions, CONSEC 01, Vancouver,B.C. Vol.1: 982-991.

Miner, M. A. (1945) "Cumulative Damage in Fatigue", Journal of Applied Mechanics, 159-164.

Mufti, A.A., Bakht, B. and Jaeger, L.G. (1991) "FRC Deck Slabs With Diminished Steel Reinforcement", Proceedings, IABSE Symposium, Leningard, USSR, 388-389.

Mufti, A.A., Memon, A.H., Bakht, B. and Banthia, N. (2002) "Fatigue Investigation of the Steel-Free Bridge Deck Slabs", ACI International SP- 206: 61-70.

Mufti, A.A., Newhook, J.P. and Khanna, O.S. (1999) "Predicting the Punching Behaviour of Reinforced Concrete Bridge Decks", Proceedings of the Canadian Society for Civil Engineering Annual Conference, Vol. 1: 95-104.

Mufti, A.A., Newhook, J.P. and Mahoney, M.A. (1999) "Salmon River Bridge Field Assessment", Proceedings of the Canadian Society for Civil Engineering Annual Conference, Vol.1: 51-61.

Mufti, A.A. and Newhook, J.P. (1998) "Punching Shear Strength of Restrained Concrete Bridge Deck Slabs," ACI Structural Journal, 95(4): 375-381.

Mufti, A.A., Jaeger, L.G., Bakht, B. and Wegner, L.D. (1993) "Experimental Investigation of FRC Slabs without Internal Steel Reinforcement," Canadian Journal of Civil Engineering, Vol. 20 (3): 398-406.

Newhook, J.P. and Mufti, A.A. (1996) "A Reinforced Steel-Free Concrete Deck Slab for the Salmon River Bridge", Concrete International, Vol. 18(6): 30-34.

Newhook, J.P. and Mufti, A.A. (1998) "Punch Program User Manual," Nova Scotia CAD/CAM Centre Dalhousie University, Halifax, Nova Scotia.

Newhook, J.P., Mufti, A.A. and Wegner, L.D. (1995) "Fibre-reinforced Concrete Deck Slabs Without Internal Reinforcement – Half-Scale Testing and Mathematical Formulation", Research Report No. 1-1995, Technical University of Nova Scotia – Nova Scotia CAD/CAM Center.

Newhook, J.P. (1997) "The Behaviour of Steel-Free Concrete Bridge Deck Slabs under Static Loading Conditions", Doctor of Philosophy Thesis, Technical University of Nova Scotia, Halifax, Nova Scotia, Canada.

OHBDC 1979, 1983, 1992. Ontario Highway Bridge Design Code, Ministry of Transportation of Ontario, Downsview, Ontario, Canada.

Perdikaris, P.C. and Beim, S. (1988) "RC Bridge Decks under Pulsating and Moving Load". ASCE, Journal of Structural Engineering, Vol.114(3): 591-607.

Petrou, M. F., PerdiKaris, P. C. and Wang, A. (1994) "Fatigue Behaviour of Noncomposite Reinforced Concrete Bridge Deck Models", Transportation Research

Record No. 1460, Journal Article Published by National Research Council, Washington, DC, USA: 73-80.

Selvadurai, A.P.S. and Bakht, B. (1995) "Simulation of Rolling Wheel Loads on an FRC Deck Slab", Proceedings, 2nd University-Industry Workshop on FRC, Toronto, ON, 273-287.

Thorburn, J. and Mufti, A. A. (2001) "Design Recommendation for an externally Restrained Highway Bridge Deck", ASCE Journal of Bridge Engineering.

Thorburn, J. and Mufti, A.A. (1995) "Full-Scale Testing of Externally Reinforced FRC Bridge Decks On Steel Girders", Proceedings of the Canadian Society of Civil Engineering Annual Conference, Ottawa, ON, Vol. (II): 543-552.

Wegner, L. D. and Mufti, A.A. (1994) "Finite Element Investigation of Fiber-Reinforced Concrete Deck Slabs without Internal Steel Reinforcement", Canadian Journal of Civil Engineering, Vol. 21: 231-236.

Youn, S.G. and Chang, S.P. (1998) "Behaviour of Composite Bridge Decks Subjected to Static and Fatigue Loading", ACI Structural Journal, Vol. 95(3): 249-258.

Appendix – A1

Details of concrete mix proportions for Grade – 35 and properties

Batch Weight

Type – 10 Cement	323	(kgs/m^3)
Coarse Aggregate (20mm stone)	996	(kgs/m^3)
Fine Aggregate (sand)	787	(kgs/m^3)
Class C Fly Ash	57	(kgs/m^3)
Water	145	(kgs/m^3)
Water Reducing Admixture (Poly 997)	2470	(mls/m^3)
Air-entraining Admixture (MBVR)	152	(mls/m^3)

Properties

Properties	Batch 1	Batch 2 (Without Fibres)	Batch 2 (With Fibres)
Slump (mm)	80	50	-
Flow Test (sec.)	-	-	12
Air Content (%)	5.0	4.0	4.5
Density of Concrete (kgs/m^3)	2395	2403	2377

Appendix – A2

Compressive strength of concrete cylinders (f_c')

Type	f_c' @ 3 days (MPa)	f_c' @ 7 days (MPa)	f_c' @ 28 days (MPa)	f_c' @ 150 days (MPa)
Batch 1	37.3	38.2	50.2	51.9
Batch 2	36.0	40.3	53.5	51.4
Batch 2 with fibres	38.7	46.0	57.7	56.1

Tensile strength of concrete cylinders (f_t)

Type	f_t @ 28 days (MPa)	f_t @ 150 days (MPa)
Batch 1	3.1	3.9
Batch 2	3.6	4.2
Batch 2 with fibres	4.1	4.6